ANTIBIOTIC-LOADED POLYMERIC MICROSPHERES FOR PASSIVE LUNG TARGETING AFTER INTRAVENOUS ADMINISTRATION

by

MONICA AGNOLETTI

M.Sc., University of Parma, 2016

A DISSERTATION SUBMITTED IN PARTIAL FULFILLMENT OF THE REQUIREMENTS FOR THE DEGREE OF

DOCTOR OF PHILOSOPHY

in

THE FACULTY OF GRADUATE AND POSTDOCTORAL STUDIES

(Pharmaceutical Sciences)

THE UNIVERSITY OF BRITISH COLUMBIA

(Vancouver)

July 2020

UNIVERSITY OF COPENHAGEN
FACULTY OF HEALTH AND MEDICAL SCIENCES

PhD Thesis

Monica Agnoletti

Antibiotic-loaded polymeric microspheres for passive lung targeting after intravenous administration

This thesis has been submitted to the Graduate School of Health and Medical Sciences, University of Copenhagen on March 15, 2020

The following individuals certify that they have read, and recommend to the Faculty of Graduate and Postdoctoral Studies for acceptance, the dissertation entitled:

Antibiotic-loaded polymeric microspheres for passive lung targeting after intravenous adminiatration

submitted by Monica Agnoletti in partial fulfillment of the requirements for the degree of Doctor of Philosophy in Pharmaceutical Sciences

Examining Committee:

Susan Weng Larsen, Faculty of Health and Medical Sciences, University of Copenhagen
University Examiner

Marcel Bally, Faculty of Medicine, University of British Columbia
University Examiner

Simon Bjerregaard, Ferring Pharmaceuticals
External Examiner

Additional Supervisory Committee Members:

-
Supervisory Committee Member

-
Supervisory Committee Member

Academic Advisors

Urs Otto Häfeli
Professor, PhD
Department of Pharmacy
Faculty of Health and Medical Sciences
University of Copenhagen, Denmark
and Faculty of Pharmaceutical Sciences
University of British Columbia, Canada

Hanne Mørck Nielsen
Professor, PhD
Department of Pharmacy
Faculty of Health and Medical Sciences
University of Copenhagen, Denmark

Katayoun Saatchi
Research Associate, PhD
Faculty of Pharmaceutical Sciences
University of British Columbia, Canada

Assessment Committee

Susan Weng Larsen (Chair)
Associate Professor, PhD
Department of Pharmacy
Faculty of Health and Medical Sciences
University of Copenhagen, Denmark

Simon Bjerregaard
Senior Scientist in Pharmaceutical Development, PhD
International PharmaScience Center
Ferring Pharmaceuticals, Denmark

Marcel Bally
Professor, PhD
Department of Pathology and Laboratory Medicine
Faculty of Medicine
University of British Columbia, Canada

Preface

The present thesis entitled "*Antibiotic-loaded polymeric microspheres for passive lung targeting after intravenous administration*" was submitted to the Faculty of Health and Medical Sciences, University of Copenhagen and the Graduate and Postdoctoral Studies, University of British Columbia. This dissertation is formatted in accordance with the regulations of University of Copenhagen and submitted in partial fulfillment of the requirements for a PhD degree awarded jointly by University of Copenhagen and the University of British Columbia. Versions of this dissertation will exist in the institutional repositories of both institutions.

The experimental work was conducted in the Drug Delivery and Biophysics of Biopharmaceuticals group headed by Professor Hanne Mørck Nielsen, PhD, Department of Pharmacy, University of Copenhagen, and in the Nanomedicine, Drug Delivery and Radiopharmaceuticals group headed by Professor Urs Otto Häfeli, PhD, Faculty of Pharmaceutical Sciences, University of British Columbia.

The project has been performed in affiliation with the Drug Research Academy at the University of Copenhagen and the Pharmaceutical Sciences Graduate Program at the University of British Columbia. This project was financially supported by the Lundbeck Foundation, Denmark.

The research conducted over the course of the PhD project has resulted in one published scientific manuscript, included in the Appendix and reproduced with permission.

> **Agnoletti M**, Rodrıguez-Rodriguez C, Kłodzinska SN, Esposito TVF, Saatchi K, Mørck Nielsen H, Häfeli UO. Monosized Polymeric Microspheres for Passive Lung Targeting: Biodistribution and Pharmacokinetics after Intravenous Administration. *ACS Nano.* 2020, 14, 6693-6706.

I designed and conducted the experiments, analyzed and interpreted the experimental data, made all figures, and wrote, edited and prepared the manuscript for submission. My supervisors, Professor Hanne Mørck Nielsen and Professor Urs Otto Häfeli, provided guidance in the study design and interpretation of the results, and were involved in the preparation and editing process of the manuscript. Cristina Rodrıguez-Rodriguez contributed to the execution and interpretation of the SPECT/CT, biodistribution and histology studies. Sylvia Natalie Kłodzinska contributed to the execution of the antimicrobial activity study and to the writing of the first draft of the manuscript. Tullio Vito Francesco Esposito provided expert advice on the cytotoxicity, radiolabeling and SPECT/CT studies as well as the initial design of the histology study. Kathy Saatchi modified the microspheres with the chelator and oversaw the radiolabeling study. All authors approved the final manuscript. My total contribution to this research was >90%. Etics approval for the animal studies was obtained from the Animal Care Committee of the University of British Columbia under the approved protocol A16-0150.

In addition to the included study, the project has involved collaboration on the preparation of the following manuscripts, which are not discussed in the current thesis.

Klodzińska SN[†], Esposito TVF[†], **Agnoletti M,** Rodriguez-Rodriguez C, Blackadar C, Wu L, Thakur A, Saatchi K, Rades T, Häfeli UO, Mørck Nielsen H. Pharmacokinetics of LL-37 and nanogel-encapsulated LL-37 after pulmonary administration: a SPECT/CT study. *In preparation.*

Geczy R, **Agnoletti M,** Hansen MF, Kutter JP, Saatchi K, Häfeli UO. Microfluidic Approaches for the Production of Monodisperse, Superparamagnetic Microspheres in the Low Micrometer Size Range. *J. Magn. Magn. Mater.* 2019, 471, 286–293.

Acknowledgements

I would like to thank my main supervisor Professor Urs Otto Häfeli for the competent mentoring, valuable advice and kind support throughout the duration of the PhD project. Thanks for pushing me to perform at my highest level and for giving me the opportunity to be a Joint PhD at UCPH and UBC. A special thanks goes to my main co-supervisor Professor Hanne Mørck Nielsen for her excellent guidance, constructive feedback on my work, and never ending professional and moral support throughout the three years. I would also like to thank my co-supervisor Research Associate Kathy Saatchi for the positive attitude, encouragement, and the scientific support and guidance with the radiolabeling experiments.

I would like to thank everyone who was involved in the collaboration between UCPH and UBC, especially the Head of the Department of Pharmacy at UCPH Flemming Madsen, the former Vice-Dean at the Faculty of Health and Medical Sciences at UCPH Professor Sven Frøkjær, the Dean at the Faculty of Pharmaceutical Sciences at UBC Professor Michael Coughtrie, and the Associate Dean of Graduate Studies at UBC Professor Tom Chang. You were all crucial in making the collaboration happen, and I am very grateful for the wonderful opportunity I have been given. A special thanks goes to Samra Alam and Marianne Wieslander Jørgensen at UCPH for their patience and help with the financial and administrative issues – your advice has truly been valuable when I needed help navigating the procedures of the University. I would like to thank the Lundbeck Foundation for providing financial support for my project, and the Graduate School of Health and Medical Sciences at UCPH for supporting my stay abroad at UBC in Vancouver.

I owe a special thanks to Cristina Rodriguez-Rodriguez, Sylvia Klodzinska and Tullio Esposito. Thanks to Cristina for helping with the *in vivo* studies, for the great discussions and support during the days at CCM – I really enjoyed working with you in "our" very organized way. Thanks to Sylvia for helping with the antibacterial activity experiments, for being a fantastic office mate and for the support given from day one. Thanks to Tullio for the extraordinary scientific inputs, help and support in the Hafeli Lab. I would also like to thank Mai Bay Stie for translating the Abstract of my thesis in the Danish Resumé.

A big thanks goes to all the wonderful colleagues I had both at the Drug Delivery and Biophysics of Biopharmaceuticals group at UCPH and at the Hafeli Lab at UBC. Thanks to Sofie Fogh Hedegaard, Sylvia Klodzinska, Ditlev Birch for the lunches, push-up challenges and fun times in the office 417. Thanks to Danai Panou, Mai Bay Stie, Sara Malekkhaiat, Kate Browning, Elisa Parra Ortiz and Reka Geczy for the "hyggeligt" working environment and for always providing a good mood. Thanks to Marco van de Weert for the support and for regularly bringing chocolate in the PhD office. Thanks to the technician Karina Juul Vissing for the excellent support in the lab. Thanks to Lennart Bohrmann, Marta Bergamo, Tullio Esposito, and Zeynab Nosrati for creating an enjoyable working environment in the Hafeli Lab, for supporting me in the ups and downs, and for the beautiful hikes in British

Columbia. Thanks to Lukas Hohenwarter, Roland Böttger, Ravi Gaikwad and all the graduate students of PharGS at UBC for the great social activities.

I owe a special thanks to my friends outside the lab. Thanks to Alejandra, Elia, Marco, Fabio and Fabio, Andrea, Filippo, Riccardo, Viktor, Alessandro, Federico, Nicola for being the family in Copenhagen and bringing a little bit of Italy in Denmark; Michela and Jess for sharing good laughs while learning Danish. Thanks to Thea and Thomas for welcoming me in Copenhagen. Thanks to my friends in Italy, especially Silvia, Giulia, Margherita and Federica for the great friendship and for always listening to my vocal messages.

Above all, I would like to thank my boyfriend Oliver for his patience, support and for making me happy every day. A big thanks goes to my aunt Fiorisa and my uncle Pasquale for their wise advice and positive spirit. Finally, I would like to thank my parents, Lorella and Massimo, and my sister Alessandra, for their endless love and encouragement, wherever I am.

Monica Agnoletti, Copenhagen, March 2020

Table of Contents

Abbreviations

^{111}In	^{111}Indium
AMPs	Antimicrobial peptides
CDC	Centers for Disease Control and Prevention
COPD	Chronic obstructive pulmonary disease
Cu	Copper
CP	Continuous phase
DP	Dispersed phase
DTPA	*p*-SCN-Bn-DTPA, S-2-(4-isothiocyanatobenzyl)-diethylenetriamine pentaacetic acid
EDTA	Ethylenediaminetetraacetic acid
EMA	European Medicines Agency
FIB-SEM	Focused ion beam-scanning electron microscopy
logD	Distribution coefficient
MDR	Multidrug-resistant
MIC	Minimum inhibitory concentration
MRSA	Methicillin-resistant *Staphylococcus aureus*
MTT	3-(4,5-dimethylthiazol-2-yl)-2,5-diphenyltetrazolium bromide
O/W	Oil/water
PDR	Pandrug-resistant
PEG	Polyethylene glycol
PLA	Poly(lactic acid)
PLGA	Poly(lactic-co-glycolic) acid
PVA	Polyvinyl alcohol
Q_{CP}	Flow rate of the CP
Q_{DP}	Flow rate of the DP
R^2	Correlation coefficient
RMSE	Root mean squared error
SEM	Scanning electron microscopy
SPECT/CT	Single-photon emission computed tomography
US FDA	United States Food and Drug Administration
W/O/W	Water/oil/water
WHO	World Health Organization
XDR	Extensively drug-resistant

Abstract

Low respiratory tract bacterial infections are currently amongst the leading causes of mortality worldwide. Current treatments consist of oral or intravenous administration of antibiotics. Today´s treatments of pulmonary bacterial infections are often not sufficiently effective due to the difficulty of drugs reaching the infection deep in the lungs, the insufficient drug doses at the site of infection, the development of multi-drug resistance, and the side effects caused by some of the currently used and effective antibiotics. Lung-targeted delivery of antibiotics by using injectable drug-loaded microspheres is a promising alternative to the traditional antibiotic solutions as they achieve local therapeutic concentrations of antibiotics and minimise unwanted off-target effects. This delivery strategy offers potential, especially in the case of patients with compromised lung function or obstruction of the respiratory tract, due to inflammation, infection or significant mucus production, while they still have normal lung perfusion.

The aim of this project was to explore the use of polymeric microspheres as carriers for lung delivery of antibiotics to increase the efficacy of these drugs against bacterial respiratory infections, specifically by selectively targeting the lung capillaries after intravenous administration.

Biodegradable poly(lactic-co-glycolic) acid (PLGA) microspheres encapsulating levofloxacin were prepared with a flow-focusing microfluidic chip and characterized for their physico-chemical properties, and their *in vitro* and *in vivo* performance. The PLGA microspheres were highly homogeneous in size with a mean diameter of ~12 μm and coefficient of variation <5.2%. The microspheres slowly released the encapsulated levofloxacin in a controlled fashion over five days and slightly reduced its antibacterial activity against *Pseudomonas aeruginosa*, *Escherichia coli* and *Staphylococcus aureus*. The microspheres degradation studies showed changes in the internal structure and in the surface morphology, and a faster degradation kinetic *in vivo* than *in vitro*. The microspheres showed low toxicity for endothelial and alveolar epithelial cell lines, and did not cause lysis of red blood cells. The biodistribution and pharmacokinetics study showed that ^{111}Indium-labeled microspheres distributed almost exclusively and homogenously in the lungs after intravenous administration. Overall, intravenous administration of 12 μm PLGA microspheres is suitable for passive lung targeting and is promising for pulmonary therapy.

Resumé

Infektioner, som skyldes bakterier i de nedre luftveje, er blandt de hyppigste dødsårsager på verdensplan. De mest almindelige behandlinger af denne type infektioner består af antibiotika administreret enten oralt eller intravenøst. Nuværende behandlinger af bakterielle infektioner i lungerne er ofte ikke tilstrækkeligt effektive grundet begrænset levering af lægemidlet dybt ned i lungerne, for lav koncentration af lægemiddelstoffet i infektionsområdet, udvikling af multiresistens hos bakterierne samt bivirkninger ved lægemidlet. Levering af antibiotika direkte til lungerne ved hjælp af mikrosfærer doseret som et injicerbart lægemiddel er et lovende alternativ til de traditionelle formuleringer af antibiotika, da det herved er muligt at opnå terapeutiske koncentrationer af antibiotika lokalt og samtidig minimere uønskede bivirkninger i andre dele af kroppen. Denne strategi har lovende potentiale især for patienter med normal lungeperfusion, men med nedsat lungefunktion eller patienter med kronisk obstruktion af luftvejene på grund af inflammation, infektion eller høj produktion af mucus.

Formålet med dette projekt var at undersøge polymer mikrosfærer til målrettet levering af antibiotika til blodkapillærer ved alveolerne i lungerne efter intravenøs administration med henblik på at øge virkningen af disse lægemidler mod bakterielle luftvejsinfektioner.

Bionedbrydelige poly(lactic-co-glycolic) acid (PLGA) mikrosfærer med levofloxacin blev fremstillet ved hjælp af en flow-fokuseret mikrofluid chip og karakteriseret for deres fysisk-kemiske egenskaber og deres virkning *in vitro* og *in vivo.* PLGA-mikrosfærerne udviste en homogen størrelsesfordeling med en gennemsnitlig diameter på ~12 µm og en variationskoefficient <5,2%. Levofloxacin blev frigivet langsomt fra mikrosfærerne på kontrolleret vis over fem dage, og den antibakterielle aktivitet var let reduceret overfor *Pseudomonas aeruginosa*, *Escherichia coli* og *Staphylococcus aureus* i forthold til det ikke indkapslede stof. Nedbrydning af mikrosfærerne blev evalueret og viste ændringer i deres indre struktur og overflademorfologi samt en hurtigere nedbrydningskinetik *in vivo* end *in vitro*. Mikrosfærerne udviste lav toksicitet for endotel- og alveolære epitelcellelinjer og forårsagede ikke lysering af røde blodlegemer. En undersøgelse af biodistribusions og farmakokinetik viste, at ^{111}Indium-mærkede mikrosfærer udviste en homogen distribution næsten udelukkende til lungerne efter intravenøs administration. Samlet set, er intravenøs administration af 12 µm PLGA mikrosfærer velegnet til passiv lungemålretning og er lovende for lungeterapi.

Lay Summary

Bacterial infections in the respiratory tract are currently one of the leading causes of mortality worldwide. Today´s treatments are often not sufficiently effective due to the difficulty of drugs reaching the infection deep in the lungs, the insufficient drug doses at the site of infection, the development of multi-drug resistance, and the side effects caused by some of the currently used and effective antibiotics.

The aim of this project was to investigate the use of polymeric microspheres as carriers for lung delivery of antibiotics after intravenous administration. The antibiotic-loaded microspheres were prepared and characterized with a wide range of methods and assays to gain a comprehensive understanding of their *in vitro* and *in vivo* performance.

The findings of this work showed that injectable drug-loaded microspheres are a promising alternative to the traditional therapies and are expected to improve the treatments of bacterial lung infections and, potentially, other lung diseases.

1 Setting the Scene

Lung infections, such as pneumonia, tuberculosis, bacterial infections associated with cystic fibrosis or non-cystic fibrosis bronchiectasis, are amongst the top ten causes of death worldwide [1,2]. Of the responsible pathogens that populate the respiratory tract (*e.g.,* viruses, bacteria, fungi), bacteria, such as *Pseudomonas aeruginosa, Staphylococcus aureus, Streptococcus pneumoniae*, have attracted special attention since they are responsible for most of the hospital-acquired infections and are associated with high morbidity and mortality [3,4]. The recommended treatment for bacterial infections includes oral or intravenous administration of antibiotics [5]. Only in the case of *P. aeruginosa* infections associated with cystic fibrosis, inhalable antibiotics are applied [6]. However, the success of the antibiotic treatment is dependent on the right amount of the drug reaching the target site and is further highly challenged currently by the increasing appearance of pathogens resistant to the traditional antibiotics. Specifically, in the case of systemic administration, distribution to non-infected sites occurs, thus the antibiotics do not always reach therapeutically active concentrations in the lungs and side effects in non-targeted organs may appear.

To overcome the challenges associated with the use of antibiotics, different approaches can be used, including drug delivery systems to selectively target the lungs. Several lipid- and polymer-based nano- and micro-particles are currently investigated to localize antibiotics to infection sites in the periphery of the lungs after inhalation [7]. Other aims include obtaining maximum targeting and thus therapeutic efficacy, while maintaining low drug levels at non-target sites. However, in patients with respiratory tract obstruction (*e.g.,* due to inflammation or mucus plugs) or compromised lung function (*e.g.,* due to bronchial narrowing), the delivery of antibiotics by inhalation is challenging and often not sufficiently effective to eliminate all the pathogens present in the lungs. In these cases, the deposition of inhaled drugs in the lung periphery is in fact limited and heterogeneous.

Therefore, targeted drug delivery to infected lungs tissue from the vascular side by using drug delivery systems is a promising approach that could be a valid alternative to conventional administration routes or a complementary therapy to inhaled antibiotics. After intravenous injection, drug delivery systems with diameters slightly larger than the diameter of lung capillaries (*i.e.,* 7.5 ± 2.3 µm for healthy adults [8,9], 6.6 ± 1.6 µm, and 7.5 ± 1.7 µm in rats and dogs, respectively [10]) will be trapped in the lung capillaries. While the matrix of the drug delivery system degrades, the encapsulated antibiotic is released and can freely diffuse into the alveolar space. Amongst the few formulations investigated, polymeric microspheres are of particular interest, specifically those composed of biodegradable and biocompatible polymers.

1.1 Hypothesis and Aims

The overall hypothesis leading to this project is that it is possible to design a suitable drug delivery system for lung targeting of antibiotics through embolization of pulmonary capillaries in the form of drug-loaded microspheres to improve the treatment of bacterial infections in the respiratory tract. In comparison to intravenously administered solutions of antibiotics, the use of particles will hypothetically result in higher drug concentration in the respiratory zone, *i.e.*, at the site of infection, thus lowering administered doses of antibiotic, and reducing risk of systemic toxicity. This drug delivery approach could therefore improve the treatment of low respiratory tract infections (*e.g.,* pneumonia) and/or complement inhaled therapy in patients with pulmonary disease with compromised lung function or respiratory tract obstruction (*e.g.,* cystic fibrosis).

To support the hypothesis, the specific aims in this project were:

Aim I: To develop monodisperse poly(lactic-co-glycolic acid) (PLGA) microspheres loaded with levofloxacin, with properties suitable for passive lung targeting and with sufficient antibacterial activity.

Aim II: To evaluate the pharmacokinetics and biodistribution of the radiolabeled PLGA microspheres to the lungs and other organs by single-photon emission computed tomography (SPECT/CT) imaging.

2 Background

2.1 The Respiratory System

The respiratory system is highly specialized and designed to enable gas exchange between the respiratory tract and the vasculature. Anatomically, it can be divided into upper and lower respiratory tract. The upper respiratory tract includes the nasal cavity, the pharynx and the larynx. The lower respiratory tract comprises the trachea, which bifurcates into the bronchi. The primary bronchi continue to branch into smaller bronchioles, which end with the alveolar sacs [11,12] (**Figure 1**). Functionally, the respiratory system can be divided into a conductive zone and a respiratory zone. The conductive zone is mainly responsible for carrying, filtering, humidifying and warming the incoming air. It includes larynx, trachea, bronchi, bronchioles, and terminal bronchioles. The respiratory zone consists of respiratory bronchioles, alveolar ducts, alveolar sacs, and is directly responsible for gas exchange [11,12] (**Figure 1**).

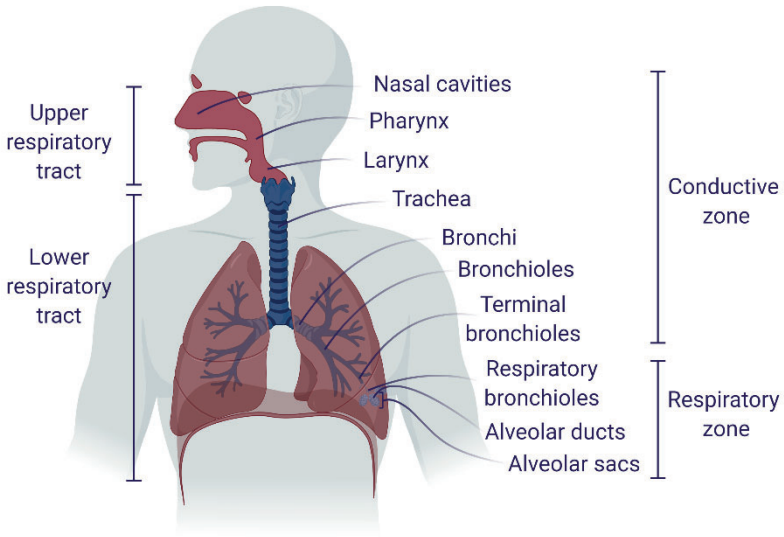

Figure 1. Anatomical and functional division of the respiratory system. Figure created with BioRender.com.

2.1.1 The Respiratory Zone

The key function of the respiratory system is gas exchange, which takes place in the alveoli. There, the respiratory tract and the pulmonary vasculature are in very close proximity over a large surface area allowing carbon dioxide waste to be removed from the blood and to be replaced by inhaled oxygen.

Structurally, the alveolar sacs are clusters of many individual alveoli, with each alveolus representing a functional unit of the respiratory tract. The alveolar wall consists of a thin monolayer of type I alveolar epithelial cells (also known as pneumocytes), interspersed with few type II pneumocytes (**Figure 2**) [9,12–16]. Type I pneumocytes are directly involved in gas exchange, while type II pneumocytes synthesize and secrete phospholipids and proteins, which constitute the alveolar lining fluid. This alveolar lining fluid is a thin (from 0.2 µm on flat alveolar walls to 0.9 µm in the alveolar corners [17,18]) continuous liquid layer that covers the apical surface of the epithelium (**Figure 2**), prevents alveolar collapse during breathing by decreasing the surface tension, and contains alveolar macrophages and various complement proteins and antimicrobial proteins, such as defensins [13,15,16].

The alveoli have an epithelial surface area of ~140 m^2 in humans and ~125 cm^2 in mice, ~ 90% of which is occupied by pulmonary capillaries organized in a dense network [9,19]. The pulmonary capillaries originate from branches of the pulmonary arteries (also called axial arteries), that run along the side of the bronchi, and from supernumerary arteries, that branch out of axial arteries and enter the lung parenchyma [19,20]. The pulmonary capillaries subsequently merge into pulmonary veins, which drain into the left atrium (**Figure 2**). Structurally, the lung capillaries have an average diameter of 5-8 µm (7.5 ± 2.3 µm for healthy adults [8,9], 6.6 ± 1.6 µm, and 7.5 ± 1.7 µm in rats and dogs, respectively [10]) and have the basal side of the epithelium surrounded by a thin endothelial cell monolayer (**Figure 2**).

Taken together, the alveolar epithelium, the monolayer of endothelial cells, and the very thin interstitial compartment inbetween form the alveolar-capillary barrier [19] (**Figure 2**), which is ~300 nm thick in mice, ~400 nm in rats, ~500 µm in dogs, and ~600 nm in humans [21]. This thin barrier provides the structural basis for exchange of gas, ions and small molecules by simple diffusion.

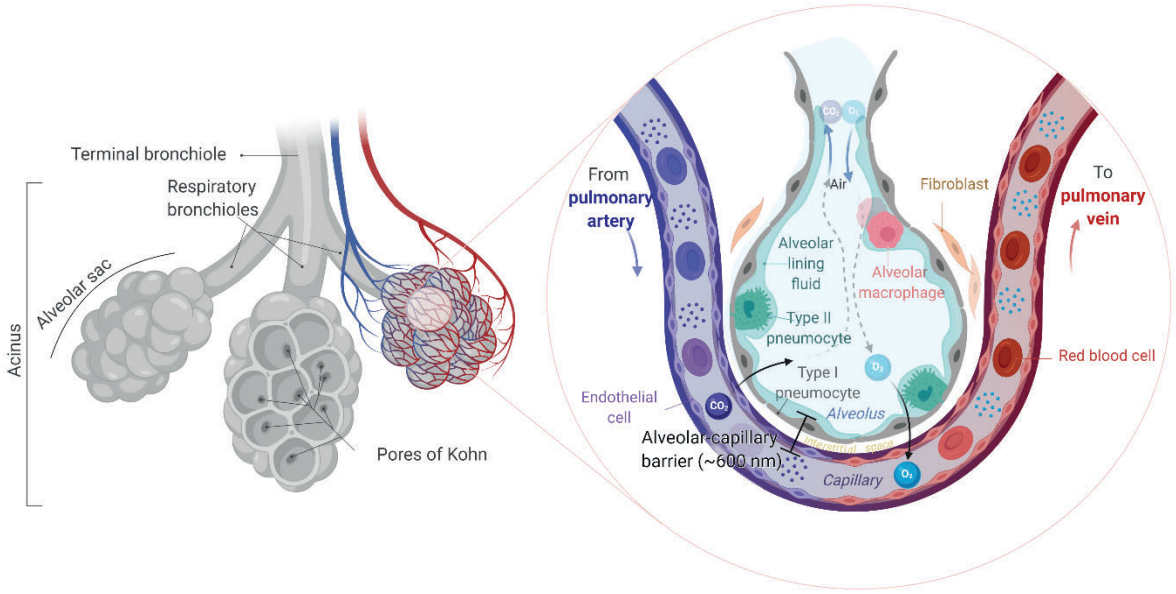

Figure 2. The respiratory zone and the structures responsible for in the gas exchange. Figure created with BioRender.com.

2.1.2 Protective Mechanisms of the Respiratory System

The respiratory tract has developed protective mechanisms against microorganisms, particulate materials, and toxic gases to which it is exposed with the inhaled air.

In the conductive zone, the oropharyngeal area entraps particles larger than 10 µm. Further down the respiratory tract, an important anatomical barrier is represented by the geometry of the respiratory tract, which bifurcates ~16 times and gradually narrow down in diameter before reaching the alveoli. This tree-like structure facilitates the deposition of particles of ~5-10 µm by impaction in the conductive zone, which can then be removed either by absorption into the systemic circulation or by the mucociliary clearance [22,23]. Insoluble particles are removed by the mucociliary escalator that consists of mucus and cilia that are present on the apical surface of the epithelial cells. The epithelium of the respiratory tract is in fact ciliated from the trachea to the terminal bronchioles and is covered by the epithelial lining fluid (**Figure 3**) [14,24,25]. This protective layer is composed of two sublayers: a low-viscosity fluid layer (known as periciliar layer) and a more viscous mucus layer on top [24]. The periciliar layer is ~7 µm thick throughout all the conductive respiratory tract [14], while the mucus layer varies in thickness depending on the localization: from 10-30 µm to 70 µm in the trachea, and 2-5 µm in the bronchioles [14,18,24,26,27] (**Figure 3**). The mucus layer is produced by secretory cells in the epithelium (*i.e.,* goblet cells and Clara cells) and serous cells of the submucosal glands (**Figure 3**) [14]. The mucus traps the inhaled substances and the upward cilia movements carry them out of the lungs before being expelled by coughing or being swallowed and eliminated by the gastrointestinal tract [12,23,28].

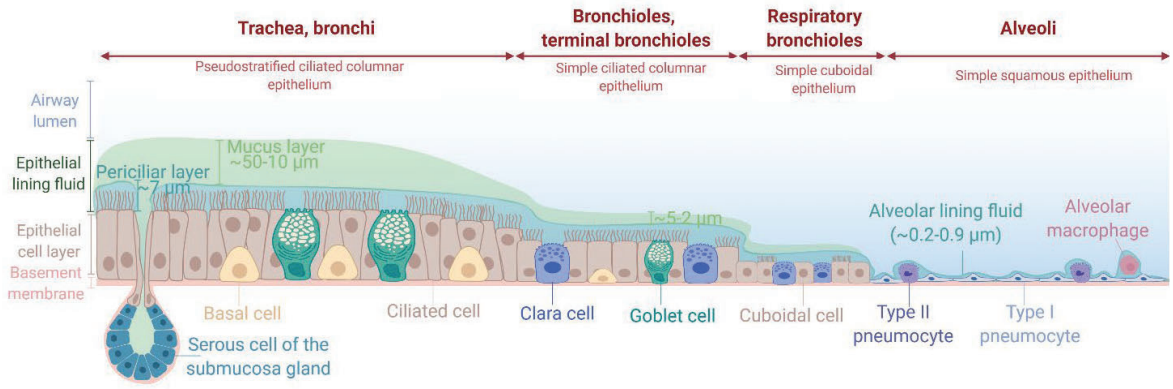

Figure 3. The mucosa and the epithelium with the structures contributing to the protection of the respiratory tract. Figure created with BioRender.com with inspiration from [29] with permission.

In the respiratory zone, the protection is provided by the alveolar macrophages (12-14 per alveolus in healthy non-smokers [30]), which phagocytose small (< 5 µm) insoluble particles and pathogens deposited in the alveoli [12,23,28]. Macrophages can also initiate an inflammatory response by secreting inflammatory factors and recruiting neutrophils.

In contrast to particulate matter, solubilized molecules may be absorbed from both the conductive and respiratory zone into the systemic circulation or the lymphatic system through the epithelium by passive diffusion or by active transport mechanisms [12,22,23,28]. The rate and mechanism of absorption depends on the physico-chemical properties of the molecule in relation to the absorption site.

2.2 Bacterial Infections in the Respiratory Zone

The defense mechanisms that protect the respiratory tract can fail, *e.g.,* as a consequence of diseases, of a large invasion of pathogens, of a highly virulent microorganism, or of medical treatments that damage the tissue and/or the immune system. A failure results in respiratory diseases, which can be classified based on the anatomical division of the respiratory system or based on the etiology. In the first case diseases are described as being related to the upper respiratory tract (*e.g.,* acute and chronic infections, nasopharyngeal carcinoma, laryngeal tumors) and of the lower respiratory tract, such as the bronchi (*e.g.,* bronchitis, bronchiectasis), the smaller bronchi and bronchioles (*e.g.,* bronchiolitis), the alveolar ducts and alveoli (*e.g.,* pneumonia) [31]. The etiologic classification distinguishes viral infections (*e.g.,* viral pneumonia, influenza), bacterial infections (*e.g.,* bacterial pneumonia, tuberculosis), allergic diseases (*e.g.,* asthma, hay fever), acute diseases of the bronchi (*e.g.,* bronchitis, bronchiolitis, bronchiectasis), airflow obstruction diseases or chronic obstructive pulmonary disease (COPD, *e.g.,* chronic bronchitis, pulmonary emphysema), and lung cancer [31].

Of the pulmonary diseases (**Table 1**), the lower respiratory tract infections are one of the major clinical challenges, as they represent among the primary causes of mortality worldwide for all ages and the leading cause of death among children under 5 years of age [1,2]. Many lung infections are frequently acute self-limiting viral infections and not lethal unless a secondary bacterial infection develops. These co-infections frequently worsen the clinical outcome and increase the severity of the infection [32]. In a hospital setting, respiratory bacterial infections are more numerous than viral infections and are usually associated to significant morbidity and mortality in sick patients [33].

These bacterial infections are located in the respiratory or conductive zones. In the respiratory zone, the bacteria are either in the lung parenchyma (*e.g.,* in pneumonia) [34] or in the alveolar macrophages (*e.g.,* in tuberculosis) [35,36]. In both cases, their proximity to the thin alveolar barrier makes the two conditions dangerous since the pathogens may cross the barrier and distribute systemically. Bacterial infections (*e.g.,* caused by *Pseudomonas* spp) can also localize in some structures of the conductive zone (*e.g.,* bronchi, bronchioles), and co-occur with or be a consequence of chronic lung disorders with impaired respiratory tract clearance (*e.g.,* cystic fibrosis, bronchiectasis, COPD) or immune compromising conditions (*e.g.,* human immunodeficiency virus, diabetes mellitus). Regarding cystic fibrosis, for

example, the genetic mutation of the cystic fibrosis transmembrane conductance regulator gene results in deficiencies in the pulmonary physiology, including alteration of the osmolarity of the respiratory tract surface liquid layer and hypersecretion of thick mucus that cannot be cleared sufficiently by the mucociliary escalator [37]. Overall, this environment together with inflammation responses promotes the development of recurring viral and chronic bacterial infections that are difficult to eradicate and can lead to host tissue damage, respiratory failure, or, eventually, death [37]. The major responsible bacteria of these secondary infections in cystic fibrosis are *S. aureus, P. aeruginosa*, *Haemophilius influenza, Achromobacter xylosoxidans* and *Burkholderi cepacia* complex. They are particularly dangerous, especially if resistant to antibiotics (*e.g.,* multidrug-resistant *P. aeruginosa*, methicillin-resistant *S. aureus* (MRSA)) and if able to switch to a biofilm mode of growth (*i.e.,* mucoid phenotype) [6,38]. The mucoid phenotype populates not only the conductive zone, but also the respiratory zone [6].

Table 1. Main pulmonary diseases [31,39].

	Disease	Anatomic site	Major pathologic changes	Etiology	
Infections	Acute infections	Larynx, trachea	Laryngitis, inflammation of the trachea	Viruses (rhinovirus, adenovirus, RSV, influenza virus)	
	Pneumonia	Alveolar sacs	Alveoli filled with inflammatory exudate	CAP	Bacteria (*S. pneumoniae*, *H. influenzae*, *M. pneumoniae* - less frequently *S. aureus*, *P. aeruginosa*), viruses (RSV, parainfluenza virus (children), influenza A and B (adults))
				HAP	*Enterobacteriaceae* (*Klebsiella* spp., *E. coli*), *Pseudomonas* spp., *S. aureus* (usually MRSA)
	Tuberculosis	Alveoli (alveolar macrophages)	Caseous granulomas and cavitation, as consequences of lung tissue hypersensitivity to tubercular antigens and lung tissue destruction	*M. tuberculosis, Mycobacterium avium complex*	
COPD	Chronic bronchitis/ bronchiolitis	Bronchi/ bronchioles	Hypertrophy and hyperplasia of the mucus glands, mucus hypersecretion	Tobacco smoke, air pollutants (*e.g.,* sulfur dioxide, nitrogen dioxide), viruses (*e.g.,* RSV), and less frequently bacteria (*e.g., M. pneumoniae*).	
	Bronchiectasis	Bronchi	Destruction of smooth muscle and the supporting elastic tissue, permanent dilation of bronchi and bronchioles.	Secondary to persistent or severe infections	
	Emphysema	Acini	Enlargement of the air spaces distal to the terminal bronchioles, destruction of the alveolar walls	Tobacco smoke, α1-anti-trypsin deficiency	

Allergies	Asthma	Bronchi	Smooth muscle hypertrophy and hyperplasia, excessive mucus, inflammation	Outdoor allergens (*e.g.,* pollens from grass, trees, weeds), undefined causes
	Hay fever	Nose	Edema of the nasal mucosa	Outdoor allergens (*e.g.,* pollens from grass, trees, weeds), indoor allergens (*e.g.,* pet hair, dust mites, mold)
Vascular diseases	Pulmonary embolism	Pulmonary arteries	Occlusion of the pulmonary arteries	Blood clot (thrombus) that usually arise by the large deep veins of the legs (condition known as deep vein thrombosis), clump of material (*e.g.,* fat from the bone marrow, air bubbles)
	Pulmonary hypertension	Pulmonary vasculature	Increase in pulmonary vascular resistance, pressures at rest ≥ 25 mm Hg	Diseases that cause decrease in the cross-section of the pulmonary vascular bed or increase of pulmonary vascular blood flow (*e.g.,* COPD, interstitial lung disease, mitral stenosis, systemic sclerosis)
Cancers	Adenocarcinoma	Small airway epithelial and type II pneumocytes	Transformation of benign cells in neoplastic cells, in some cases metastasis (*e.g.,* small-cell lung carcinoma) or intrathoracic spread (*e.g.,* squamous cell carcinoma)	Tobacco smoke - less frequently: environmental exposure (*e.g.,* asbestos, tar, soot), genetic polymosphisms of P-450 (*e.g.*, CYP1A1)
	Squamous cell carcinoma	Bronchi		
	Large cell carcinoma	Bronchi		
	Small cell carcinoma	Small airway epithelial and type II pneumocytes		

COPD: Chronic obstructive pulmonary diseases, RSV: respiratory syncytial virus, CAP: community-acquired pneumonia, HAP: hospital-acquired (nosocomial) pneumonia, MRSA: Methicillin-resistant *Staphylococcus aureus.*

2.2.1 Treatment of Bacteria Lung Infections

Treating the bacterial infections is important to reduce the mortality of respiratory tract infections, and it is currently done with antibiotics. Antibiotics are molecules that *via* one or more targets on the bacteria cause inhibition of growth (if bacteriostatic) or preferably cell death (if bactericidal). Antibiotics target the cellular membrane (*e.g.,* β-lactams, glycopeptides), intracellular components that are essential for the synthesis of protein (*e.g.,* macrolides, amphenicols, tetracycline, aminoglycosides) or nucleic acids (*e.g.,* quinolones), or metabolic pathways (*e.g.,* sulfonamides) (**Figure 4**) [40–42].

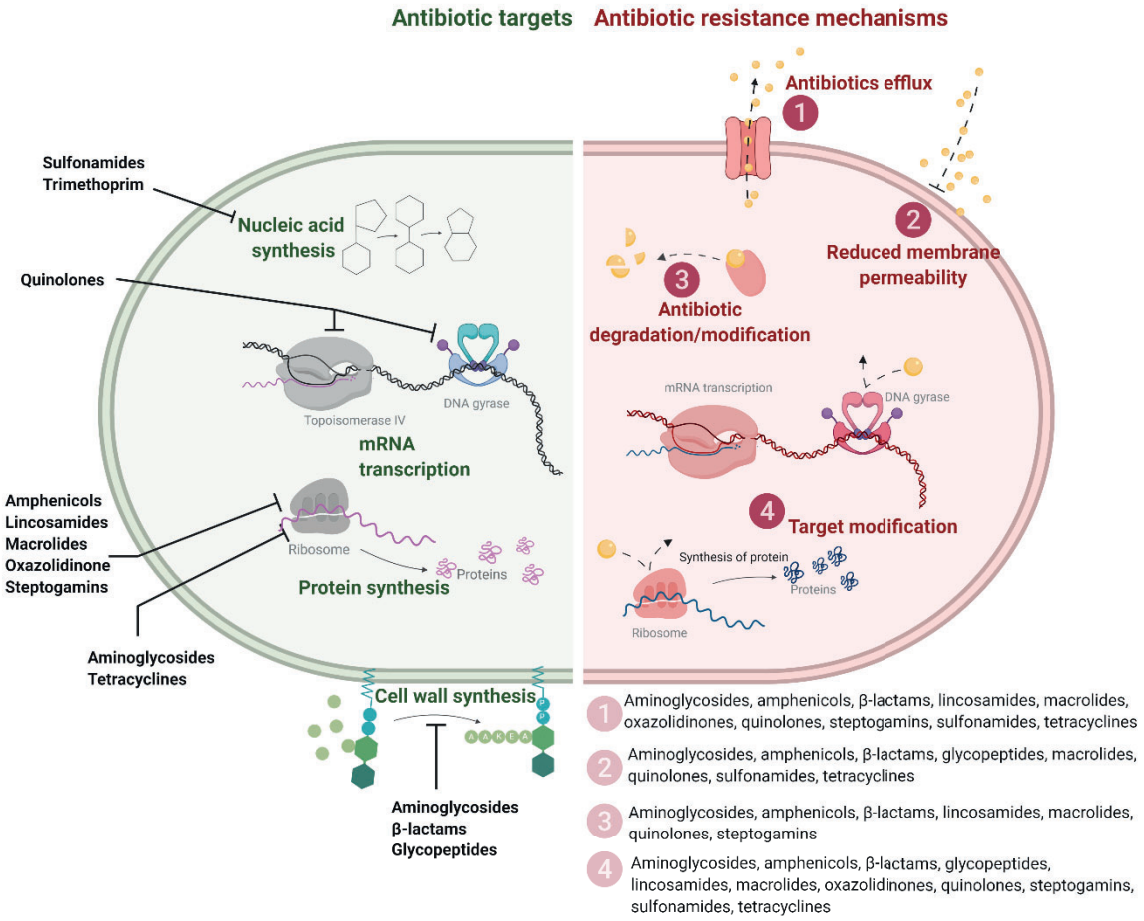

Figure 4. Antibiotics targets and resistance mechanisms in bacteria cell. Figure created with BioRender.com with inspiration from [43] with permission.

For treatment of bacterial respiratory infections, different classes of antibiotics are used alone or in combination. The selection of the treatment regimen is based on several factors, including the severity of the disease (*e.g.,* localization in the respiratory tract, presence of biofilm, re-occurring infection), whether treatment will be done in the community or hospital setting, patient-specific factors (*e.g.,* age, antibiotic allergies), the local epidemiology (*e.g.,* national/local antimicrobial resistance), and the presence of risk factors for infection with drug-resistant organisms.

In general, the guidelines from the European Society of Clinical Microbiology and Infectious Diseases and the European Respiratory Society recommend treatments by oral or intravenous administration of antibiotics, depending on the severity of the disease. Amoxicillin and tetracyclines are first-choice antibiotics, while newer macrolides (*e.g.,* azithromycin, clarithromicin) and some fluoroquinolones (*e.g.,* levofloxacin, moxifloxacin) are good alternatives when clinically relevant bacterial resistance against all first-choice agents is observed. In case of pseudomonal infections, co-administration of antipseudomonal fluoroquinolones (*e.g.,* levofloxacin, ciprofloxacin) with an antipseudomonal β-lactam antibiotic (*e.g.,* aztreonam, cefepime, ceftazidime, imipenem, meropenem) is recommended [5] (**Table 2**).

The treatment of infections with cystic fibrosis, particularly by *P. aeruginosa*, includes systemic and inhaled antibiotics (*i.e.,* tobramycin, levofloxacin, aztreonam, colistin [6,38,44,45]), either alone or combined, in order to reach high concentrations both in the lung lining fluid in the conductive zone (*via* inhalation) and in the respiratory zone (*via* oral or intravenous administration) [6].

Table 2. Antibiotic treatments for bacterial infections in the lower respiratory tract, according to European and American guidelines.

LRTI type	Severity/sub-group	Treatment	
		Preferred	**Alternative ***
Community setting			
LRTI [5,46]	All	Oral amoxicillin + doxycycline	Oral co-amoxiclav, clarithromycin/azithromycin, levofloxacin/moxifloxacin
Hospital setting			
Pneumonia [5,46–48]	Moderate/severe	Oral co-amoxiclav + azithromycin/clarithromycin	Oral levofloxacin, moxifloxacin
	+ risk factors for *P. aeruginosa*	IV meropenem/imipenem/cefepime + ciprofloxacin/levofloxacin	
	+ risk factors for MRSA	Oral or IV vancomycin/linezolid + levofloxacin/moxifloxacin	
Infections in bronchiectasis [5,49,50]	No risk factors for *P. aeruginosa*	Oral co-amoxiclav, levofloxacin, moxifloxacin	
	+ risk factors for *P. aeruginosa*	Oral ciprofloxacin, IV beta-lactam+aminoglycoside, inhaled colistin/tobramycin/gentamicin	
Infections (primarily *P. aeruginosa*) in cystic fibrosis [51–54]	Moderate/severe	Inhaled tobramycin/aztreonam/colistin ± oral ciprofloxacin	IV amikacin/ceftazidime/tobramycin/colistin/meropenem
COPD [5]	Mild	Oral amoxicillin, doxycycline	Oral co-amoxiclav, clarithromycin, azithromycin, levofloxacin, moxifloxacin
	Moderate/severe	Oral co-amoxiclav	Oral levofloxacin, moxifloxacin
	+ risk factors for *P. aeruginosa*	Oral ciprofloxacin	
Tuberculosis [55,56]	Severe	Oral or IV rifampin + oral pyrazinamide + oral, IV or IM isoniazid + oral ethambutol	Oral or IV levofloxacin/moxifloxacin/gatifloxacin + IV or IM amikacin/capreomycin + 2 amongst ethionamide/oral cycloserine/linezolid/clofazimine ± bedaquiline/imipenem/meropenem

COPD: chronic obstructive pulmonary disease, IV: intravenous, LRTIs: lower respiratory tract infections, MRSA: methicillin-resistant *Staphylococcus aureus*.
*In case of hypersensitivity to preferred drugs or national/local prevalence of clinically relevant resistance

2.2.2 Challenges with Antibiotic Treatments

Today´s treatments of bacterial infections, including pulmonary infections, are often not sufficiently effective. The above mentioned treatments are all mainly based on intravenous or oral administration of antibiotics dissolved in aqueous medium or formulated in oral dosage forms (*e.g.,* capsules, tablets), respectively. Even though these routes of administration are characterized by high systemic bioavailability, this does not ensure high enough concentrations of the antibiotic at the actual target site as required to efficiently treat the infections [33,44].

If the antibiotic concentration is not sufficient to kill the bacteria at the site(s) of infection, the pathogens may instead be able to develop mechanisms to resist the effect of the specific antibiotic. These mechanisms include: *(i)* antibiotic efflux (*e.g.,* expression of efflux pumps, such as the ATP-binding cassette transporters or the major facilitator superfamily transporters that transport tetracyclines, glycopeptides, and macrolides out of cells), *(ii)* inhibition of drug entry in the cell (*e.g.,* decrease in the expression of outer membrane porins of Gram-negative bacteria that usually facilitate the entry of hydrophilic antibiotics such as some β-lactams), *(iii)* production of enzymes that degrade and inactivate antibiotics (*e.g.,* β-lactamases that hydrolyse the β-lactam ring of β-lactams, aminoglycoside modifying enzymes that acetylate, phosphorylate or adenylate aminoglycosides) and *(iv)* modification of the target site (*e.g.,* mutations of penicillin-binding proteins that are responsible for bacterial cell wall synthesis and are usually bound and inactivated by β-lactams, production of modified peptidoglycan precursor with lower affinity for glycopeptides, rRNA methylation at sites that usually bind macrolides, lincosamides, streptogamins and aminoglycosides) (**Figure 4**) [41–43,57,58]. These genetic resistance modifications can also be transferred from a resistant to a susceptible bacterium, resulting in the distribution between genera and species [57,58]. As a consequence, many pathogens responsible for serious diseases have become resistant to various classes of antibiotics, and some evolving into multidrug-resistant (MDR), extensively drug-resistant (XDR), or even pandrug-resistant (PDR) types, in which cases they are resistant to more than one, almost all, or all approved antibiotics, respectively [59].

Clinically, high doses (250-750 mg) of antibiotics are administered orally or intravenously to obtain the local drug concentrations to effectively treat the infection. As a consequence of the systemic levels of antibiotics, part of the dose may reach non-infected tissues, alter the growth of harmless and useful organisms (*e.g.,* bacteria in the intestine) [33,44], and/or be responsible for toxicity at not-targeted site(s) [33,44]. For example, prolonged administration of high doses of the aminoglycoside tobramycin can cause acute and chronic nephrotoxicity, by decreasing glomerular filtration rate and altering excretion of electrolytes [60,61].

Overall, this leads to inefficiency of existing approaches to treat infection. Antimicrobial resistance has now become a global public health concern and has directed the focus of many organizations, such as the Centers for Disease Control and Prevention (CDC) and the

World Health Organization (WHO), to identify the bacteria responsible for serious infections and prone to develop resistance, in order to focus the attention and develop strategies to treat these pathogens. These bacteria are classified as urgent, serious and concerning threats by the CDC [62] and, similarly, as pathogens with critical, high, medium priority by the WHO [63]. Urgent threats include carbapenem-resistant *Acinetobacter, c*arbapenem-resistant *Enterobacteriaceae*, and *Clostridioides difficile.* Serious threats include extended-spectrum beta-lactamase-producing *Enterobacteriaceae*, MDR *P. aeruginosa,* MRSA, drug-resistant *S. pneumoniae,* MDR and XDR Mycobacterium *tuberculosis*, vancomycin-resistant *Enterococci* [62].

2.2.3 New Strategies to Treat Bacterial Infections

The challenges and obstacles that are associated with antibiotic treatments have directed the attention to new strategies to treat bacterial infections in the future, such as the discovery of new classes of antibiotics, and the improvement of the therapeutic effect of existing compounds [33,44].

Discovery and development of new compounds that are potent and effective especially against MDR bacteria is expected to likely be one of the best options to fight infections worldwide, according to the Global Action Plan against antimicrobial resistance proposed by WHO in 2015 [64]. Since 2000, 29 new antibiotic drugs (including three multidrug combinations) have been approved by United States Food and Drug Administration (US FDA) and European Medicines Agency (EMA) [65] (**Table 3**) and 42 are currently in clinical trials or under regulatory evaluation for treating bacterial infections (as of September 2019) [66]. Unfortunately, even though the total number of antibiotics has increased, the majority are analogues of currently marketed drugs and have shown to be susceptible to similar mechanisms of resistance, already seen for the known classes of antibiotics. Moreover, of the antibiotics currently in the development pipeline only 11 have the potential activity to act against at least one of the pathogens that are resistant to carbapenems classified as urgent threats according to the CDC [67]. Only ~ one in five drugs in the pipeline has an innovative component, such as being a novel class (new scaffold, new pharmacophore) and/or hitting a novel target (new binding site, and, therefore, novel mechanism of action).

Table 3. Antibiotics and combinations US FDA (https://www.accessdata.fda.gov/scripts/cder/daf/) and EMA (https://www.ema.europa.eu/en/medicines) approved from 2000 to 2019. Adapted from [65,66,68–70] with permission.

Year approved	Drug name	Drug class	Route of administration	Indication(s)	Innovation?*
2019	Pretomanid	Nitroimidazole	Oral	MDR- and XDR-TB	-
2018	Omadacycline	Tetracycline	IV, oral	CABP, ABSSSI	-
2018	Eravacycline	Tetracycline	IV	cUTI	✓
2018	Plazomicin	Aminoglycoside	IV	cUTI	-
2017	Meropenem+ vaborbactam	β-lactam + (cyclic boronate) β-lactamase inhibitor	IV	cUTI	✓
2017	Delafloxacin	Fluoroquinolone	IV, oral	ABSSSI	-
2015	Ozenoxacin	Quinolone	Cutaneous	Impetigo	-
2015	Ceftazidime + avibactam	β-lactam + diazabicyclooctane β-lactamase inhibitor	IV	cIAI, cUTI, HABP, VABP	✓
2014	Finafloxacin	Fluoroquinolone	Otic	AOE	-
2014	Nemonoxacin	Quinolone	IV	CABP	-
2014	Ceftolozane+tazobactam	β-lactam + β-lactamase inhibitor	IV	cUTI, cIAI	-
2014	Tedizolid phosphate	Oxazolidinone	IV, oral	ABSSSI	-
2014	Oritavancin	Glycopeptide	IV	ABSSSI	-
2014	Dalbavancin	Glycopeptide	IV	ABSSSI	-
2014	Delamanid	Nitroimidazole	Oral	MDR-TB	-
2012	Bedaquiline	Diarylquinoline	Oral	MDR-TB	✓
2012	Fidaxomicin	Tiacumicin	Oral	*C. difficile*-associated diarrhea	✓
2010	Ceftaroline fosamil	Cephalosporin	IV	ABSSSI, CABP	-
2009	Besifloxacin	Fluoroquinolone	Ophthalmic	Bacterial conjunctivitis	-
2009	Telavancin	Glycopeptide	IV	cSSSI	-

2007	Garenoxacin #	Quinolone	IV, oral	CABP, cSSSI, cIAI, acute pelvic infections	-
2007	Retapamulin	Pleuromutilin	Cutaneous	Impetigo	✓
2005	Tigecycline	Tetracycline	IV	cSSSI, cIAI, CABP	-
2005	Doripenem	Carbapenem	IV	cIAI, cUTI	-
2004	Gemifloxacin	Fluoroquinolone	Oral	CABP, AECB	-
2003	Daptomycin	Lipopeptide	IV	cSSSSI, *S. aureus* bloodstream infections	✓
2002	Ertapenem	Carbapenem	IV, IM	cIAI, cSSSI, CABP, cUTI, acute pelvic infections	-
2001	Telithromycin	Macrolide	Oral	CABP	-
2000	Linezolid	Oxazolidinone	IV, oral	VRE infections, CABP, HABP, VABP, cSSSI, uSSSI	-

ABSSSI: acute bacterial skin and skin structure infections, AECB: acute bacterial exacerbation of chronic bronchitis, AOE: acute otitis externa, CABP: community-acquired bacterial pneumonia, HABP: hospital-acquired bacterial pneumonia, cSSSI: complicated skin and skin structure infections, cUTI: complicated urinary tract infections, cAIA: complicated intra-abdominal infections, IV: intravenous, IM: intramuscular, MDR- and XDR-TB: multi-drug resistant and extensively drug-resistant tuberculosis, uSSSI: uncomplicated skin and skin structure infections, VABP: ventilation-acquired bacterial pneumonia, VRE: vancomycin-resistant *Enterococci*.

* intended as being a novel class (new scaffold, new pharmacophore) and/or hitting a novel target (new binding site, novel mechanism of action).

withdrawn by EMA and US FDA.

Among the compounds in the clinical development with a certain degree of novelty (**Table 4**), antimicrobial peptides (AMPs) are promising alternatives to traditional antibiotics. They have different mechanisms of action (*e.g.,* disruption of the cell membrane, immunomodulation, intracellular penetration and damage to intracellular biomolecules [71]) and often a broad spectrum of antimicrobial activity, not only against bacteria, but also against viruses, fungi and parasites [72,73]. For bacterial infections, they have been studied as monotherapies, giving their effective bacterial growth killing [72,74–77], but also as adjuvants to traditional antibiotics to provide a synergistic effect [72,74,76]. To date, only one (*i.e.,* daptomycin) AMP has been approved clinically as antibiotic for monotherapy [73].

The antibiotics currently used in the clinic have different mechanisms of action against vital processes or structures of the bacteria. However, as mentioned above, their action against a single target frequently causes the development of resistance in bacteria. Using them in combination therapy instead would result in hitting different targets at the same time, and overcome the antibiotic tolerance that often result in therapeutic failure [78]. Not only the combination of antibiotics from different classes (*e.g.,* colistin and tigecycline, rifampin, meropenem[79]*)* or antibiotics and inhibitors (*e.g.,* amoxicillin and clavulanate) has already showed synergistic effect, but also their combination with new classes of anti-infectives (*e.g.,* AMPs, quorum sensing inhibitors) [44,76]. For example, the synergistic effect of antibiotics and AMPs has recently shown to be effective against infections caused by critical and high-priority pathogens [80] (*e.g.,* azithromycin and LL-37 for MDR *P. aeruginosa* and MDR *Acinetobacter baumannii* [81], ampicillin and nisin for *Salmonella enterica* [82], chloramphenicol and brevinin-2 CE for MRSA [83], and ampicillin and cryprdin-2 for *S. enterica* [84]). Despite the promising results, currently there are not combinations of classes planned to be introduced in the market in the near future, a part from one (*i.e.,* imipenem/cilastatin + relebactam (MK-7655A))[66].

Another more recently applied strategy is interfering with the growth of bacteria through targeting the bacterial communication systems (*i.e.,* quorum sensing), used by the bacteria to communicate with each other, to develop biofilm, and to produce secondary metabolites and virulence factors [85,86]. Quorum sensing is mediated by species-specific and strain-specific signalling molecules, which are produced and released by the bacteria [85]. These are also known as autoinducers, such as acyl-homoserine lactones (used by *Pseudomonas* spp., *Acinobacter* spp.), fatty acids (used by *Xanthomonas* spp., *Burkholderia* spp.), ketones (used by *Legionella* spp.) or quinolones (used by *P. aeruginosa*) [85]. By interfering with the production, by scavenging or by degrading the autoinducers, quorum sensing inhibitors *(e.g.,* 5-fluorouracil, eugenol, farnesol), quorum quenching antibodies (*e.g.,* Fab RS2-1G9) and macromolecules (*e.g.,* α-cyclodextrin), or quorum quenching enzymes (*e.g.,* acylase Pvdq, lactonase AiiA), respectively, disrupt this molecular communication system making the bacteria more sensitive to antibiotics and decrease biofilms [85]. These molecules are promising anti-infective agents that could be used to complement antibiotic therapy, especially in the case of biofilm-related infections [85,86]. However, to date, no quorum sensing inhibitors have been applied clinically.

Table 4. Antibiotics containing a degree of innovation (novel class or novel target) currently in clinical development or under regulatory evaluation at the beginning of 2020. Adapted from [66,67] with permission.

Development phase	Drug name	Drug class	Mechanism of action (target)	Route of administration	Expected activity against pathogens	Potential indication(s)
NDA	Lefamulin	Pleuromutilin	Protein synthesis inhibitor (50S ribosomal subunit at the peptidyl transferase center)	IV, oral	*S. aureus*	ABSSSI, CABP, HABP, VABP
III	Murepavidin (POL-7080)	AMP mimetic	Interference with the biogenesis of lipopolysaccharide of the outer membrane (β-barrel protein LptD)	IV, inhalation	Carbapenem-resistant *P. aeruginosa* **	HABP, VABP, ABSSSI, bloodstream infection, cIAI
III	Ridinilazole (SMT 19969)	Bis-benzimidazole	Inhibition of cell division and reduction of toxin production (drug target unknown)	Oral	*C. difficile***	*C. difficile* infections
II	SQ-109	Diamine	Inhibition of cell wall synthesis (MmpL3 membrane transporter)	Oral	*M. tuberculosis*	TB
II	Telacebec (Q-203)	Imidazopyridine amide	Inhibition of ATP synthesis (qcrB subunit of the cytochrome bc1 complex)	Oral	*M. tuberculosis*	TB
II	Macozinone	Benzothiazinone	Inhibition of cell wall synthesis (flavoenzyme DprE1)	Oral	*M. tuberculosis*	TB
II	OPC-167832	Carbostyril	Inhibition of cell wall synthesis (flavoenzyme DprE1)	Oral	*M. tuberculosis*	TB
II	Gepotidacin (GSK-2140944)	Triazaacenaphthylene	Topoisomerase II inhibitor (novel A subunit site)	IV, oral	*S. aureus, N. gonorrhoeae, Enterobacteriaceae*	uUTI, cUTI, ABSSSI, urogenital gonorrhea, CABP

II	Zoliflodacin (ETX0914)	Spiropyrimidinetrione	Topoisomerase II inhibitor (novel site)	Oral	*S. aureus*, *N. gonorrhoeae*	Uncomplicated gonorrhea
II	Brilacidin (PMX-30063)	Defensin mimetic	Cell membrane	IV	*S. aureus*	ABSSSI
II	CG-400549	Benzyl pyridinone	FabI inhibitor	Oral	MRSA*	ABSSSI
II	MGB-BP-3	Distamycin	DNA minor groove binding	Oral	*C. difficile***	*C. difficile* infections
II	Afabicin (Debio-1450)	Benzofuran naphthyridine	FabI inhibitor	IV, oral	*S. aureus*	ABSSSI, bone or joint infections due to *S. aureus*
I	GSK-070 (GSK3036656)	Oxaborole	Inhibition of protein synthesis (Leucyl-tRNA synthetase)	Oral	*M. tuberculosis*	TB
I	TBA-7371	Azaindole	Inhibition of cell wall synthesis (flavoenzyme DprE1)	Oral	*M. tuberculosis*	TB
I	CRS3123	Diaryldiamine	Methionyl-tRNA synthetase	Oral	*E. faecium, S. aureus, C. difficile***	*C. difficile* infections

ABSSSI: acute bacterial skin and skin structure infections, AMP: antimicrobial peptide, CABP: community-acquired bacterial pneumonia, HABP: hospital-acquired bacterial pneumonia, cUTI: complicated urinary tract infections, cAIA: complicated intra-abdominal infections, IV: intravenous, LptD: lipopolysaccharide transport protein D, MRSA: methicillin-resistant *Staphylococcus aureus*, NDA: new drug application, TB: tuberculosis, uUTI: uncomplicated urinary tract infections, VABP: ventilation-acquired bacterial pneumonia.

**and* indicate the bacteria classified as urgent and serious threats, respectively, according to the Centers for Disease Control and Prevention (CDC) [62].

Another strategy currently under investigation is represented by damaging the bacterial membrane and/or by altering bacteria metabolic pathways (*e.g.,* the respiration system), as a consequence of intracellular oxidative stress [87–89]. Normally, in the bacterial cell the production and clearance of reactive oxygen species are in equilibrium, ensuring physiological conditions for survival. However, excessive oxidative stress can be induced by nanoparticles of various metals (*e.g.,* silver, zinc, copper, gold, titanium), resulting in inhibition of bacterial growth or death [87–89]. The research of this class of non-traditional antibiotics is still at the preclinical phase.

While new compounds, new combinations, and new targets are heavily investigated, another approach that can contribute to increasing the therapeutic efficacy of antibiotic treatments is to ensure optimized effect at the specific site of infection by *e.g.*, re-formulation of existing or new antibiotics into novel drug delivery systems, *e.g.,* nano- and micronsized particles. Re-formulation of existing and/or new antibiotics in more advanced drug delivery systems can increase the efficacy of the treatment [44,90] by selective delivery of the antibiotic to the infection site and exposure of the bacteria to a higher dose of the antibiotic, resulting in more effective and rapid bacteria killing, lowered risk of development antibacterial resistance, and decreased risk of systemic off-target effects [33]. In addition to site-specific delivery, drug delivery systems are also able to protect the drug from chemical and/or enzymatic degradation as well as from the interaction with other molecules, to locally release a sufficient dose of drug in a controlled manner, and to improve drug transport across biological barriers [33,44]; all contributing enhanced drug bioavailability. Thus, for efficient pulmonary delivery of antibiotics to treat lung infections it is important that the carrier of the drug delivery systems is biocompatible and biodegradable, so that toxicity from its accumulation is prevented and repeated dose administration is possible. High doses of antibiotics are usually required, thus, delivery systems with high drug loading capacity are preferred [44].

2.3 Lung Targeting

Several drug delivery systems have been developed and investigated to specifically target the lungs, and in particular the respiratory zone. Such drug delivery systems can target the lungs directly *via* inhalation or indirectly *via* intravenous administration.

2.3.1 Direct Lung Targeting *via* Inhalation

Compared to the traditional approaches with oral and intravenous administration, inhalation has some advantages, including being non-invasive and needle-free, avoiding 'first-pass' metabolism and antibiotic exposure to the gastrointestinal microflora [33], and, most importantly, being able to deliver relatively high drug doses directly to the target site, *e.g.* the infected lung tissue [91]. Thus, antibiotics encapsulated, entrapped, or adsorbed on the surface of drug delivery systems can be delivered directly to the pulmonary site of infection by inhalation. As shown in **Figure 5**, after inhalation the particulate drug delivery system enter the respiratory tract and deposit deep in the respiratory tree (*e.g.,* in the alveoli) with subsequent release of the active component(s).

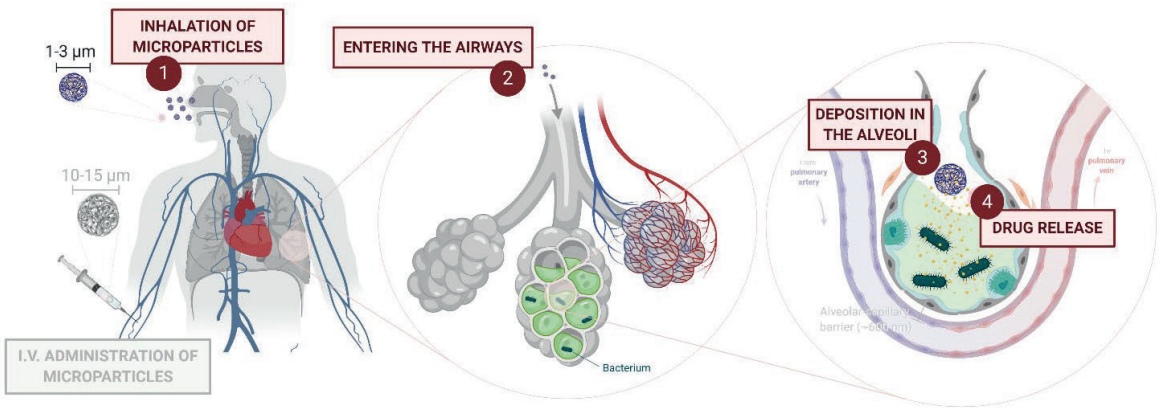

Figure 5. Lung targeting *via* inhalation of drug delivery systems. Figure created with BioRender.com

Antibiotic drug delivery to the lungs by inhalation, however, present some disadvantages, such as the possibility of systemic antibiotic absorption and the difficulty to control the antibiotic dose at the infection site [33,38]. Other challenges are related to the complexity of the pulmonary anatomy and physiology, and to the mechanisms of deposition of particulates. To be effective for the treatment of pulmonary infections, the inhaled drug delivery systems have to first reach the respiratory zone, then be able to avoid the macrophages, penetrate any bacterial biofilm, release the drug into the low volume of lung fluid so that it can exert its effect on the target bacteria [92]. Achieving this will depend on the

characteristics of the inhaled formulation (*e.g.,* mass median aerodynamic particle size, particle size distribution, surface and particle morphology, density, surface charge and hygroscopicity [12]), physico-chemical properties of the antibiotic, inhalant device, patient (*e.g.,* inspiratory flow velocity and flow regime, patient´s lung volume, respiratory tract geometry) and disease state [23,93,94]. For example, the particles or nebulised droplets carrying the antibiotic should have a particle size of 1-5 μm to be deposited deep in the lower respiratory tract and in the alveoli by gravitational sedimentation or by Brownian diffusion, respectively, without impacting in the larger airways or being exhaled [33]. Particles of a size below 500 nm may also deposit, although to a limited extent as they have a high risk of being exhaled resulting in reduced deposition [33]. If deposited in the respiratory tract and if they have a neutral surface charge, smaller nano-sized particulate carriers may, to some extent, permeate the mucus in the upper respiratory tract and any associated bacterial biofilm by diffusing through the network formed by its components (cut-off of 500 nm in healthy people, 300-100 nm in patients with cystic fibrosis) [45].

The formulations applied for pulmonary delivery are either liquid (solutions or suspensions) or dry powders, and require inhalation devices for administration, nebulizers or dry powder inhalers, respectively [95]. Many dry powders and nebulized suspensions of drug delivery systems are currently investigated at preclinical and clinical stages for local delivery of drug to treat different pulmonary diseases, including asthma, cystic fibrosis, COPD, lung infections, lung hypertension, and lung cancer [7]. Among these, there are micelles, liposomes, polymeric nanoparticles, microparticles and nano-embedded microparticles, as shown in **Table 5.**

To date, only one inhaled formulation of an antibiotic in drug delivery systems has been approved and has entered the market. It is a liposomal suspension of amikacin designed for nebulization, and approved by the US FDA for the treatment of *Mycobacterium avium complex* lung disease. Two other formulations are undergoing clinical trials. Ciprofloxacin, formulated in liposomes (Lipoquin) and in a mixture of non-encapsulated ciprofloxacin with ciprofloxacin-encapsulated liposomes (Pulmaquin), has been tested in phase III clinical trials for the treatment of non-cystic fibrosis bronchiectasis patients with chronic *P. aeruginosa* pulmonary infections. However, US FDA and EMA recently denied the market authorization [96]. A liposomal formulation of tobramycin (Tobramycin Fluidosomes™) received the orphan drug designation for use in respiratory tract infections associated to cystic fibrosis, and entered the clinical trials. Interestingly, all these formulations have been designed for *P. aeruginosa* treatment in cystic fibrosis.

This lack of success for inhaled nanomedicines with antibiotics compared to inhaled antibiotics that have been approved for the treatment of lung infections (*i.e.,* tobramycin (as solution for inhalation, TOBI®, Bramitob® [97] or dry powder, TOBI® Podhaler® [98]), levofloxacin (as solution for inhalation, Quinsair® [99]), aztreonam (as solution for inhalation, Cayston® [100]), and colistimethate sodium (as dry powder, ColoBeathe® [101]), is related to the higher complexity of these novel drug delivery systems for inhalation compared to the

current formulations. This means that efficient scale-up of production ensuring good manufacturing practice can be challenging and expensive. Other obstacles to develop such systems are associated with the unique lung microenvironment and its defence mechanisms and to the high doses usually required for anti-infective treatments, as mentioned above [33,44,102].

Table 5. Examples of lipid and polymeric inhaled formulations for the treatment of lung infections approved and under development.

Drug delivery system		Therapeutic indication	Status	Ref
Carrier	**Drug**			
Liposomes	Amikacin	Lung disease caused by *M. avium* complex	Approved, 2018 (ALIS/Arikayce®)	103,104
Liposomes	Tobramycin	Respiratory infections in CF	Phase II (2016) (Tobramycin Fluidosomes™)	105
Liposomes	Ciprofloxacin	Non-CF bronchiectasis	Phase III (2018), NDA denied (2019) [96] (Lipoquin®, Pulmaquin®)	91
Liposomes	Clarithromycin	*P. aeruginosa* infections in CF	Preclinical	106
PLA MP	Rifampicin	Pulmonary infections	Preclinical	107
PLGA MP	Curcumin	CF	Preclinical	108
PLGA MP	Levofloxacin	CF	Preclinical	109
PLGA MP	Rifampicin	TB	Preclinical	110
PLGA NP/MP	Tobramycin	CF	Preclinical	111
PLGA NP	Levofloxacin	*P. aeruginosa* biofilm infections	Preclinical	112
PLGA NP	Ciprofloxacin	CF	Preclinical	113
PLA MP	Rifampicin /isoniazid	TB	Preclinical	114
PLA MP	Rifampicin	TB	Preclinical	115
Chitosan	Rifampicin	TB	Preclinical	115
Chitosan-coated PLGA MP	Rifampicin	TB	Preclinical	115
Chitosan	Moxifloxacin	Respiratory infections	Preclinical	116
Chitosan	Levofloxacin	*P. aeruginosa* infections in CF	Preclinical	117

CF: cystic fibrosis, MP: microparticles, NDA: new drug application, NP: nanoparticles, PLA: poly(lactic acid), PLGA: poly(lactic-co-glycolic) acid, TB: tuberculosis.

2.3.2 Passive Lung Targeting *via* Intravenous Administration

An alternative approach to target the lungs is from the vasculature around the thin alveolar epithelium taking advantage of the mechanical filter properties of the lung capillaries. After intravenous administration, antibiotic-loaded particulate carrier systems are pumped through the heart into the pulmonary blood circulation. The restricted capillary diameter of the pulmonary capillary bed (*i.e.,* 7.5 ± 2.3 µm for healthy adults [8,9], 6.6 ± 1.6 µm and 7.5 ± 1.7 µm in rats and dogs, respectively [10]) (**Figure 6**) will lead to entrapment of particles with a slightly higher diameter in the capillaries surrounding the alveolar epithelium. This is known as passive lung targeting. As the matrix of the drug delivery system degrade, the antibiotic is released and can freely diffuse through the thin alveolar-capillary barrier into the alveolar space, and exert the bacteriostatic or bactericidal effect.

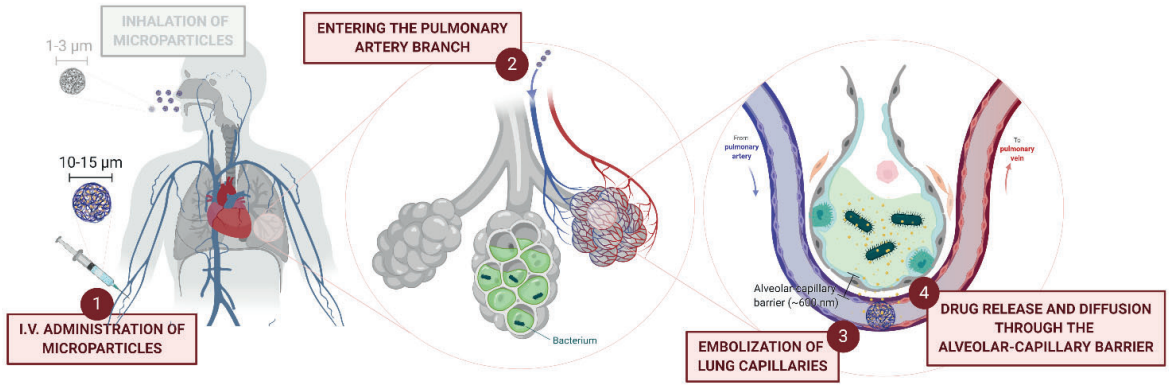

Figure 6. Lung targeting *via* intravenous administration of drug delivery systems.

The passive lung targeting is particularly interesting and a valid approach in case of seriously ill patients with compromised lung function or respiratory tract obstruction (*e.g.,* due to inflammation and mucus plugs), such as in patients with pneumonia or cystic fibrosis. Here, in fact, respiratory tract narrowing may result in compromised ventilation and inhomogeneous distribution of the inhaled drug delivery systems in the lungs, and thus in inefficient treatment [118–120]. Moreover, in these cases, lung perfusion is rarely compromised to a high degree compared to ventilation [121]. To date, the passive lung targeting strategy is approved and used only in a diagnostic nuclear medicine procedure to determine the lung perfusion in humans with ^{99m}Tc-labeled albumin macroaggregates, commercialized as Pulmolite® or DraxImage® albumin macroaggregates (Montreal, Canada).

This approach is naturally challenged by the safety concern of embolizing lung capillaries. However, this may be tailored as it is directly related to the particle size and distribution of the particulate delivery systems, the administered dose, the compatibility, and the carrier biodegradation. It is thus highly relevant that the particulate carrier system has a narrow size

distribution around an average value within the 10-15 μm range. In this way, only capillaries and not larger vessels (*e.g.,* arterioles with a diameter of ~20 μm [122]) are embolized, and, thus, the microvascular hemodynamics of the pulmonary circulation is maintained normal and an acute massive embolism as a consequence of vascular occlusion is avoided. The administered dose of the particulate carrier system should be low enough to only embolize a small percentage (< 1%) of the 280 billion capillaries in humans[122,123], so that the remaining non-embolized capillaries allow the lungs to continue to work normally. As with inhaled drug delivery systems, the passively targeted carrier has to be biocompatible as well as biodegradable, so that embolization is reversible, toxicity from carrier accumulation is prevented and repeated dosing is possible. As for other routes of administration it is important that the drug-related properties of the formulations should be tuned and selected according to their use. The properties (*e.g.,* solubility and hydrophobicity) of both the drug and the carrier are thus important. Further, the preparation method for the drug delivery system constitutes a key factor to develop high-content drug carriers. The carrier must release the loaded drug within the time range suitable for the specific application ensuring appropriate pharmacokinetics. In the case of pulmonary infections, it is optimal to have a sufficiently high and sustained drug release during a few (*i.e.*, three-six) days so that it is possible to fight the infection and at the same time minimize the dosing frequency. Finally, the drug has to be able to diffuse and permeate the alveolar-capillary barrier.

Due to the severity of many pulmonary diseases, *e.g.*, cancer and infections, and the demonstrated possibility of controlled embolization of alveolar capillaries, the design of drug-loaded particulate carrier systems to treat lung diseases after intravenous administration has attracted attention. Different biodegradable polymers (*e.g.,* PLGA, poly (lactic acid) (PLA), albumin, gelatin) have been recently tested as carrier systems for cisplatin [124], rifampicin [125], erythromycin [126], azithromycin [127], ofloxacin [128] and cefquinome [129] for the treatment of lung tumors and pulmonary infections (**Table 6**). Many of these previous works have tested *in vitro* performance as well as *in vivo* release and biodistribution of the loaded drugs. However, in the majority of the studies the drug did not accumulate exclusively in the lungs, but distributed to non-targeted organs, such as the liver, kidneys and spleen [126–129], which may be attributed to their large particle size distribution (range 3-50 μm) and/or to the non-optimal release profile. Up to now, the drug-loaded delivery systems have been investigated at the preclinical stage without testing the real-time kinetics or efficacy of the delivery system in terms of treatment of *in vivo* models.

Table 6. Examples of injectable diagnostic and therapeutic drug delivery systems for passive lung targeting approved or under development.

	Drug delivery system		Particle size and % lung targeting *	Status	Ref
	Carrier	Drug			
Diagnostic lung perfusion	Albumin macro-aggregates (MAA)	-	- 10-90 um (90%), all < 150 - MAA in lungs ~99.4% (10 min)	Approved (1976)	130
	Polystyrene MP	-	- 10-12 µm - MP in lungs 97.7% (1 h) ~95% (48 h)	Preclinical	131
	PLA MS	-	- 9.0 ± 0.4 µm, - MS in lungs 99.4% (15 min)	Preclinical	132
	PLGA-PEG MS	-	- 10-50 µm (~80%) - MS in lungs 25% (15 min)	Preclinical	133
	PLGA MS	-	- 10-50 µm (~93%) - MS in lungs 30% (15 min)	Preclinical	133
Respiratory infections	Albumin MS	Azithromycin (AZI)	- 3.9-19.8 µm - AZI in lungs ~70% (30 min), ~90% (12 h)	Preclinical	127
	PLGA MS	Cefquinome (CEQ)	- 5-50 µm - CEQ in lungs ~55% (15 min), ~90% (12 h)	Preclinical	134
	Gelatin MS	Cefquinome (CEQ)	- 5-30 µm - CEQ in lungs ~50% (15 min), ~90% (12 h)	Preclinical	129
	Albumin MS	Ofloxacin (OFX)	- 5-25 µm - OFX in lungs ~75% (10 min), ~90% @ 12 h	Preclinical	128
Cancer	PLGA MS	Cisplatin (CisPt)	- 5-30 µm - CisPt in lungs ~95% (15 min), ~95% @ 24 h	Preclinical	124
	Gelatin MS	Carboplatin (CPt)	- 5.0-28.6 µm - CPt in lungs 47% (15 min), 64% (12 h)	Preclinical	135
	Gelatin MS	5-fluorouracil (5FU)	- 5-15 µm - 5FU in lungs 60% (10 min), 85% (12 h)	Preclinical	136

MP: microparticles, MS: microspheres, PLA: poly (lactic acid), PLGA: poly (lactic-co-glycolic acid)
* % lung targeting intended as distribution of the carrier or the drug (released by the carrier) in the lungs compared to other organs at different times post injection (indicated in brackets).

3 Scientific Outcome

3.1 Research Manuscript

Title

Monosized Polymeric Microspheres for Passive Lung Targeting: Biodistribution and Pharmacokinetics after Intravenous Administration

(Appendix)

Aim

The aim of this study was to prepare and characterize biodegradable microspheres suitable for targeted delivery of antibiotics to the lungs after intravenous administration.

Outcome

PLGA microspheres encapsulating levofloxacin were prepared with a flow-focusing microfluidic chip. They optimized microspheres showed a suitable particle size and physico-chemical properties for passive lung targeting. The microspheres encapsulated levofloxacin and preserved its antibacterial activity against *P. aeruginosa, E.coli* and *S. aureus*. The PLGA microspheres degraded within three weeks *in vitro* and within one week *in vivo*, while slowly releasing ~85% of the encapsulated levofloxacin over five days. The PLGA microspheres showed low toxicity towards endothelial, alveolar epithelial and red blood cells. The microspheres were radiolabeled with the gamma emitter ^{111}Indium and intravenously administered in mice to assess their pharmacokinetics and tissue distribution. Immediately after tail vein injection, the ^{111}In-labeled PLGA microspheres distributed homogenously throughout the lungs, from where they cleared within one week.

Overall, monodisperse PLGA microspheres with a diameter of 12 µm demonstrated to be a promising targeted delivery system to transport and release antibiotics for the treatment of pulmonary infections.

4 Discussion

4.1 Levofloxacin-Loaded PLGA Microspheres as Drug Delivery Systems

Different drug delivery systems can be used to target the lungs. Among these, biodegradable polymeric micro- and nanoparticles are particularly interesting due to their controlled drug delivery properties. Of the biodegradable polymers (*e.g.,* polyesters, hyaluronan, chitosan), PLGA is one of the most characterized and widely used for the preparation of nano- and microparticles. PLGA is a copolymer of PLA and poly(glycolic acid) (PGA), and it degrades *in vivo* by hydrolysis producing the two non-toxic monomers (**Figure 7**), which are further metabolized and eliminated from the body though normal metabolic pathways (*i.e.,* tricarboxylic acid cycle) as water and carbon dioxide [137,138]. The PLGA polymer is biodegradable and biocompatible and US FDA and EMA approved for use in different drug delivery systems in humans and for a range of administration routes (including intravenous administration) to treat various diseases (*e.g.,* cancer, diabetes mellitus, bipolar disorders) [137,138]. Drug delivery systems composed of PLGA and approved by US FDA have been well summarized by Li *et al*.[139], Pandey *et al.* [140], and Zhong *et al.* [141]. Additionally, they have shown to encapsulate different classes of drugs *(e.g.,* small molecules, proteins, nucleic acids) with different solubilities (*i.e.,* hydrophilic, hydrophobic) [138,142], and release them in a controlled manner. Particles composed of PLGA can also be easily surface-functionalized or modified (*e.g.,* with polyethylene glycol (PEG) to increase their blood circulation half-life) [137,138]. Moreover PLGA's degradation and release kinetics can be tuned according to the application by choosing one of the commercially available PLGAs with specific copolymer composition (*i.e.,* PLA:PGA molar ratio), molecular weight and end group [137,138,143].

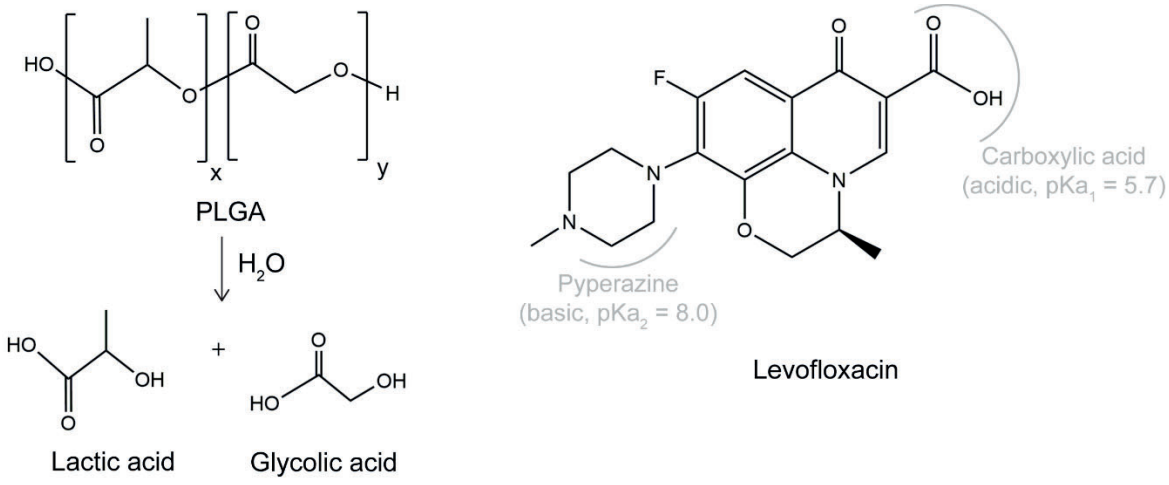

Figure 7. Chemical structures of PLGA and levofloxacin.

In this project, the drug of choice for the PLGA microspheres was levofloxacin (**Figure 7**), a third generation fluoroquinolone antibiotic that inhibits the bacterial DNA gyrase and the topoisomerase IV, two enzymes responsible for the DNA synthesis and replication [144]. Levofloxacin is a broad spectrum antibiotic active against Gram-positive, Gram-negative and atypical bacteria [144]. Due to its exceptional activity against pathogens responsible for respiratory infections (*e.g., S. pneumoniae, H. influenza, S. aureus*) [145], it is colloquially called the "respiratory quinolone" together with the other molecules of its class (*e.g.,* moxifloxacin, gemifloxacin). Clinically, it is currently indicated for the treatment of respiratory infections (*e.g.,* acute bacterial exacerbations of chronic bronchitis, community-acquired and nosocomial pneumonia) [144,146], skin and skin structure infections[144,147], genitourinary infections [144,148]. In solid form, levofloxacin is a light yellowish crystalline powder with a molecular weight of 370.38 g/mol. At physiological pH, it exists mainly (~75% of the total amount of levofloxacin) as a zwitterion due to the ionization of both ionisable groups (*i.e.,* the 3-carboxyl proton with $pKa_1 = 5.7$, and the piperazinyl nitrogen with $pKa_2 = 8.0$ [149]). It is sparingly soluble in water at physiological pH and soluble in common solvents such as dichloromethane, chloroform, dimethyl sulphoxide. The distribution coefficient in octanol/buffer system ($logD_{oct/buffer}$) at pH 7.4 is 0.51, showing its affinity for both the lipophilic phase and the hydrophilic phase [149]. According to the Biopharmaceutics Classification System, it belongs to class I, *i.e.,* drugs with high solubility, high permeability and rapid dissolution. Regarding the pharmacokinetics, the oral and intravenous formulations are considered bioequivalent, as the bioavailability after oral administration is 99%. It has a plasma half-life of 6-8 h after oral, intravenous and pulmonary administration [99,150,151]. It is mainly eliminated (>85%) through the kidneys in the urine [99,150,151]. After systemic administration, its intrapulmonary concentration (*i.e.,* in the epithelial lining fluid and in the alveolar macrophages) is 1.5-6 times higher than in the plasma compartment [152–154], confirming the desired distribution for the treatment of pulmonary infections. Levofloxacin is generally considered safe and one of the most tolerable fluoroquinolones [155,156]. Very few adverse events on the gastrointestinal tract and skin includes photosensitivity reactions, nausea or vomiting, diarrhoea, pseudomembranous colitis [155,156]. However, levofloxacin and other fluoroquinolones have recently showed long-lasting and potentially permanent adverse reactions associated to the musculoskeletal and nervous systems (*e.g.,* tendon inflammation and rupture, depression, problems with memory and sleeping), and their use has been restricted in patients with underlying conditions, that predispose them to side effects [157,158]. Current delivery routes of levofloxacin include oral, intravenous and inhalation. At the preclinical phase, levofloxacin has been encapsulated in various drug delivery systems intended for intravenous and pulmonary administration, such as PLGA nanoparticles [90,112], chitosan nanoparticles [117,159,160], liposomes [90], hybrid lipid-polymer nanoparticles [161,162], niosomes (*i.e.,* non-ionic surfactant vesicles) [163], conjugated gold nanoparticles [164], hybrid polymer-calcium carbonate microparticles [165,166], and polymeric microparticles [109].

4.2 Preparation of Microspheres

PLGA microspheres can be prepared by various bulk methods, such as conventional single or double emulsification, membrane emulsification, spray drying, but also with microfluidic techniques [137,142,167–171]. To achieve the highest uniformity in particle size, the microspheres were in this project prepared and loaded with levofloxacin using a microfluidic emulsification technique in a glass chip with a flow-focusing geometry (**Figure 8**). To make the microspheres, an aqueous solution (*i.e.,* continuous phase (CP)) containing an emulsifier (*i.e.,* polyvinyl alcohol) was introduced in the outer inlet channels. At the same time, an organic solution (*i.e.,* dispersed phase (DP)) of dichloromethane containing both PLGA and levofloxacin was introduced in the central inlet at lower (~30 ×) flow rate. The DP was hydrodynamically focused into the orifice (*i.e.,* the junction point of the inlet channels) and, because of the shear force exerted by the CP, broken into oil/water (O/W) emulsion droplets containing polymer and drug [172]. Subsequently, each of the droplets shrunk and turned into solid polymeric microspheres as the result of extraction of the organic solvent in the external water phase.

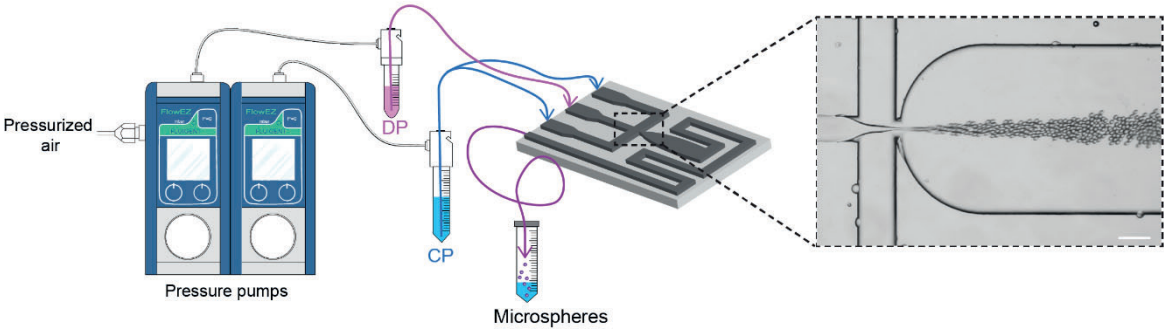

	Dispersed phase (DP, in DCM)	Continuous phase (CP, in water)
F0, F0i*	5% PLGA	2% PVA
F1	5% PLGA + 0.8% aLVX	2% PVA
F2	5% PLGA + 0.8% aLVX	2% PVA + 0.1% aLVX
F3	5% PLGA + 2.2% hLVX	2% PVA + 2% hLVX

Figure 8. Preparation of microspheres on a flow-focusing microfluidic chip. aLVX: anhydrous LVX, hLVX: hemihydrate LVX, PVA: polyvinyl alcohol, *F0i contains 50% (w/w) PLGA-PEG-NH_2 for radioactive imaging. Inset of the microfluidic chip is the snapshot during the production of droplets taken with optical microscope. Scale bar: 150 µm.

The microfluidics technique was chosen over the conventional bulk emulsification for its high reproducibility and superior control of the emulsification process [173–176]. Because each droplet was formed individually and sequentially under constant and identical forces, more homogenous emulsions were produced, making it a very good platform for the continuous synthesis of microparticles with high monodispersity and low batch-to-batch variation [174–177]. Various parameters are important for the droplet formation, with channel geometry

(particularly the orifice width), flow rates, and fluid viscosity showing the largest impact [175]. By controlling the fluid dynamics through the experimental and formulation parameters (*e.g.,* flow rates, viscosity of the DP and CP, and polymer concentration) in the microfluidic system, it is in fact possible to control the entire production process and tune the physico-chemical properties of the resulting microspheres [175].

A systematic optimization was carried out to select the best conditions to obtain the microspheres with the desired characteristics for targeted delivery of antibiotics to the lungs after intravenous administration, *i.e.,* monodisperse microspheres with size range of ~10-20 µm, with high antibiotic content and the ability to slowly release the loaded drug. The variables that were first tested were the flow rates of the DP (Q_{DP}) and CP (Q_{CP}), followed by the composition of the DP, and lastly the flow control system.

Different flow rates and flow ratios were investigated for their effect on the droplet break-off and on the droplet size. In general, there are four regimes of droplet formation: squeezing, dripping, jetting, thread formation [178]. Several combinations of Q_{DP} (0.5-5 µL/min) and Q_{CP} (30-150 µL/min) were screened. At low flow rate ratios (Q_{CP} /Q_{DP} < 20), the DP fully blocked the orifice, deformed and squeezed until break-off. This droplet generation regime is known as squeezing, and produces droplets larger than the orifice width. Here the size of the droplets and particles is mainly controlled by the dimension of the orifice and the viscosity of the fluids in lieu of the flow rate ratio [178]. By gradually increasing the Q_{CP} (30-150 µL/min), and thus the flow ratio (Q_{DP} /Q_{CP} = 20-120), the particle size decreased and the regime moved from squeezing to dripping (in which the droplets form near the orifice) or to jetting (in which the droplets form further downstream from the orifice at a distance < 20× the orifice width). This happens because the shear force imposed by the CP to the DP increases with increasing Q_{CP} for a fixed Q_{DP}. Above a certain value of flow ratio (Q_{DP} /Q_{CP} > 150), the shear force on the thread of the DP by the CP caused instability in the system, transition of the break-up pattern to an elongated thread yielding a jet of small (few micron) and polydisperse droplets. The best conditions for the production of monodisperse microspheres of 10-15 µm were found to be Q_{DP} = 3 µL/min, Q_{CP} = 90 µL/min, associated to the dripping regime.

By keeping the flow rates constant, other formulation-related parameters, specifically the organic solvent, the PLGA concentration in the DP, the PLGA lactide/glycolide ratio composition, and different PLGA molecular weights were tested and/or carefully chosen based on literature to maintain the desired particle size and distribution, and at the same time allow for the highest levofloxacin loading possible.

For the droplet generation in a flow focusing chip, the organic solvent chosen as DP needs to be volatile and able to dissolve the polymer and the drug. Moreover, it has to be immiscible in the aqueous CP, yet still be able to diffuse to the external water phase resulting in the formation of solid particles. Three types of organic solvents (*i.e.,* chloroform, dichloromethane and dimethyl carbonate) with different water solubility values and

toxicities were tested as DP. By keeping the flow rates constant at Q_{DP} = 3 µL/min, Q_{CP} = 90 µL/min, monodisperse particles were obtained with both chloroform and dichloromethane as the DP, while higher polydispersity was observed with dimethyl carbonate. This may be related to the much higher water solubility of dimethyl carbonate (13.9% for dimethyl carbonate [179], compared to 0.8% for chloroform, 1.75% for dichloromethane) and lower interfacial tension between the DP and CP (due to its partial solubility in water), resulting in an unstable emulsion being formed [180]. Between chloroform and dichloromethane, the latter was chosen as it shows lower toxicity [180], lower boiling point (dichloromethane 39.6 °C and chloroform 61.2 °C, meaning that it can more easily be removed in the washing step), and diffuses faster in the aqueous phase (~20 sec [181]) leading to faster solidification of the particles.

Higher solidification rates are also desirable when amphiphilic or hydrophilic drugs are encapsulated in hydrophobic polymers [172]. Amphiphilic drugs, such as levofloxacin, but also hydrophilic drugs have intermediate/low logD values, which means that in a biphasic organic/aqueous system they distribute in both the aqueous and organic phases or at the interfase between the two phases (if amphiphilic) or preferably in the water phase (if hydrophilic). In the single O/W emulsion system, the distribution of the drug into the excess of the external aqueous phase is associated with low encapsulation efficiency [172]. Therefore to optimize the drug content in the PLGA microspheres the drug partitioning (or diffusion) from the organic (*i.e.,* DP) to the aqueous phase (*i.e.,* CP) should be reduced as much as possible during the preparation. Experimentally, it can be achieved by accelerating the solvent extraction (and thus, droplet solidification), strengthening the drug-PLGA interaction, increasing the viscosity of the DP by using a higher PLGA concentration or a higher molecular weight PLGA, or by reducing the drug solubility in the aqueous phase [172]. For all these reasons, the optimal DP composition was found to be a 5% (w/v) PLGA (7-17 kDa, 50:50 PLA:PGA ratio, carboxylic-terminated end group) solution in dichloromethane.

The choice of the flow control system plays an important role for the use of microfluidic tools, and here it has shown to be a critical aspect especially for the preparation of homogenous microspheres, where the flow rates used were very low (in the order of µL/min) and had to be stable during the entire collection of microspheres in order to form uniform and reproducible results. This resulted in a very sensitive setup. It was especially critical for the DP, since that flow is responsible for the formation of the uniform monodisperse droplets, while small fluctuation in the CP flow did not represent a high enough percentage of the total flow rate to matter. Three different systems were tested: basic syringe pumps, high-precision syringe pumps (neMESYS, Cetoni) and pressure-controlled pumps (Flow EZ pressure pumps, Fluigent). The syringe pumps are one of the most established flow control systems in microfluidics. However, in the case of the basic version with a rather simple drive motors built in, flow fluctuations occurred because of the increments of the stepper motor, resulting in rather polydisperse microspheres and low day-to-day reproducibility. Almost negligible oscillations and, thus, better performance were obtained with the high-precision syringe pumps. Pressure pumps showed, however, the best

performance by precisely controlling the pulseless and stable flow of both the DP and CP with sub-second response time and fast equilibration time.

4.3 Physico-Chemical Characterization

Based on the best conditions found in the optimization phase, non-loaded (*i.e.,* formulation F0) and three levofloxacin-loaded (*i.e.,* formulations F1, F2, F3) PLGA microspheres were prepared by varying the theoretical drug content in the DP and the composition of the CP, and further characterized.

All the resulting microspheres had an average diameter of 12 µm and a narrow size distribution with coefficient of variation < 5.2% (**Table 7**). The formation of homogenous microspheres with a smooth surface was confirmed by scanning electron microscopy (SEM) (**Appendix, Figure S1**). These properties of the microspheres are highly desirable, as spherical and monodisperse size-distributed particles are expected to limit the variation in the rate of microparticle degradation and reduce burst drug release, compared to particles prepared with conventional emulsification methods [170]. Additionally, the size range perfectly matched the optimal size needed for passive lung targeting.

Table 7. Particle size, drug content and encapsulation efficiency of fresh and freeze-dried non-loaded and levofloxacin-loaded PLGA microspheres.

Formulation (#, form)	Particle size (µm)	CV (%)	Theoretical LVX loading (% w/w)	LVX loading (% w/w)	EE (% w/w)
F0, fresh	12.3 ± 0.4 ^{ns}	3.5	-	-	_
F0, freeze-dried	12.5 ± 0.6 ^{ns}	4.6	-	-	_
F0i, fresh	11.4 ± 0.5 ^{ns}	4.5	-	-	_
DTPA-F0i, fresh	12.0 ± 0.6 ^{ns}	4.7	-	-	_
F1, fresh	12.2 ± 0.4 ^{ns}	3.5	15	2.2 ± 0.1 (ns)	13.7 ± 2.0
F1, freeze-dried	11.5 ± 0.4 ^{ns}	3.3	15	* 1.8 ± 0.5 (ns)	12.2 ± 3.10
F2, fresh	12.7 ± 0.5 ^{ns}	3.9	15	* 3.9 ± 0.6 (ns)	26.5 ± 3.9
F2, freeze-dried	12.1 ± 0.5 ^{ns}	4.7	15	* 3.5 ± 0.4 (ns)	23.4 ± 2.9
F3, fresh	12.5 ± 0.5 ^{ns}	3.3	30	5.6 ± 0.4 (ns)	18.4 ± 0.8
F3, freeze-dried	12.1 ± 0.6 ^{ns}	5.2	30	5.0 ± 0.3 (ns)	16.3 ± 1.1

CV: coefficient of variation (calculated based on 500 MS), EE: encapsulation efficiency, LVX: levofloxacin, *$p < 0.05$, calculated based on 3 independent batches (N = 3), ns: not significantly different. For particle size, statistical multiple comparison between all formulations were done. For LVX loading and EE, multiple comparison between fresh and freeze-dried formulations as well as the different loaded formulations were done. The statistical analysis of the EE followed the analysis of the loading

The drug content was measured with ultraviolet-visible spectroscopy after microsphere disintegration. The levofloxacin-loaded PLGA microspheres had a levofloxacin content of ~2-5.5% (**Table 7**). The drug loading (*i.e.,* drug-to-polymer ratio) and the encapsulation efficiency (*i.e.,* encapsulated drug-to-initially included drug) doubled by saturating the CP with anhydrous levofloxacin (**Table 7**, F1 *vs* F2). This confirms that limiting the drug diffusion from the organic to the aqueous phase is a good strategy to increase the encapsulation of highly water soluble drugs in hydrophobic particles, as previously shown [109]. Doubling the theoretical drug loading along with replacing the anhydrous form with the hemihydrate form of levofloxacin further improved the final drug loading but lowered the encapsulation efficiency (**Table 7**, F1 *vs* F2). These results indicated a saturation of the loading capacity under the used preparation conditions. The hemihydrate form of the drug was used because its solubility in dichloromethane was higher and more drug molecules were loaded as a result hereof.

The drug loading, although low, was satisfactory when considering the nature of the polymer and the drug together with the single O/W emulsification preparation method. Previous work showed that ~2 μm PLGA microspheres could be loaded with levofloxacin with up to 10.5% drug loading when prepared with a double emulsion water/oil/water (W/O/W) by saturating the external water phase, and that the further addition of lauric acid to the organic phase resulted in further increase of levofloxacin loading (18.4%) and encapsulation efficiency (44.4%), possibly due to complexation between the molecules through electrostatic interactions between the lauric acid and the basic piperazinyl group of levofloxacin [109,159]. Other studies showed that gentamicin loading in PLGA microspheres increased from 2.7% to 6.2% when the PLGA concentration in the organic phase was doubled from 10% to 20% [182]. Overall, these results show that the encapsulation of small hydrophilic and amphiphilic drugs in PLGA microspheres is challenging and requires optimization of the preparation method and formulation-related parameters to obtain efficient loading [172].

4.4 *In Vitro* Characterization

The performance of the prepared PLGA microspheres were assessed *in vitro*. Specifically, the levofloxacin release from the microspheres and the associated degradation of the polymeric matrix was assessed. The antimicrobial activity upon encapsulation in the microspheres was also determined. Finally, the compatibility on endothelial, epithelial and red blood cells was tested.

4.4.1 Levofloxacin Release and Microspheres Degradation

The release of levofloxacin from the PLGA microspheres is an important aspect of the drug delivery system, being the precondition for drug diffusion through the alveolar-capillary barrier and for its antibacterial effect.

All the PLGA microspheres slowly released the encapsulated levofloxacin over a period of five days following a biphasic diffusion-driven mechanism [183]. A fast release corresponding to ~10-20% of the encapsulated levofloxacin associated to the diffusion of the levofloxacin close to the particle surface was followed by a slow and gradual release of the loaded levofloxacin that diffused out through water-filled pores of the polymeric matrix. After five days, up to 85% of the loaded levofloxacin was released (**Figure 9**). No burst effect was observed, probably due to the fact that most of the levofloxacin was encapsulated in the polymeric matrix, instead of being bound or adsorbed on the surface.

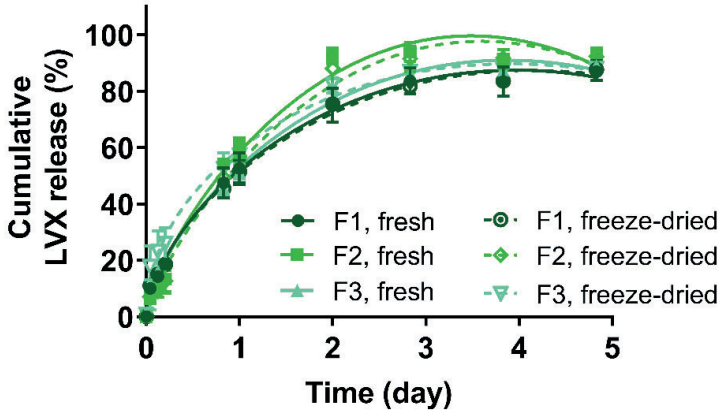

Figure 9. *In vitro* cumulative release profiles of levofloxacin from PLGA microspheres. F1 fresh (—●—) and freeze-dried (-⊙-); F2, fresh (—■—) and freeze-dried (-◈-), F3, fresh (—▲—) and freeze-dried (-▽-)) in phosphate buffered saline (PBS) and 37 °C, fitted by the Peppas-Sahlin model. Results are expressed as mean ± SD (N = 3, n = 1).

Five mathematical models (*i.e.,* Zero order, First order, Higuchi, Korsmeyer-Peppas, Peppas-Sahlin [184]) were tested to fit the experimental data and describe the drug release from PLGA microspheres. Of the 5, the Peppas-Sahlin model best fitted the drug release profiles, as it showed the highest correlation coefficient values ($R^2 = 0.9847 – 0.9964$) and the lowest root mean squared error (RMSE = 2.04 – 4.83) (**Appendix, Table S2, Figure S2**). According to this model, the drug release happens as a consequence of two events, *i.e.,* the drug diffusion (first term of Peppas-Sahlin Eq., **Appendix, Table S2**) and the relaxation of the polymeric chains with transition from a semi-rigid to a flexible state (second term of Peppas-Sahlin Eq., **Appendix, Table S2**) [184,185]. However, in this case the diffusion of the drug was the main mechanism with a small, but not negligible, contribution of the chain relaxation, as shown by the much higher Fickian diffusion constant compared to the

relaxation constant in the Eq. (k_1 = 65.1–76.8 >> k_2 = -11.7 – -16.5, **Appendix, Table S2**) [184,185].

As mentioned above, the levofloxacin release profile is important in relation to the antibacterial activity, since it controls the drug concentrations available at the target tissue. The PLGA microspheres showed a favourable slow and controlled release profile, which would ideally contribute to levofloxacin diffusing through the alveolar-capillary barrier and reaching the bacteria in the alveolar space over a longer time period, and minimize the risk of systemic side effects. Moreover, prolonged release profiles may improve patience compliance given the reduced frequency of administration needed to have therapeutic concentration at the infected site. However, a critical point is related to the fact that the released levofloxacin at the infected site has to be at concentrations the above-minimum inhibitory concentration (MIC) for the specific bacteria at all time points in order to have a pharmacological effect and reduce the risk of development of antibiotic resistance. Based on the release experiments performed, the concentration of levofloxacin in the epithelial lining fluid of mice upon release from the PLGA microspheres can be predicted to almost instantly be higher than the MIC for *P. aeruginosa* and *S. aureus* (4 μg/mL) and for E. coli (0.03 μg/mL, see section 4.4.2).

For PLGA microspheres, drug release occurs together with and as a consequence of microsphere degradation. Therefore, by choosing a PLGA with a convenient degradation behaviour, the release profile (mono-, bi-, tri-phasic), rate and the duration could be tuned. Specifically, the degradation rate is faster for PLGA with a low molecular weight [183], amorphous nature, with more hydrophilic end groups (*e.g.,* carboxylic acid [186]), and with higher content of the glycolic acid, as shorter polymer chains require less time to degrade and as hydrophilicity of the matrix increases water absorption, and thus degradation and release rates [137,142]. Based on these considerations, PLGA with PLA:PGA molar ratio of 50:50, molecular weight of 7-17 kDa and carboxylic end groups was chosen. Importantly, the polymer composition (*i.e.,* molar ratio of PLA to PGA), molecular mass, end functionalities and polymer crystallinity are only some of the factors that control the release profile. Others are associated to the encapsulated drug (*e.g.,* nature of the drug [187], the initial drug loading [188], the location of the drug in the microspheres), to the physico-chemical properties of the microspheres (*e.g.,* size, polydispersity, porosity of the microspheres) and to *in vitro* conditions (*e.g.,* temperature, stirring, pH of the release medium, composition of the release medium) [185]. In an *in vivo* environment, the effect of enzymes, lipids and immune system should also be considered [185].

PLGA degradation mechanism is well-known and occurs *via* hydrolysis: Water molecules first penetrate into the polymeric matrix causing some swelling, then break the ester bonds in the PLGA backbone. This results in the formation of oligomers (*i.e.,* PLA, PGA) and monomers (*i.e.,* LA, GA), which gradually dissolve in the release medium in a process known as erosion (*i.e.,* mass loss [143,185]) of the polymer matrix until complete polymer degradation. This creates internal water-filled pores available for drug diffusion out of the

particles. Importantly, the degradation products contain acidic groups, which themselves catalyse the hydrolysis, and thus, increase the formation of pores [142,143,185].

To confirm and validate the diffusion-based release and the associated microsphere degradation pattern, changes in the surface morphology and internal structure of the polymeric matrix were investigated over time by using a focused ion beam (FIB)-SEM. During the first days (**Figure 10**, day 1-2), the microspheres showed a partially collapsed spherical shape (appearing as "deflated balls") with small pores on the surface and in the internal matrix. The pores grew in size and eventually merged with near pores to form larger pores and opening channels towards the surface (**Figure 10**, day 5 *vs* day 1-2), while more prominent wrinkles appeared on the surface (**Appendix, Figure S3**, up to day 21). In agreement with previous work on PLGA films [189,190] and the above mentioned PLGA degradation mechanism, the polymer chains hydrolysis caused the formation of degradation products that contributed to the process *via* autocatalysis. Faster autocatalysis is expected in the matrix compared to the surface, as the molecules formed are kept locally in the bulk and were not neutralized and removed by the buffer solution (as it may have happened for the monomers produced on the microspheres surface) [143].

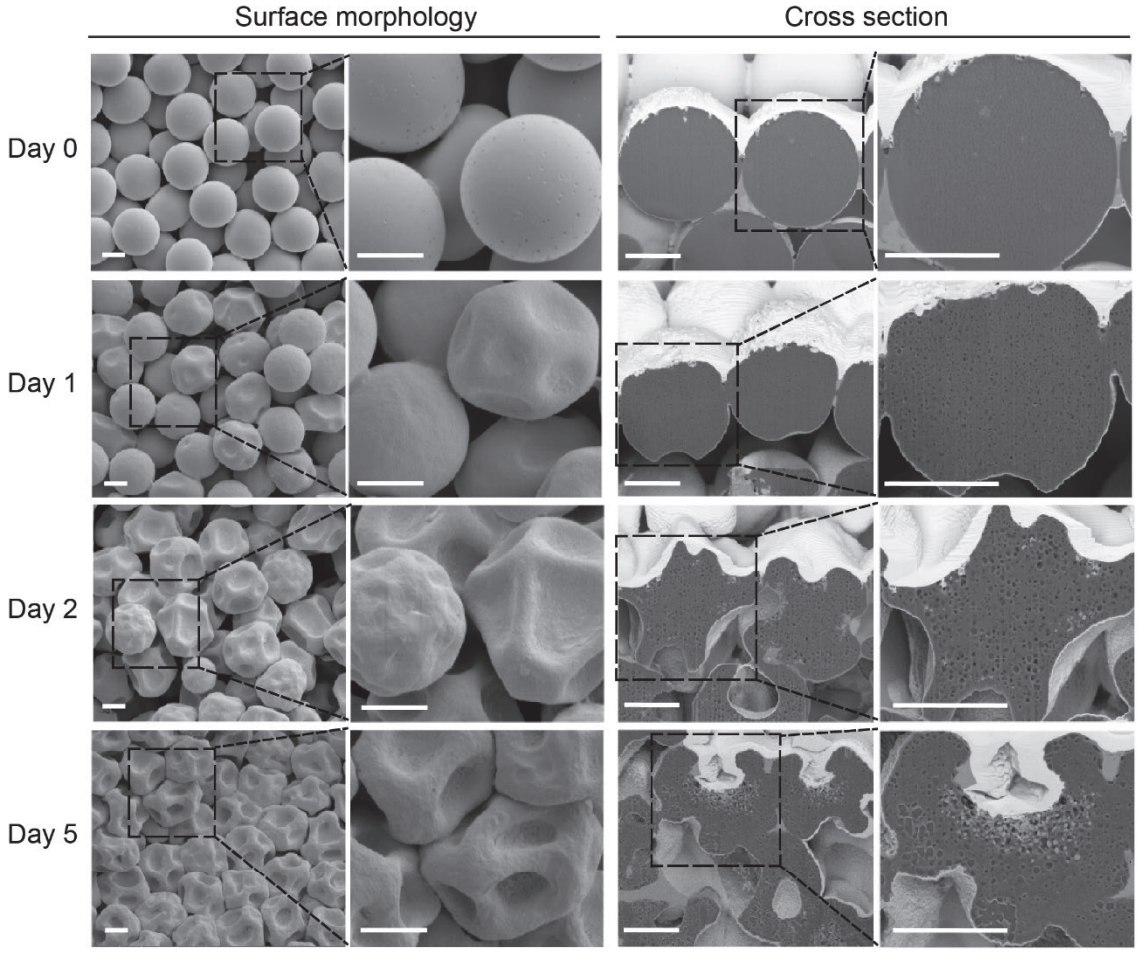

Figure 10. SEM images of F2 PLGA microspheres and their cross section during degradation. Scale bars: 5 µm.

4.4.2 Antibacterial Activity

The antibacterial activity of the levofloxacin-loaded microspheres was evaluated using the broth microdilution method, which is a standard assay for determination of MIC. The assay was performed on *S. aureus*, a Gram-positive, as well as *E. coli, P. aeruginosa*, which are Gram-negative bacteria. The chosen pathogens are relevant for the tested indications as they frequently are associated to nosocomial infections in e.g., the respiratory tract. The non-loaded PLGA microspheres did not display any antibacterial activity against the tested bacteria, in agreement with previous studies where no bacterial growth inhibition was observed at concentration below 1 mg/mL [191]. The MICs of non-formulated levofloxacin were 0.03 µg/mL, 1 µg/mL, and 0.5 µg/mL for *E. coli*, *P. aeruginosa*, *S. aureus*, respectively (**Appendix, Table 2**), in good agreement with previous studies for *E.coli* [192] and *P. aeruginosa* [193], and in the middle of the quoted MICs (0.15 to 4 µg/mL) for *S. aureus* [193,194]. The three PLGA microspheres containing levofloxacin showed MIC values of 0.25-1 µg/mL for *E. coli*, 4 µg/mL for *P. aeruginosa*, and 2-4 µg/mL for *S. aureus*. This shows that encapsulating LVX in PLGA microspheres reduces the antimicrobial activity of levofloxacin by a factor of two to five. This decrease may be due to the slow and controlled drug release profile for the PLGA microspheres, which results in progressively release of levofloxacin from the microspheres, as previously shown for PLGA nanoparticles loaded with netilmicin [195] and ciprofloxacin [196].

Despite the decrease of antibacterial activity of levofloxacin upon encapsulation in the microspheres, the dose of levofloxacin delivered is expected to have a bactericidal effect in mice. Levofloxacin, in fact, has shown bactericidal effect against *P. aeruginosa* and *S. pneumoniae* at concentrations 1-4× the respective MICs [197–200]. As alveolar lining volumes of mice are not available in literature, based on body weight-dependant calculation from a 70 kg human who has ~36 mL of alveolar lining fluid [15], a 25 g mouse may have a volume of ~13 µL of alveolar lining fluid. The levofloxacin delivered and released already after 1 h from the 3 mg dose of PLGA microspheres (*i.e.,* ~22 µg) is ~400× higher than the amount needed to reach the MIC values in the alveolar lining fluid in mice (*i.e.,* 0.051 µg). In humans, however, the amount of levofloxacin needed to have a concentration higher than MIC in the alveolar lining fluid (*i.e.,* 145 µg) is theoretically only reached after four days, showing that optimization of the formulation or higher doses are needed to have a pharmacological effect.

4.4.3 Cytotoxicity and Hemocompatibility

A desired characteristic of a drug delivery system is low toxicity of not only the carrier but also the drug-loaded delivery system against host eukaryotic cells. The PLGA microspheres were tested for cytotoxicity to endothelial (HUVEC), epithelial (alveolar lung epithelial A549 and human lung epithelial H1299), and red blood cells, as they were designed for intravenous administration and embolization in the lung capillaries. Cell toxicity was

evaluated by assessing the function of metabolic activity in mitochondria by measuring the potential of living cells to reduce the colorless 3-(4,5-dimethylthiazol-2-yl)-2,5-diphenyltetrazolium bromide (MTT) into a blue formazan.

The non-loaded and levofloxacin-loaded PLGA microspheres showed similar reduction in cell viability of the tested endothelial and epithelial cell lines (**Figure 11A-C**). This could be related to the relatively low levofloxacin loading shown for all the formulations, and thus no additional effect on the cytotoxicity, as previously shown for levofloxacin -loaded PLGA nanoparticles on bronchial Calu-3 cells [109]. The PLGA microspheres showed IC_{50} values of 1.4–2 mg/mL for HUVEC, 2.5–3.5 mg/mL for A549 and 0.7–1.5 mg/mL for H1299. These values correspond to concentrations of levofloxacin of 0.03–0.08 mg/mL for HUVEC, 0.06–0.09 mg/mL for A549, and 0.01–0.04 mg/mL for H1299. The observed decrease in cell viability was concluded to be associated to the high concentration of PLGA microspheres used in the experiments and not to the initial fast release of levofloxacin, as the levofloxacin-loaded PLGA microspheres showed higher reduction in cell viability compared to non-encapsulated levofloxacin at the corresponding levofloxacin concentrations (**Appendix, Figure S5**).

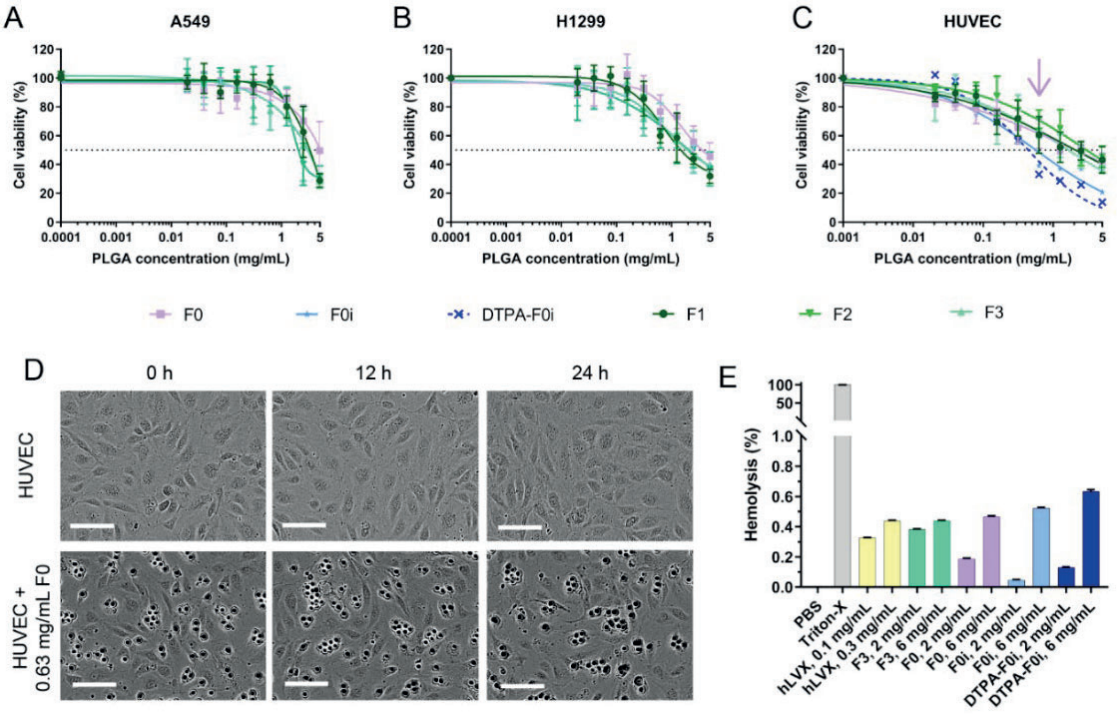

Figure 11. Cytotoxicity and hemocompatibility of PLGA microspheres. **(A,B,C)** Cell viability (%) of A549, H1299 and HUVEC cells incubated for 24 h with F0 (),F0i (), DTPA-F0i (), F1 (), F2 (), F3 () and hemihydrate (). The dotted line represents 50% viability. Data are presented as mean ± SD, N = 3, except for F0i and DTPA-F0i where N = 1. **(D)** Representative phase contrast images of HUVEC cells taken using the IncuCyte® Live-Cell Analysis System at 0, 12, 24 h after treatment with media (control, top) or F0 at 0.63 mg/mL PLGA concentration (concentration indicated with the pink arrow in Figure C) (bottom). Scale bars: 100 µm. **(E)** Hemolysis (%) of human red blood cells caused by free LVX, non-loaded PLGA MS and LVX-loaded PLGA MS were assessed after 1 h incubation at different concentrations. Data are presented as mean ± SD (N = 1, n = 3).

Despite the cytotoxicity shown at high PLGA concentrations, 3 mg was chosen as the dose for *in vivo* experiments to control if the minimum PLGA dose needed to reach a therapeutic level of levofloxacin in the alveolar lining fluid, *i.e.,* above MIC in humans (*i.e.,* > 2.8 mg of PLGA MS) could still be tolerated in an *in vivo* setting using mice. This might be expected as PLGA is a biocompatible polymer, US FDA approved for clinical administration at concentrations up to 30 mg/mL for intramuscular injection. Also, differences between *in vitro* and *in vivo* cytotoxicity results are in fact attributed to the higher susceptibility of cells in the well-controlled and confined, but also more simplistic *in vitro* environment.

Inverted phase microscopy images confirmed decreased cell viability upon exposure to PLGA microspheres and non-encapsulated levofloxacin. The representative images showed morphological changes of HUVEC cells exposed to PLGA microspheres for 24 h, when the cells appeared more round and smaller than the control. As expected, cells exposed to PLGA microspheres at a concentration of 0.6 mg/mL, showed normal cell morphology (**Figure 11D**).

The hemocompatibility (*i.e.,* blood compatibility), is another important evaluation that has to be done with drug delivery systems intended for intravenous administration, as interaction and destruction of blood components result in cellular and humoral reactions that can lead to unwanted inflammation, formation of thrombus [201], and/or clearance of the drug delivery system from the bloodstream and consequent reduction of drug delivery to the target site, and, thus, reduction of the efficacy of the treatment [202,203]. Determination of hemocompatibility includes the assessment of hemolysis, protein adsorption on the surface of the particulates, thrombogenicity and complement activation [201]. The ideal intravenous carrier should be non-hemolytic, non-thrombogenic, non-complement activating and invisible to the immune system.

The hemolysis (*i.e.,* red blood cells lysis), and subsequent leakage of free haemoglobin was assessed to estimate the toxicity of the PLGA microspheres to human red blood cells. The non-loaded and LVX-loaded PLGA microspheres were non-hemolytic, meaning that all the PLGA microsphere concentrations lysed less than 2% of the red blood cells, the permitted level in hemolysis assessment [201]. In fact, after 1 h incubation with erythrocytes, minimal hemolysis (*i.e.,* under 0.4%) was induced for all formulations at concentrations up to 6 mg/mL corresponding to 3× the dose chosen for the *in vivo* experiments (**Figure 11E**). This is in agreement with previous studies on PLGA nanoparticles, where no hemolysis was observed at PLGA concentrations up to 3 mg/mL [204] or 10 mg/mL [205].

Overall, the PLGA microspheres could be safely administered *in vivo* at a dose of 3 mg/mouse, corresponding to ~300,000 PLGA microspheres, without concerns on animal toxicity.

4.5 *In Vivo* Characterization

4.5.1 Microspheres Degradation

The microsphere degradation kinetics was assessed *in vivo* by visual investigation of their presence in the lungs capillaries of mice at different time points, after imaging 30-µm thick coronal sections. The microspheres were entrapped in the lung capillaries immediately after intravenous injection (**Figure 12**) and stayed in the lungs for one more week (**Figure 12C**). Overall, the degradation kinetic was faster in *in vivo* than *in vitro* (where it took 3 weeks for the microspheres to completely disintegrate (**Appendix, Figure S3**)). This was in agreement with the literature, as PLGA microspheres were shown to degrade 1.7-2.6 times faster *in vivo* than *in vitro*, independently of the polymer end group or molecular weight, probably due to the plasticizer effect of lipids and biological compounds *in vivo*, resulting in higher water uptake [206]. However, it was not possible to show the microstructure of the microspheres (*e.g.,* surface wrinkling) in the lung tissue. This may be due to the relatively low resolution of optical microscopy (compared to the electron microscopy) and probably also influenced by interference with surrounding tissue.

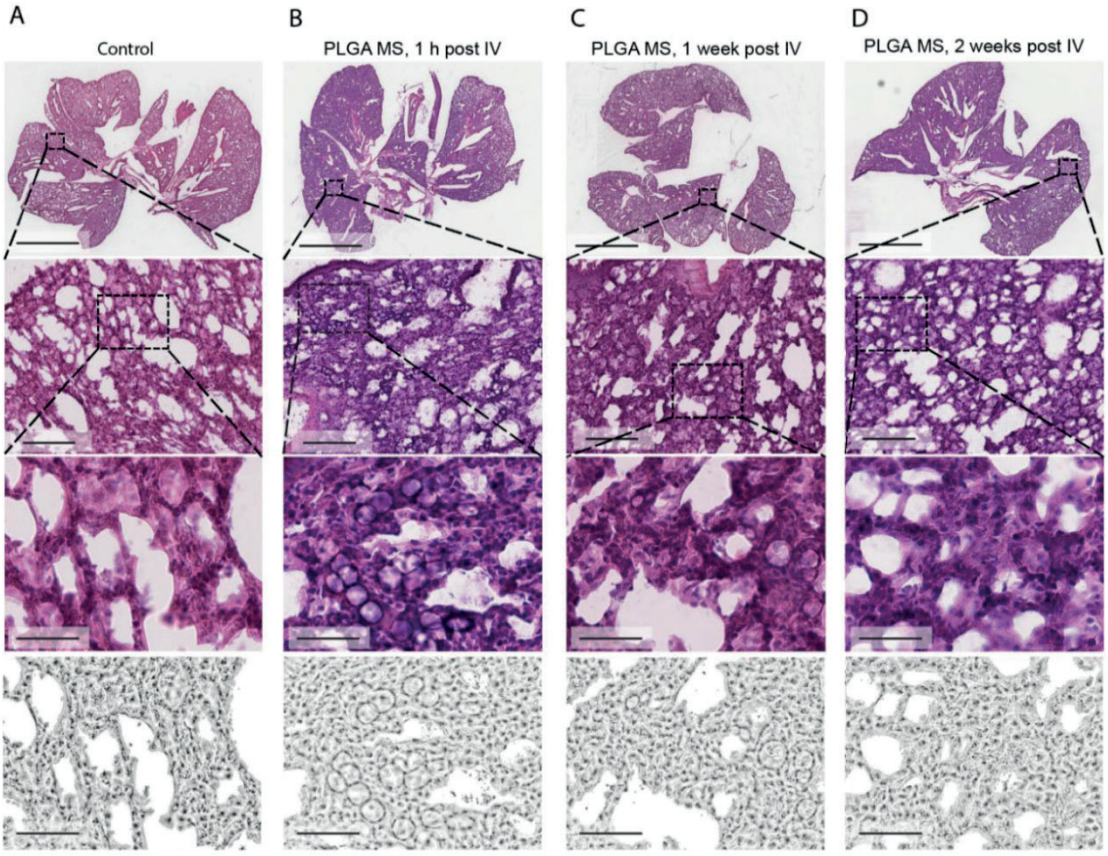

Figure 12. Representative histology images over time of lungs exposed to PLGA microspheres (F0) after IV injection. H&E stained histological 30-µm coronal lungs sections after different treatments (1st-3rd rows), and processed images after hematoxylin extraction (4th row, see **Appendix, Figure S4** for full-sized images). **(A)** Healthy and untreated lungs. **(B,C,D)** Healthy lungs after 1 h, 1 week and 2 weeks of injection of 3 mg/mouse PLGA MS (corresponding to ~300,000 PLGA MS/mouse). Scale bars: 1st row: 5 mm, 2nd row: 200 µm, 3rd and 4th row: 50 µm.

4.5.2 Lung Targeting after Intravenous Administration

The PLGA microspheres were further investigated for lung targeting, after being radiolabelled with ^{111}Indium (^{111}In).

Microspheres with a radioactive tag were prepared in order to track them after systemic administration using the nuclear imaging technique SPECT/CT. To radiolabel the microspheres, PEGylated PLGA microspheres were firstly prepared by adding PLGA-PEG-NH_2 to the PLGA in the DP to surface functionalize the resulting particles with amino groups (**1**, *i.e.,* F0i PLGA MS, **Figure 13A**). The PEGylated PLGA microspheres were then reacted with S-2-(4-isothiocyanatobenzyl)-diethylenetriamine pentaacetic acid (*p*-SCN-Bn-DTPA), resulting in DTPA-F0i PLGA MS (**2, Figure 13A**), and finally radiolabelled with ^{111}In, yielding the final product ^{111}In-DTPA-F0i PLGA MS (**3, Figure 13A**). ^{111}In was chosen amongst the gamma emitter radioisotopes due to its relatively long half-life of 2.8 days, which allows imaging for up to 10 days, and due to its ability of forming very thermodynamically stable bonds with DTPA [207].

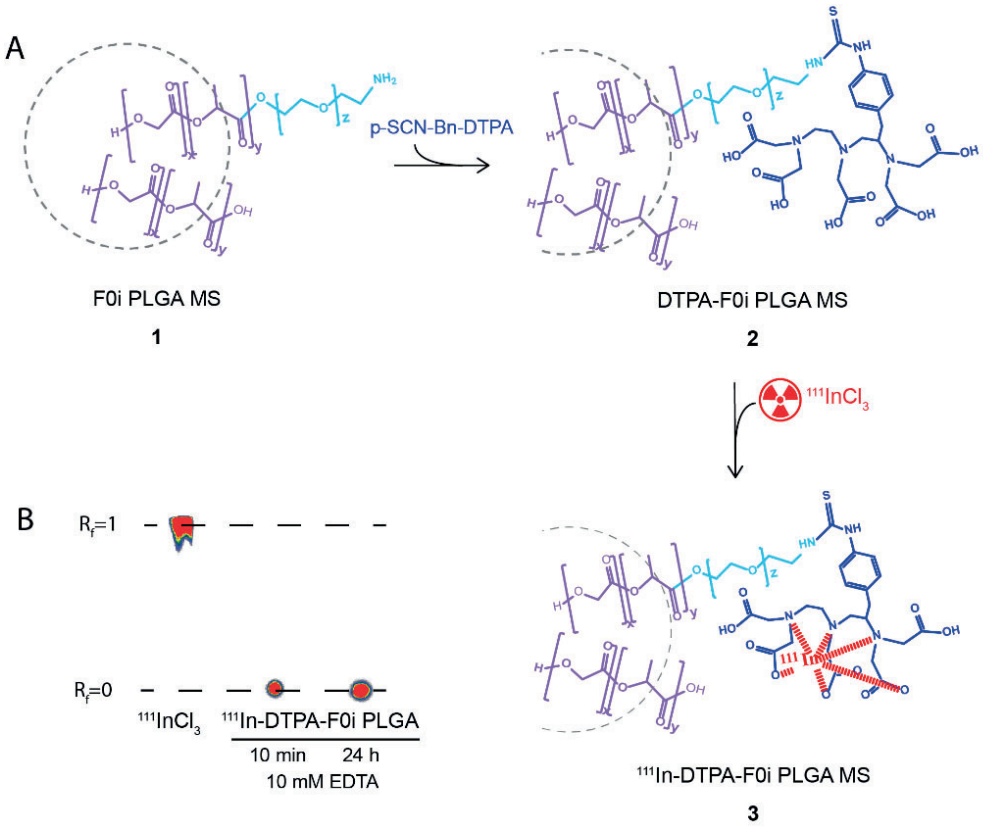

Figure 13. Synthesis of radiolabeled PLGA microspheres. **(A)** Synthesis of ^{111}In-DTPA-F0i PLGA MS. **(B)** Radiolabeling efficiency and stability over 24 h by using ITLC.

The final polymeric composition (*i.e.,* PLGA-PEG-NH_2:PLGA at 50:50 weight ratio) used to prepare the F0i PLGA microspheres was based on the optimization process, in which microspheres were prepared at different weight ratios between PLGA-PEG-NH_2 and PLGA

(*i.e.,* 5:95, 10:90, 25:75, 50:50, 100:0 (*i.e.,* 100% PLGA-PEG-NH_2)) in the DP, and characterized in terms of radiolabelling efficiency and radiochemical purity. The radiolabelling efficiency (*i.e.,* the ratio between the activity measured on the ^{111}In-DTPA-F0i PLGA MS and the initial activity) gradually increased from ~2% to ~8% proportionally to the PEGylated content in the DP mixture. These relatively low values of labelling efficiency could be associated to the presence of only few amino groups on the microspheres surface decreasing their overall reactivity with DTPA, and thus the chelation of ^{111}In. Since PLGA-PEG-NH_2 was added to the reaction mixture during the formation of microspheres, and not as surface functionalization of preformed microparticles, it may have distributed between the bulk and the surface of the microspheres [208,209]. This would align with the low radiolabeling efficiency shown by the microspheres made of 100% PLGA-PEG-NH_2. However, due to the emulsion-based preparation method, the preferred orientation of the PEG moieties in theory remains towards the aqueous phase with the more hydrophobic part of the copolymer PLGA in the PLGA matrix, resulting in the formation of PEG enriched surfaces and less PEG inside the polymeric matrix [208,209]. The resulting ^{111}In labelling was found sufficient for the planned *in vivo* studies, but further investigations on this matter could be supplemented by studying the surface functionalization with PEG and then with DTPA by FT-IR and NMR with peaks and absorbance bands of the introduced chemical groups (*e.g.,* introduction of new ether functions from the PEG fragments PEG-NH_2, DTPA, PLGA-COOH), as previously shown [210]. The radiochemical purity was tested using instant thin-layer chromatography (ITLC) after incubation of the ^{111}In-DTPA-PLGA MS with a strong chelator for ^{111}In (*i.e.,* ethylenediaminetetraacetic acid (EDTA)). From the integration of the ITLC peaks, all the F0i microspheres prepared showed high radiochemical purity, as only a small (<5%) percentage of ^{111}In migrated to the solvent front as ^{111}In-EDTA complex (retention factor, $R_f = 1$), while the ^{111}In-DTPA-PLGA MS remained at the origin ($R_f = 0$). Despite the low radiolabelling efficiency, the high radiochemical purity proved that^{111}In was strongly chelated by DTPA, making the formulations ready for the *in vivo* studies. The best *in vitro* performance was observed for ^{111}In-DTPA-PLGA MS made of polymeric blend containing 50% PEGylated PLGA, as they showed the highest labelling efficiency (*i.e,* ~5%), and thus highest activity linked to the microspheres, as well as excellent radiochemical purity (*i.e.,* 97%) and 24 h stability after EDTA challenge (**Figure 13B**). Moreover, the modification in terms of partly exchanging PLGA with PEGylated PLGA did not drastically change the composition of matter of the microspheres.

Importantly, the radiolabelling reaction did not alter the physicochemical properties of the F0i PLGA microspheres (with and without DTPA), as the particle size and size distribution (**Table 7**), the shape and surface morphology (**Appendix, Figure S1**) and the cytotoxicity (**Figure 11C,E**) did not differ significantly from F0 PLGA microspheres. This is critical for the *in vivo* performance as the microspheres biodistribution can be affected by their size and shape. However, F0i PLGA microspheres showed a faster degradation (complete degradation within ten days, compared to the F0 PLGA ones (**Appendix, Figure S3)**. This

was not surprising as it may be explained by the increased hydrophilicity due to PEG chains and, thus, their faster hydrolysis.

With the intent of performing dual-radioisotope imaging to assess the passive lung targeting of the microspheres, their ability to deliver and release levofloxacin with resulting appropriate pharmacokinetics, a cold (*i.e.,* not radioactive) copper (II) (Cu) complex with LVX and the N-donor heterocyclic ligand phenanthroline was synthesised (**Figure 14A**), as previously described [211]. The mass spectrum showed the parent ion of [Cu(levofloxacin)(phenanthroline)]$^{+}$ ternary complex (*m/z* = 605) together with the mono(levofloxacin)Cu(II) complex ([Cu(levofloxacin)]$^{+}$, *m/z* = 425) (**Figure 14B**). However, since the ternary complex had a very low solubility (< ng/mL) in organic solvents such as dichloromethane or chloroform, due to its positive charge, it was not possible to load it into the PLGA microspheres with the microfluidic O/W single emulsion method and use it in the *in vivo* evaluation.

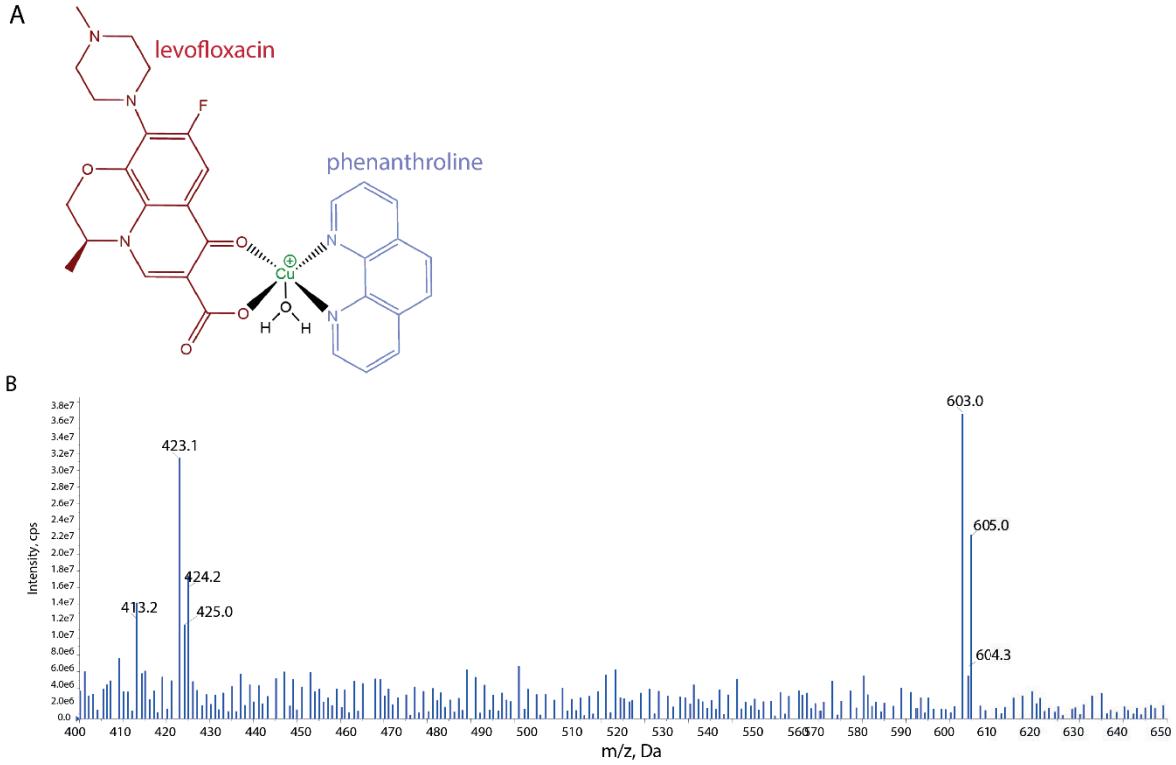

Figure 14. The Cu(II) levofloxacin complex. **(A)** Chemical structure of the cationic ternary complex [Cu(levofloxacin)(phenanthroline)(H_20)]$^{+}$. **(B)** ESI^{+} MS spectrum.

The pharmacokinetics and biodistribution of the non-loaded ^{111}In-DTPA-F0i PLGA MS were assessed by SPECT/CT imaging in healthy mice. Following intravenous administration, ~85% of the injected PLGA microspheres ended up in the lungs (**Figure 15**), as a consequence of microembolizing the pulmonary capillaries with particles larger than the diameter of the lung capillaries (*i.e.,* ~8 um). The microspheres distributed homogenously throughout the left and right lobes (**Appendix, Figure 5B**) confirming the

hypothesis that a more homogenous lung distribution can be achieved by intravenous administration of microspheres *via* passive lung targeting, compared to that obtained by inhalation [119,212,213]. This was highly desirable as regional localization in the lungs determines the clinical efficacy of the treatment.

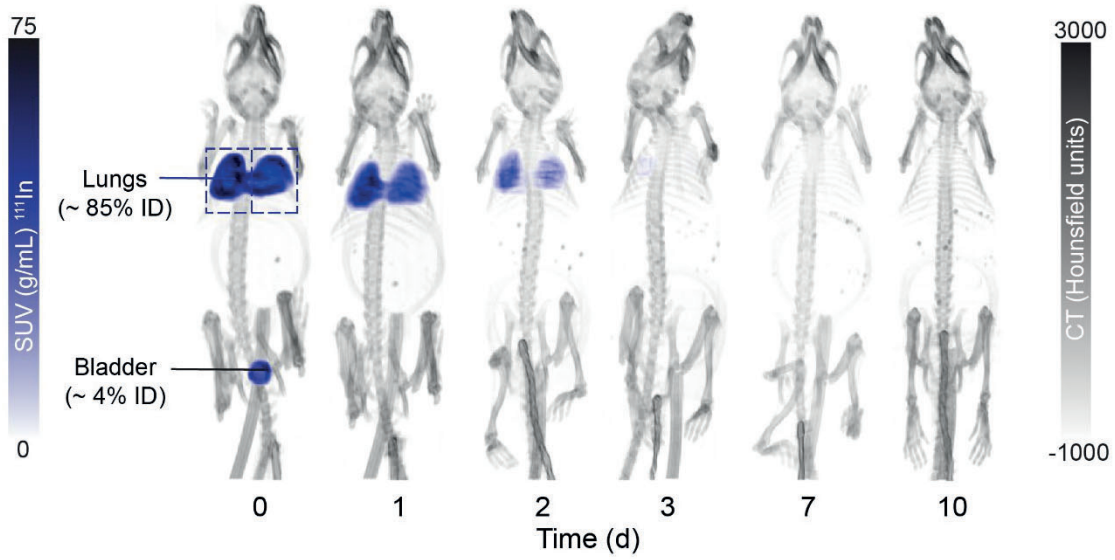

Figure 15. Pharmacokinetics and biodistribution of radiolabeled PLGA microspheres. Representative maximum intensity projections SPECT/CT overlay images (dorsal view) of healthy C57BL/6 mice showing the *in vivo* distribution of ^{111}In-DTPA-F0i PLGA microspheres after intravenous tail injection over time. The radioactivity is shown in blue. ID: injected dose.

However, ~ 4% of the injected radioactivity was immediately excreted *via* the urinary pathway (**Figure 15**, day 0). This could be due to the detachment and elimination of the ^{111}In-DTPA complex alone or linked to the PEG chains in lieu of the release of non-complexed ^{111}In. The high values of the *in vitro* radiochemical purity and stability of ^{111}In-DTPA after EDTA challenge (**Figure 13B**) favour this hypothesis. The activity in the bladder at day 0 is not likely related to un-chelated ^{111}In, as intravenously administered $^{111}InCl_3$ distributed mainly in the kidneys (~ 20% of the injected activity) and, in less extent, in the bladder (~2%) (**Appendix, Figure S7**).

The pharmacokinetics of the PLGA microspheres showed that they were slowly cleared from the lungs with only ~ 5% of the injected dose three days after administration, and 0.1% of the initial dose after seven days (**Appendix, Figure 5C**). After ten days, 0.02% of the injected activity still present in the mice was distributed to the lungs and the excretory organs, such as liver and kidneys, and to the spleen (**Appendix, Figure 5D,E**). Over time, in fact, the microspheres degrade *via* hydrolysis and decrease in particle size. When they reach sizes smaller than ~8 um, they can traverse the pulmonary arteriolar capillary bed, be transported away and accumulate in the liver and spleen, as shown for macroaggregate albumin particles and polystyrene microparticles [131,214]. The detachment of groups present on the surface, including PLGA and/or PLGA-PEG-NH_2 fragments conjugated to ^{111}In-

DTPA is also possible. At the same time, the ^{111}In-DTPA complex undergoes strong competition *in vivo* by the serum proteins (*e.g.,* transferrin), which frequently causes demetalation or transchelation of ^{111}In over prolonged exposure [215–218]. This could explain some of the isotope activity found in the kidneys, liver, spleen, and bones 2-3 days post injection, as it follows the same distribution profile of intravenously administered $^{111}InCl_3$ (**Appendix, Figure S6A**), as previously shown [219].

From these findings, the F0i PLGA MS seemed to be cleared to a larger extent from the lungs*, i.e.,* ~three days post injection (**Figure 15**, and **Appendix, Figure 5C**) following a faster kinetic rate compared to the degradation rate shown *in vitro* (**Appendix, Figure S3**). This behaviour is in line with previous studies showing 1.7-2.6 times faster degradation kinetics of PLGA microspheres *in vivo* compared to the one *in vitro*, which was hypothesized to be related to the *in vivo* plasticizing effect of lipids and other biological compounds, resulting in higher water uptake in the polymer [206]. However, further investigation is needed to confirm that the decline of radioactivity in the lungs after three days is indeed related to complete degradation of the microspheres, and not to the detachment of surface radiolabelled functionalities, giving a false-positive result.

Assuming microspheres clearance from the lungs happens within three days, prediction on the possibility of repeated administration can be made. The safety of repeated administration potentially necessary during serious lung infection therapy depends on several factors, including the total microspheres dose (*i.e.,* the number of microspheres injected, which relates to the numbers of capillaries clogged) and the degradation time (based on the polymer used and particle size (with longer degradation time for larger particles, as previously seen for albumin macroaggregates [214]). Importantly, the tested dose of 3 mg PLGA microspheres did not cause measurable alteration of pulmonary function, as the mice respiratory rate monitored during the entire *in vivo* experiments showed normal values. As mentioned above, a healthy adult has 280 billion pulmonary capillaries [122,123], and occluding a few million of them (*e.g.,* 3,000,000, corresponding to 10 repeated doses of 300,000 particles each) will thus only influence <0.1% of the capillaries. The repetition interval depends on the degradation rate and the dose, which in turn depends on its antibacterial efficacy. Ideally, the second and subsequent doses should be administered to maintain the antibiotic concentration at the site of infection above the MIC, *i.e.,* administered at a time point when the previous injected microspheres have almost completely been cleared from the lungs. With the results shown in this work, we assume that 3 mg PLGA microspheres are enough to deliver a therapeutic dose of levofloxacin for the desired pharmacological effect for three days (see section 4.4.3). Thus, it is expected that several administrations in series would be possible, as it likely would be needed for the treatment of lung infections and chronic pathologies (*e.g.,* cystic fibrosis) where periodic administrations of antibiotics are currently prescribed.

5 Conclusions and Future Perspectives

In this work, a wide range of methods was combined to develop, characterize both *in vitro* and *in vivo*, and gain a comprehensive understanding of levofloxacin-loaded PLGA microspheres to selectively target the alveolar capillaries of infected lungs after intravenous administration.

The PLGA microspheres had a monodisperse size distribution with a mean diameter of 12 µm. They degraded *in vitro* in three weeks while showing surface and internal morphological changes, and released the encapsulated levofloxacin in a controlled manner over five days. While the levofloxacin loading of the PLGA microspheres was relatively low, it still had antimicrobial activity against selected Gram-positive and Gram-negative bacteria. The microspheres showed compatibility with endothelial, alveolar epithelial and red blood cells. After tail vein injection in mice, the ^{111}In-radiolabeled PLGA microspheres distributed preferentially and homogenously throughout the lung capillaries. The microspheres were retained in the lungs for up to one week while slowly degrading and the degradation products being eliminated through the urinary pathway.

Overall, the results support the safe use of monodisperse size-distributed polymeric microspheres to target the lungs from the vascular side, and potentially deliver drugs to treat lung diseases *via* passive lung targeting. It should be noted that the levofloxacin-loaded PLGA microspheres are not directly translatable to human, and, thus, have to be further optimized to provide therapeutic levels of antibiotics in the human respiratory zone.

The flow-focusing microfluidic chip was shown to be a very good platform to prepare monodisperse microspheres while controlling their size and size distribution. However, for this strategy to be truly useful, some limitation and drawbacks should be solved/improved to have its application in larger scales, including clinical translation. The clogging of the microsized channels and/or orifice, due to the presence of contamination or precipitation of the materials in the fluid, as well as wettability and hydrophobicity of the channels, due to prolonged exposure and flow of organic solvent should be taken in consideration. To limit the number of interruptions in the continuous process, these problems should be solved, for example by using chips made of cheaper materials that could be discarded as soon as the issues arise. Importantly, the material has to be compatible with the organic solvents used for the droplet formation. The glass chip has shown to be resistant to many harsh solvents, but is associated to high fabrication costs, and thus, ideally not replaceable in case of orifice clogging or reduction of channel hydrophilicity. Cheaper materials such as polymers (*e.g.,* polydimthylsiloxane, thiol-ene) and milder solvents could be therefore considered to make the process more flexible. Another limitation of droplet-based microfluidics is the relatively limited/low productivity of a single chip (~10 mg/h, with the used conditions), which makes the production and collection of suitable amounts of microspheres tedious and lasts for many hours (in some cases). As a consequence, the DP and CP reservoirs (usually of ~2 mL and 10 mL, respectively) in this case had to be refilled halfway or during the experiment,

interrupting the continuous and stable flow, and requiring its re-equilibration, which may introduce variability in the sample. Several microfluidic chips can be connected in parallel to scale up the productivity, while larger syringe pumps (for the syringe pumps) or reservoirs (for the pressure-driven pumps) should be used in order to limit the refilling.

Drug content is one of the most important factors to confirm the success of a drug delivery system. Especially in the case of antibiotics treatments, the microspheres need to have sufficiently high drug content and preferably also high encapsulation efficiency. Here, the PLGA microspheres showed many good properties (*e.g.,* biocompatibility, sustained release without a significant burst effect, and slow degradation within one week), but also poor loading with amphiphilic drugs. This disadvantage may indeed limit their use in clinical trials. Further optimization of the levofloxacin-loaded PLGA microspheres is thus needed to increase the drug loading and obtain improved *in vivo* performance in the treatment of lung infections. The aim should be to have a high drug concentration at the site of infection and reduced dose of microspheres administered, as well as minimize the drug waste during the preparation process. Several strategies should be considered, including the modification of the preparation method (from O/W emulsification to non-aqueous emulsification methods, such as W/O/O or solid (S)/O/O), modification of the polymer to a less hydrophobic material (e.g., by functionalizing the entire surface with PEG molecules), or replacement of the amphiphilic drug with a more hydrophobic, preferably more potent molecule. However, these optimization steps should take the microfluidic approach into account as it is important to have microspheres with uniform and appropriate size distribution for a safe passive lung targeting strategy.

To confirm the sustained release of the drug observed *in vitro* and to prove the ability of the drug to diffuse through the alveolar-capillary membrane and localize in the alveoli, biodistribution and pharmacokinetics studies for the drug should be performed with the PLGA microspheres encapsulating levofloxacin, preferably in both healthy and infected animals in which efficacy study could also be performed. Dual SPECT/CT imaging could for example be done after labeling the polymer and the drug with two different gamma-emitter radioisotopes (*e.g.,* ^{111}In, ^{67}Ga, ^{67}Cu) so that both the drug and the carrier could be followed over time in the same animal. To solve the solubility problems experienced with the ternary complex of levofloxacin during the radiolabeling procedure, monoanionic ligand (*e.g.,* maltol, a natural FDA approval molecule) could be used.

Possible toxic effects should also be further evaluated. *In vivo* pulmonary toxicity studies should be performed in addition to the microscopic examination of lung tissue already performed to prove the absence of pathologic changes. Determining the minimum toxic dose and the minimum lethal dose not only in healthy, but also in infected animals is important to fully define the biocompatibility. Additionally, the effect of repeated administration should be investigated to define the possible treatment regime and maximum possible doses without toxicity. Repeated administrations can be for example tested with microspheres radiolabeled with different radioisotopes, which allows for observation of possible

differences in microspheres distribution in the lungs as well as in degradation rates between the different injections.

Finally, to provide the evidence of the therapeutic benefit of the drug delivery system for the treatment of pulmonary infections, efficacy studies in established *S. pneumoniae*, *P. aeruginosa* and/or *S. aureus* infected *in vivo* models should be performed. Ideally, susceptible and resistant strains (*e.g.,* penicillin-susceptible *S. pneumoniae* and penicillin-resistant *S. pneumoniae*) should be used to investigate its applications in case of antibiotic-resistance pathogens. Further proof of the drug delivery efficacy *via* passive lung targeting could be obtained by comparing it with current treatments (*i.e.,* oral, intravenous and pulmonary administration of levofloxacin) as well as by combining it with inhaled microparticles encapsulating levofloxacin.

6 References

(1) Troeger, C.; Blacker, B.; Khalil, I. A.; Rao, P. C.; Cao, J.; Zimsen, S. R. M.; Albertson, S. B.; Deshpande, A.; Farag, T.; Abebe, Z.; et al. Estimates of the Global, Regional, and National Morbidity, Mortality, and Aetiologies of Lower Respiratory Infections in 195 Countries, 1990–2016: A Systematic Analysis for the Global Burden of Disease Study 2016. *Lancet Infect. Dis.* **2018**, *18*, 1191–1210.

(2) Naghavi, M.; Abajobir, A. A.; Abbafati, C.; Abbas, K. M.; Abd-Allah, F.; Abera, S. F.; Aboyans, V.; Adetokunboh, O.; Ärnlöv, J.; Afshin, A.; et al. Global, Regional, and National Age-Sex Specifc Mortality for 264 Causes of Death, 1980-2016: A Systematic Analysis for the Global Burden of Disease Study 2016. *Lancet* **2017**, *390*, 1151–1210.

(3) Haque, M.; Sartelli, M.; Mckimm, J.; Bakar, M. A. Health Care-Associated Infections – an Overview. *Infect. Drug Resist.* **2018**, *11*, 2321–2333.

(4) Hernández, G.; Rico, P.; Díaz, E.; Rello, J. Nosocomial Lung Infections in Adult Intensive Care Units. *Microbes Infect.* **2004**, *6*, 1004–1014.

(5) Woodhead, M.; Blasi, F.; Ewig, S.; Huchon, G.; Leven, M.; Ortqvist, A.; Schaberg, T.; Torres, A.; van der Heijden, G.; Verheij, T. J. M. Guidelines for the Management of Adult Lower Respiratory Tract Infections. *Eur. Respir. J.* **2005**, *26*, 1138–1180.

(6) Høiby, N. Recent Advances in the Treatment of Pseudomonas Aeruginosa Infections in Cystic Fibrosis. *BMC Med.* **2011**, *9*, 205–2016.

(7) Emami, F.; Mostafavi Yazdi, S. J.; Na, D. H. Poly(Lactic Acid)/Poly(Lactic-Co-Glycolic Acid) Particulate Carriers for Pulmonary Drug Delivery. *J. Pharm. Investig.* **2019**, *49*, 427–442.

(8) Hogg, J. C.; Coxson, H. O.; Brumwell, M. L.; Beyers, N.; Doerschuk, C. M.; MacNee, W.; Wiggs, B. R. Erythrocyte and Polymorphonuclear Cell Transit Time and Concentration in Human Pulmonary Capillaries. *J. Appl. Physiol.* **1994**, *77*, 1795–1800.

(9) Townsley, M. I. Structure and Composition of Pulmonary Arteries, Capillaries, and Veins. In *Structure and composition of pulmonary arteries, capillaries, and veins. Comprehensive Physiology*; 2012; pp 675–709.

(10) Short, A. C.; Montoya, M. L.; Gebb, S. A.; Presson, R. G.; Wagner, W. W.; Capen, R. L. Pulmonary Capillary Diameters and Recruitment Characteristics in Subpleural and Interior Networks. *J. Appl. Physiol.* **1996**, *80*, 1568–1573.

(11) Smola, M.; Vandamme, T.; Sokolowski, A. Nanocarriers as Pulmonary Drug Delivery Systems to Treat and to Diagnose Respiratory and Non Respiratory Diseases. *Int. J. Nanomedicine* **2008**, *3*, 1–19.

(12) Suarez, S.; Hickey, A. J. Drug Properties Affecting Aerosol Behavior. *Respir. Care* **2000**, *45*, 652–666.

(13) Knudsen, L.; Ochs, M. The Micromechanics of Lung Alveoli: Structure and Function of Surfactant and Tissue Components. *Histochem. Cell Biol.* **2018**, *150*, 661–676.

(14) Fahy, John V., B. F. D. Airway Mucus Function and Dysfunction. *N. Engl. J. Med.* **2010**, *363*, 2233–2247.

(15) Fronius, M.; Clauss, W. G.; Althaus, M. Why Do We Have to Move Fluid to Be Able to Breathe? *Front. Physiol.* **2012**, *3*, 146.

(16) Zepp, J. A.; Morrisey, E. E. Cellular Crosstalk in the Development and Regeneration of the Respiratory System. *Nat. Rev. Mol. Cell Biol.* **2019**, *20*, 551–566.

(17) Bastacky, J.; Lee, C. Y. C.; Goerke, J.; Koushafar, H.; Yager, D.; Kenaga, L.; Speed, T. P.; Chen, Y.; Clements, J. A. Alveolar Lining Layer Is Thin and Continuous: Low-Temperature Scanning Electron Microscopy of Rat Lung. *J. Appl. Physiol.* **1995**, *79*, 1615–1628.

(18) Sanders, N.; Rudolph, C.; Braeckmans, K.; De Smedt, S. C.; Demeester, J. Extracellular Barriers in Respiratory Gene Therapy. *Adv. Drug Deliv. Rev.* **2009**, *61*, 115–127.

(19) Gil, J. Microcirculation of the Lung: Functional and Anatomic Aspects. In *Textbook of Pulmonary Vascular Disease*; Yuan, J. J., Garcia, J. G. N., West, J. B., Hales, C. A., Rich, S., Archer, S. L., Eds.; Springer, Boston, MA, 2011; pp 13–24.

(20) Rizzo, A. N.; Fraidenburg, D. R.; and Yuan, J. X.-J. Pulmonary Vascular Anatomy. In *PanVascular Medicine*; Lanzer, P., Ed.; Springer, Berlin, Heidelberg, 2015; pp 4041–4056.

(21) Maina, J. N.; West, J. B. Thin and Strong! The Bioengineering Dilemma in the Structural and Functional Design of the Blood-Gas Barrier. *Physiol. Rev.* **2005**, *85*, 811–844.

(22) Nicod, L. P. Lung Defences: An Overview. *Eur. Respir. Rev.* **2005**, *14*, 45–50.

(23) Labiris, N. R.; Dolovich, M. B. Pulmonary Drug Delivery. Part I: Physiological Factors Affecting Therapeutic Effectiveness of Aerosolized Medications. *Br. J. Clin. Pharmacol.* **2003**, *56*, 588–599.

(24) Lewis, B. W.; Patial, S.; Saini, Y. Immunopathology of Airway Surface Liquid Dehydration Disease. *J. Immunol. Res.* **2019**, *2019*, 2180409.

(25) Fröhlich, E.; Mercuri, A.; Wu, S.; Salar-Behzadi, S. Measurements of Deposition, Lung Surface Area and Lung Fluid for Simulation of Inhaled Compounds. *Front. Pharmacol.* **2016**, *7*, 1–10.

(26) Karamaoun, C.; Sobac, B.; Mauroy, B.; Van Muylem, A.; Haut, B. New Insights into the Mechanisms Controlling the Bronchial Mucus Balance. *PLoS One* **2018**, *13*, 1–20.

(27) Atanasova, K. R.; Reznikov, L. R. Strategies for Measuring Airway Mucus and Mucins. *Respir. Res.* **2019**, *20*, 1–14.

(28) Patton, J. S.; Byron, P. R. Inhaling Medicines: Delivering Drugs to the Body through the Lungs. *Nat. Rev. Drug Discov.* **2007**, *6*, 67–74.

(29) Leiva-Juárez, M. M.; Kolls, J. K.; Evans, S. E. Lung Epithelial Cells: Therapeutically Inducible Effectors of Antimicrobial Defense. *Mucosal Immunol.* **2018**, *11*, 21–34.

(30) Stone, K. C., Mercer, R. R., Gehr, P., Stockstill, B., Crapo, J. D. Allometric Relationships of Cell Numbers and Size in the Mammalian Lung. *Am. Respir. Cell Mol. Biol.* **1992**, *6*, 235–243.

(31) Bates, D. V.; Hansen-Flaschen, J. Respiratory Disease. *Encyclopædia Britannica*; Encyclopædia Britannica, 2019.

(32) Smith, A. M.; and McCullers, J. A. Secondary Bacterial Infections in Influenza Virus Infection Pathogenesis. In *Influenza Pathogenesis and Control - Volume I*; Compans, R. W., and Oldstone, M. B. A., Eds.; Springer International Publishing: Cham, 2014; Vol. 385, pp 327–356.

(33) Ritsema, J. A. S.; Van Der Weide, H.; Te Welscher, Y. M.; Goessens, W. H. F.; Van

Nostrum, C. F.; Storm, G.; Bakker-Woudenberg, I. A. J. M.; Hays, J. P. Antibiotic-Nanomedicines: Facing the Challenge of Effective Treatment of Antibiotic-Resistant Respiratory Tract Infections. *Future Microbiol.* **2018**, *13*, 1683–1692.

(34) Mackenzie, G. The Definition and Classification of Pneumonia. *Pneumonia* **2016**, *8*, 1–5.

(35) Smith, I. Mycobacterium Tuberculosis Pathogenesis and Molecular Determinants of Virulence. *Society* **2003**, *16*, 463–496.

(36) Ryndak, M. B.; Laal, S. Mycobacterium Tuberculosis Primary Infection and Dissemination: A Critical Role for Alveolar Epithelial Cells. *Front. Cell. Infect. Microbiol.* **2019**, *9*, 299.

(37) Kiedrowski, M. R.; Bomberger, J. M. Viral-Bacterial Co-Infections in the Cystic Fibrosis Respiratory Tract. *Front. Immunol.* **2018**, *9*, 3067.

(38) Gaspar, M. C.; Couet, W.; Olivier, J. C.; Pais, A. A. C. C.; Sousa, J. J. S. Pseudomonas Aeruginosa Infection in Cystic Fibrosis Lung Disease and New Perspectives of Treatment: A Review. *Eur. J. Clin. Microbiol. Infect. Dis.* **2013**, *32*, 1231–1252.

(39) Kumar, V.; Abbas, A. K.; Aster, J. C. Lungs. In *Robbins Basic Pathology*; Elsevier, 2017; pp 495–548.

(40) Sengupta, S.; Chattopadhyay, M. K.; Grossart, H. P. The Multifaceted Roles of Antibiotics and Antibiotic Resistance in Nature. *Front. Microbiol.* **2013**, *4*, 47.

(41) Sultan, I.; Rahman, S.; Jan, A. T.; Siddiqui, M. T.; Mondal, A. H.; Haq, Q. M. R. Antibiotics, Resistome and Resistance Mechanisms: A Bacterial Perspective. *Front. Microbiol.* **2018**, *9*, 2066.

(42) Peterson, E.; Kaur, P. Antibiotic Resistance Mechanisms in Bacteria: Relationships between Resistance Determinants of Antibiotic Producers, Environmental Bacteria, and Clinical Pathogens. *Front. Microbiol.* **2018**, *9*, 2928.

(43) Boolchandani, M.; D'Souza, A. W.; Dantas, G. Sequencing-Based Methods and Resources to Study Antimicrobial Resistance. *Nat. Rev. Genet.* **2019**, *20*, 356–370.

(44) Ho, D. K.; Nichols, B. L. B.; Edgar, K. J.; Murgia, X.; Loretz, B.; Lehr, C. M. Challenges and Strategies in Drug Delivery Systems for Treatment of Pulmonary Infections. *Eur. J. Pharm. Biopharm.* **2019**, *144*, 110–124.

(45) Velino, C.; Carella, F.; Adamiano, A.; Sanguinetti, M.; Vitali, A.; Catalucci, D.; Bugli, F.; Iafisco, M. Nanomedicine Approaches for the Pulmonary Treatment of Cystic Fibrosis. *Front. Bioeng. Biotechnol.* **2019**, *7*, 406.

(46) Ramirez, J. A. Overview of Community-Acquired Pneumonia in Adults. In *UpToDate*; Bond, S., Ed.; UpToDate, Waltham, MA, 2019; (accessed Mar 3, 2020).

(47) Metlay, J. P.; Waterer, G. W.; Long, A. C.; Anzueto, A.; Brozek, J.; Crothers, K.; Cooley, L. A.; Dean, N. C.; Fine, M. J.; Flanders, S. A.; et al. Diagnosis and Treatment of Adults with Community-Acquired Pneumonia. *Am. J. Respir. Crit. Care Med.* **2019**, *200*, E45–E67.

(48) Lim, W. S.; Baudouin, S.; George, R.; Hill, A.; Jamieson, C.; Le Jeune, I.; Macfarlane, J.; Read, R.; Roberts, H.; Levy, M.; et al. British Thoracic Society Guidelines for the Management of Community Acquired Pneumonia in Adults: Update 2009. *Thorax* **2009**, *64*.

(49) Polverino, E.; Goeminne, P. C.; McDonnell, M. J.; Aliberti, S.; Marshall, S. E.; Loebinger, M. R.; Murris, M.; Cantón, R.; Torres, A.; Dimakou, K.; et al. European Respiratory Society Guidelines for the Management of Adult Bronchiectasis. *Eur. Respir. J.* **2017**, *50*.

(50) Barker, A. F. Treatment of Bronchiectasis in Adults. In *UpToDate*; Hollingsworth, H., Ed.; UpToDate, Waltham, MA, 2020.

(51) UK Cystic Fibrosis Trust Antibiotic Working Group. *Antibiotic Treatment for Cystic Fibrosis – 3rd Edition*; 2009; http://www.cftrust.org.uk/aboutcf/publications/consensusdoc/Antibiotic_treatment_for_Cystic_Fibrosis.pdf.

(52) Smyth, A. R.; Bell, S. C.; Bojcin, S.; Bryon, M.; Duff, A.; Flume, P.; Kashirskaya, N.; Munck, A.; Ratjen, F.; Schwarzenberg, S. J.; et al. European Cystic Fibrosis Society Standards of Care: Best Practice Guidelines. *J. Cyst. Fibros.* **2014**, *13*, S23–S42.

(53) Castellani, C.; Duff, A. J. A.; Bell, S. C.; Heijerman, H. G. M.; Munck, A.; Ratjen, F.; Sermet-Gaudelus, I.; Southern, K. W.; Barben, J.; Flume, P. A.; et al. European Cystic Fibrosis Society Best Practice Guidelines: The 2018 Revision. *J. Cyst. Fibros.* **2018**, *17*, 153–178.

(54) Doring, G.; Conway, S. P.; Heijerman, H. G. M.; Hodson, M. E.; Hoiby, N.; Smyth, A.; Touw, D. J. Antibiotic Therapy against Pseudomonas Aeruginosa in Cystic Fibrosis. *Eur. Respir. J.* **2000**, *16*, 749–767.

(55) Migliori, G. B.; Sotgiu, G.; Rosales-Klintz, S.; Centis, R.; D'Ambrosio, L.; Abubakar, I.; Bothamley, G.; Caminero, J. A.; Cirillo, D. M.; Dara, M.; et al. ERS/ECDC Statement: European Union Standards for Tuberculosis Care, 2017 Update. *Eur. Respir. J.* **2018**, *51*.

(56) Nahid, P.; Dorman, S. E.; Alipanah, N.; Barry, P. M.; Brozek, J. L.; Cattamanchi, A.; Chaisson, L. H.; Chaisson, R. E.; Daley, C. L.; Grzemska, M.; et al. Official American Thoracic Society/Centers for Disease Control and Prevention/Infectious Diseases Society of America Clinical Practice Guidelines: Treatment of Drug-Susceptible Tuberculosis. *Clin. Infect. Dis.* **2016**, *63*, e147–e195.

(57) Laws, M.; Shaaban, A.; Rahman, K. M. Antibiotic Resistance Breakers: Current Approaches and Future Directions. *FEMS Microbiol. Rev.* **2019**, *43*, 490–516.

(58) Aslam, B.; Wang, W.; Arshad, M. I.; Khurshid, M.; Muzammil, S.; Rasool, M. H.; Nisar, M. A.; Alvi, R. F.; Aslam, M. A.; Qamar, M. U.; et al. Antibiotic Resistance: A Rundown of a Global Crisis. *Infect. Drug Resist.* **2018**, *11*, 1645–1658.

(59) Magiorakos, A. P.; Srinivasan, A.; Carey, R. B.; Carmeli, Y.; Falagas, M. E.; Giske, C. G.; Harbarth, S.; Hindler, J. F.; Kahlmeter, G.; Olsson-Liljequist, B.; et al. Multidrug-Resistant, Extensively Drug-Resistant and Pandrug-Resistant Bacteria: An International Expert Proposal for Interim Standard Definitions for Acquired Resistance. *Clin. Microbiol. Infect.* **2012**, *18*, 268–281.

(60) Mondorf, A. W.; Breier, J.; Hendus, J.; Scherberich, J. E.; Mackenrodt, G.; Shah, P. M.; Stille, W.; Schoeppe, W. The Effect of Aminoglycosides on Proximal Tubular Membranes of Human Kidneys. *Infection* **1979**, *7*, 133–142.

(61) Prayle, A.; Watson, A.; Fortnum, H.; Smyth, A. Side Effects of Aminoglycosides on the Kidney, Ear and Balance in Cystic Fibrosis. *Thorax* **2010**, *65*, 654–658.

(62) Centers for Disease Control and Prevention. *Antibiotic Resistance Threats in the United States*; 2019; https://www.cdc.gov/drugresistance/biggest-threats.html.

(63) Tacconelli, E.; Carrara, E.; Savoldi, A.; Harbarth, S.; Mendelson, M.; Monnet, D. L.; Pulcini, C.; Kahlmeter, G.; Kluytmans, J.; Carmeli, Y.; et al. Discovery, Research, and Development of New Antibiotics: The WHO Priority List of Antibiotic-Resistant Bacteria and

Tuberculosis. *Lancet Infect. Dis.* **2018**, *18*, 318–327.

(64) World Health Organization. *Global Action Plan on Antimicrobial Resistance*; 2015; https://www.who.int/antimicrobial-resistance/publications/global-action-plan/en/.

(65) Butler, M. S.; Blaskovich, M. A.; Cooper, M. A. Antibiotics in the Clinical Pipeline at the End of 2015. *J. Antibiot. (Tokyo).* **2017**, *70*, 3–24.

(66) Pew Research Center. *Antibiotics Currently in Clinical Development*; 2019; http://www.pewtrusts.org/en/multimedia/data-visualizations/2014/antibiotics-currently-in-clinical-development.

(67) Theuretzbacher, U.; Gottwalt, S.; Beyer, P.; Butler, M.; Czaplewski, L.; Lienhardt, C.; Moja, L.; Paul, M.; Paulin, S.; Rex, J. H.; et al. Analysis of the Clinical Antibacterial and Antituberculosis Pipeline. *Lancet Infect. Dis.* **2019**, *19*, e40–e50.

(68) Pew Research Center. *Antibiotics Currently in Clinical Development*; 2018; http://www.pewtrusts.org/en/multimedia/data-visualizations/2014/antibiotics-currently-in-clinical-development.

(69) Pew Research Center. *Antibiotics Currently in Clinical Development*; 2015; http://www.pewtrusts.org/en/multimedia/data-visualizations/2014/antibiotics-currently-in-clinical-development.

(70) Pew Research Center. *Antibiotics Currently in Clinical Development*; 2017; https://www.pewtrusts.org/en/research-and-analysis/data-visualizations/2014/antibiotics-currently-in-clinical-development.

(71) Guilhelmelli, F.; Vilela, N.; Albuquerque, P.; Derengowski, L. da S.; Silva-Pereira, I.; Kyaw, C. M. Antibiotic Development Challenges: The Various Mechanisms of Action of Antimicrobial Peptides and of Bacterial Resistance. *Front. Microbiol.* **2013**, *4*, 353.

(72) Lewies, A.; Du Plessis, L. H.; Wentzel, J. F. Antimicrobial Peptides: The Achilles' Heel of Antibiotic Resistance? *Probiotics Antimicrob. Proteins* **2019**, *11*, 370–381.

(73) Koo, H. B.; Seo, J. Antimicrobial Peptides under Clinical Investigation. *Pept. Sci.* **2019**, *111*, e24122.

(74) Gordon, Y. J.; Romanowski, E. G.; McDermott, A. M. Mini Review: A Review of Antimicrobial Peptides and Their Therapeutic Potential as Anti-Infective Drugs. *Curr. Eye Res.* **2005**, *30*, 505–515.

(75) Guaní-Guerra, E.; Santos-Mendoza, T.; Lugo-Reyes, S. O.; Terán, L. M. Antimicrobial Peptides: General Overview and Clinical Implications in Human Health and Disease. *Clin. Immunol.* **2010**, *135*, 1–11.

(76) Zharkova, M. S.; Orlov, D. S.; Golubeva, O. Y.; Chakchir, O. B.; Eliseev, I. E.; Grinchuk, T. M.; Shamova, O. V. Application of Antimicrobial Peptides of the Innate Immune System in Combination with Conventional Antibiotics-a Novel Way to Combat Antibiotic Resistance? *Front. Cell. Infect. Microbiol.* **2019**, *9*, 128.

(77) Pletzer, D.; Hancock, R. E. W. Antibiofilm Peptides: Potential as Broad Spectrum Agents. *J. Bacteriol.* **2016**, *198*, 2572–2578.

(78) Lewis, K. Platforms for Antibiotic Discovery. *Nat. Rev. Drug Discov.* **2013**, *12*, 371–387.

(79) Geladari, A.; Simitsopoulou, M.; Antachopoulos, C.; Roilides, E. Dose-Dependent Synergistic Interactions of Colistin with Rifampin, Meropenem, and Tigecycline against

Carbapenem- Resistant Klebsiella Pneumoniae Biofilm. *Antimicrob. Agents Chemother.* **2019**, *63*, 1–10.

(80) World Health Organization. *Antibacterial Agents in Clinical Development: An Analysis of the Antibacterial Clinical Development Pipeline, Including Tuberculosis*; 2017.

(81) Lin, L.; Nonejuie, P.; Munguia, J.; Hollands, A.; Olson, J.; Dam, Q.; Kumaraswamy, M.; Rivera, H.; Corriden, R.; Rohde, M.; et al. Azithromycin Synergizes with Cationic Antimicrobial Peptides to Exert Bactericidal and Therapeutic Activity Against Highly Multidrug-Resistant Gram-Negative Bacterial Pathogens. *EBioMedicine* **2015**, *2*, 690–698.

(82) Dosler, S.; Alev Gerceker, A. In Vitro Activities of Antimicrobial Cationic Peptides; Melittin and Nisin, Alone or in Combination with Antibiotics against Gram-Positive Bacteria. *J. Chemother.* **2012**, *24*, 137–143.

(83) Zhang, Y.; Liu, Y.; Sun, Y.; Liu, Q.; Wang, X.; Li, Z.; Hao, J. In Vitro Synergistic Activities of Antimicrobial Peptide Brevinin-2CE with Five Kinds of Antibiotics against Multidrug-Resistant Clinical Isolates. *Curr. Microbiol.* **2014**, *68*, 685–692.

(84) Rishi, P.; Preet, S.; Bharrhan, S.; Verma, I. In Vitro and in Vivo Synergistic Effects of Cryptdin 2 and Ampicillin against Salmonella. *Antimicrob. Agents Chemother.* **2011**, *55*, 4176–4182.

(85) Rémy, B.; Mion, S.; Plener, L.; Elias, M.; Chabrière, E.; Daudé, D. Interference in Bacterial Quorum Sensing: A Biopharmaceutical Perspective. *Front. Pharmacol.* **2018**, *9*, 203.

(86) Kalia, V. C. Quorum Sensing Inhibitors: An Overview. *Biotechnol. Adv.* **2013**, *31*, 224–245.

(87) Wang, L.; Hu, C.; Shao, L. The Antimicrobial Activity of Nanoparticles: Present Situation and Prospects for the Future. *Int. J. Nanomedicine* **2017**, *12*, 1227–1249.

(88) Kumar, M.; Curtis, A.; Hoskins, C. Application of Nanoparticle Technologies in the Combat against Anti-Microbial Resistance. *Pharmaceutics* **2018**, *10*, 1–17.

(89) Shaikh, S.; Nazam, N.; Rizvi, S. M. D.; Ahmad, K.; Baig, M. H.; Lee, E. J.; Choi, I. Mechanistic Insights into the Antimicrobial Actions of Metallic Nanoparticles and Their Implications for Multidrug Resistance. *Int. J. Mol. Sci.* **2019**, *20*, 1–15.

(90) Derbali, R. M.; Aoun, V.; Moussa, G.; Frei, G.; Tehrani, S. F.; Del'Orto, J. C.; Hildgen, P.; Roullin, V. G.; Chain, J. L. Tailored Nanocarriers for the Pulmonary Delivery of Levofloxacin against Pseudomonas Aeruginosa: A Comparative Study. *Mol. Pharm.* **2019**, *16*, 1906–1916.

(91) Cipolla, D.; Blanchard, J.; Gonda, I. Development of Liposomal Ciprofloxacin to Treat Lung Infections. *Pharmaceutics* **2016**, *8*, 1–31.

(92) d'Angelo, I.; Conte, C.; La Rotonda, M. I.; Miro, A.; Quaglia, F.; Ungaro, F. Improving the Efficacy of Inhaled Drugs in Cystic Fibrosis: Challenges and Emerging Drug Delivery Strategies. *Adv. Drug Deliv. Rev.* **2014**, *75*, 92–111.

(93) Labiris, N. R.; Dolovich, M. B. Pulmonary Drug Delivery. Part II: The Role of Inhalant Delivery Devices and Drug Formulations in Therapeutic Effectiveness of Aerosolized Medications. *Br. J. Clin. Pharmacol.* **2003**, *56*, 600–612.

(94) Darquenne, C.; Fleming, J. S.; Katz, I.; Martin, A. R.; Schroeter, J.; Usmani, O. S.; Venegas, J.; Schmid, O. Bridging the Gap Between Science and Clinical Efficacy: Physiology, Imaging, and Modeling of Aerosols in the Lung. *J. Aerosol Med. Pulm. Drug Deliv.* **2016**, *29*, 107–126.

(95) Patil, T. S.; Deshpande, A. S. Nanostructured Lipid Carriers-Based Drug Delivery for Treating Various Lung Diseases: A State-of-the-Art Review. *Int. J. Pharm.* **2018**, *547*, 209–225.

(96) Bronchiectasis News Today. FDA Maintains Refusal of Aradigm ' s Bronchiectasis Bacteria Therapy and Recommends Further Study https://bronchiectasisnewstoday.com/2019/02/28/fda-maintains-refusal-of-aradigms-apulmiq-recommends-future-trial/ (accessed Mar 10, 2020).

(97) European Medicines Agency. *Bramitob - EMA/612853/2015*; 2015; https://www.ema.europa.eu/documents/psusa/spironolactone-list-nationally-authorised-medicinal-products-psusa/00002780/201803_en.pdf.

(98) European Medicines Agency. *Tobi Podhaler - EMEA/H/C/002155 - IAIN/0042*; 2011; https://www.ema.europa.eu/en/medicines/human/EPAR/tobi-podhaler.

(99) European Medicines Agency. Quinsair - EMEA/H/C/002789 - R/0022, 2015.

(100) European Medicines Agency. *Cayston - EMEA/H/C/000996*; 2009.

(101) European Medicines Agency. *Colobreathe - EMEA/H/C/001225 - IAIN/0043*; 2012; https://www.ema.europa.eu/en/medicines/human/EPAR/colobreathe.

(102) Iyer, R.; Hsia, C.; Nguyen, K. Nano-Therapeutics for the Lung: State-of-the-Art and Future Perspectives. *Curr. Pharm. Des.* **2015**, *21*, 5233–5244.

(103) Shirley, M. Amikacin Liposome Inhalation Suspension: A Review in Mycobacterium Avium Complex Lung Disease. *Drugs* **2019**, *79*, 555–562.

(104) Li, Z.; Zhang, Y.; Wurtz, W.; Lee, J. K.; Malinin, V. S.; Durwas-Krishnan, S.; Meers, P.; Perkins, W. R. Characterization of Nebulized Liposomal Amikacin (Arikace^{TM}) as a Function of Droplet Size. *J. Aerosol Med. Pulm. Drug Deliv.* **2008**, *21*, 245–253.

(105) Rukavina, Z.; Vanić, Ž. Current Trends in Development of Liposomes for Targeting Bacterial Biofilms. *Pharmaceutics* **2016**, *8*, 18.

(106) Alhajlan, M.; Alhariri, M.; Omri, A. Efficacy and Safety of Liposomal Clarithromycin and Its Effect on Pseudomonas Aeruginosa Virulence Factors. *Antimicrob. Agents Chemother.* **2013**, *57*, 2694–2704.

(107) Priemel, P. A.; Wang, Y.; Bohr, A.; Water, J. J.; Yang, M.; Mørck Nielsen, H. Poly(Ethylene Carbonate)-Containing Polylactic Acid Microparticles with Rifampicin Improve Drug Delivery to Macrophages. *J. Pharm. Pharmacol.* **2018**, *70*, 1009–1021.

(108) Hu, Y.; Li, M.; Zhang, M.; Jin, Y. Inhalation Treatment of Idiopathic Pulmonary Fibrosis with Curcumin Large Porous Microparticles. *Int. J. Pharm.* **2018**, *551*, 212–222.

(109) Gaspar, M. C.; Pais, A. A. C. C.; Sousa, J. J. S.; Brillaut, J.; Olivier, J. C. Development of Levofloxacin-Loaded PLGA Microspheres of Suitable Properties for Sustained Pulmonary Release. *Int. J. Pharm.* **2019**, *556*, 117–124.

(110) Liu, Z.; Li, X.; Xiu, B.; Duan, C.; Li, J.; Zhang, X.; Yang, X.; Dai, W.; Johnson, H.; Zhang, H.; et al. A Novel and Simple Preparative Method for Uniform-Sized PLGA Microspheres: Preliminary Application in Antitubercular Drug Delivery. *Colloids Surfaces B Biointerfaces* **2016**, *145*, 679–687.

(111) Ernst, J.; Klinger-Strobel, M.; Arnold, K.; Thamm, J.; Hartung, A.; Pletz, M. W.; Makarewicz, O.; Fischer, D. Polyester-Based Particles to Overcome the Obstacles of Mucus

and Biofilms in the Lung for Tobramycin Application under Static and Dynamic Fluidic Conditions. *Eur. J. Pharm. Biopharm.* **2018**, *131*, 120–129.

(112) Cheow, W. S.; Hadinoto, K. Enhancing Encapsulation Efficiency of Highly Water-Soluble Antibiotic in Poly(Lactic-Co-Glycolic Acid) Nanoparticles: Modifications of Standard Nanoparticle Preparation Methods. *Colloids Surfaces A Physicochem. Eng. Asp.* **2010**, *370*, 79–86.

(113) Günday Türeli, N.; Torge, A.; Juntke, J.; Schwarz, B. C.; Schneider-Daum, N.; Türeli, A. E.; Lehr, C. M.; Schneider, M. Ciprofloxacin-Loaded PLGA Nanoparticles against Cystic Fibrosis P. Aeruginosa Lung Infections. *Eur. J. Pharm. Biopharm.* **2017**, *117*, 363–371.

(114) Sharma, R.; Saxena, D.; Dwivedi, A. K.; Misra, A. Drug Combinations to Target Alveolar Macrophages for Treatment of Pulmonary Tuberculosis. *Pharm. Res.* **2001**, *18*, 1405–1410.

(115) Manca, M. L.; Mourtas, S.; Dracopoulos, V.; Fadda, A. M.; Antimisiaris, S. G. PLGA, Chitosan or Chitosan-Coated PLGA Microparticles for Alveolar Delivery?. A Comparative Study of Particle Stability during Nebulization. *Colloids Surfaces B Biointerfaces* **2008**, *62*, 220–231.

(116) Ventura, C. A.; Tommasini, S.; Crupi, E.; Giannone, I.; Cardile, V.; Musumeci, T.; Puglisi, G. Chitosan Microspheres for Intrapulmonary Administration of Moxifloxacin: Interaction with Biomembrane Models and in Vitro Permeation Studies. *Eur. J. Pharm. Biopharm.* **2008**, *68*, 235–244.

(117) Gaspar, M. C.; Sousa, J. J. S.; Pais, A. A. C. C.; Cardoso, O.; Murtinho, D.; Serra, M. E. S.; Tewes, F.; Olivier, J. C. Optimization of Levofloxacin-Loaded Crosslinked Chitosan Microspheres for Inhaled Aerosol Therapy. *Eur. J. Pharm. Biopharm.* **2015**, *96*, 65–75.

(118) Dolovich, M. B. 18F-Fluorodeoxyglucose Positron Emission Tomographic Imaging of Pulmonary Functions, Pathology, and Drug Delivery. *Proc. Am. Thorac. Soc.* **2009**, *6*, 477–485.

(119) Porra, L.; Dégrugilliers, L.; Broche, L.; Albu, G.; Strengell, S.; Suhonen, H.; Fodor, G. H.; Peták, F.; Suortti, P.; Habre, W.; et al. Quantitative Imaging of Regional Aerosol Deposition, Lung Ventilation and Morphology by Synchrotron Radiation CT. *Sci. Rep.* **2018**, *8*, 1–10.

(120) Colombo, C.; Alicandro, G.; Gambazza, S.; Mileto, P.; Mari, A.; Grespan, E.; Nazzari, E.; Russo, M. C.; Battezzati, A. Ventilation Inhomogeneity Is Associated with OGTT-Derived Insulin Secretory Defects in Cystic Fibrosis. *Pediatr. Pulmonol.* **2019**, *54*, 141–149.

(121) Bajc, M.; Jonson, B. Ventilation/Perfusion SPECT for Diagnosis of Pulmonary Embolism and Other Diseases. *Int. J. Mol. Imaging* **2011**, *2011*, 1–7.

(122) Weibel, E. R.; Gomez, D. M. Architecture of the Human Lung. *Science (80-.).* **1962**, *137*, 577–585.

(123) Bajc, M.; Neilly, J. B.; Miniati, M.; Schuemichen, C.; Meignan, M.; Jonson, B. EANM Guidelines for Ventilation/Perfusion Scintigraphy : Part 1. Pulmonary Imaging with Ventilation/Perfusion Single Photon Emission Tomography. *Eur. J. Nucl. Med. Mol. Imaging* **2009**, *36*, 1356–1370.

(124) Huo, D.; Deng, S.; Li, L.; Ji, J. Studies on the Poly(Lactic-Co-Glycolic) Acid Microspheres of Cisplatin for Lung-Targeting. *Int. J. Pharm.* **2005**, *289*, 63–67.

(125) Zhang, W.; Jiang, X.; Hu, J.; Fu, C. Rifampicin Polylactic Acid Microspheres for Lung Targeting. *J. Microencapsul.* **2000**, *17*, 785–788.

(126) Fan, Y.; Shan-Guang, W.; Yu-Fang, P.; Feng-Lan, S.; Tao, L. Preparation and Characteristics of Erythromycin Microspheres for Lung Targeting. *Drug Dev. Ind. Pharm.* **2009**, *35*, 639–645.

(127) Ramaiah, B.; Harsha Nagaraja, S.; Kapanigowda, U. G.; Boggarapu, P. R.; Subramanian, R. High Azithromycin Concentration in Lungs by Way of Bovine Serum Albumin Microspheres as Targeted Drug Delivery: Lung Targeting Efficiency in Albino Mice. *DARU J. Pharm. Sci.* **2016**, *24*, 1–11.

(128) Harsha, S.; R, C.; Rani, S. Ofloxacin Targeting to Lungs by Way of Microspheres. *Int. J. Pharm.* **2009**, *380*, 127–132.

(129) Qu, S.; Dai, C.; Yang, F.; Huang, T.; Xu, T.; Zhao, L. A Comparison of Two Methods for the Preparation Cefquinome-Loaded Gelatin Microspheres for Lung Targeting https://link.springer.com/article/10.1007%2Fs11095-018-2342-4 (accessed Feb 18, 2020).

(130) Rhodes, B. A.; Zolle, I.; Buchanan, J. W.; Wagner, H. N. Radioactive Albumin Microspheres for Studies of the Pulmonary Circulation. *Radiology* **1969**, *92*, 1453–1460.

(131) Kutscher, H. L.; Chao, P.; Deshmukh, M.; Singh, Y.; Hu, P.; Joseph, L. B.; Reimer, D. C.; Stein, S.; Laskin, D. L.; Sinko, P. J. Threshold Size for Optimal Passive Pulmonary Targeting and Retention of Rigid Microparticles in Rats. *J. Control. Release* **2010**, *143*, 31–37.

(132) Häfeli, U. O.; Saatchi, K.; Elischer, P.; Misri, R.; Bokharaei, M.; Ren??e Labiris, N.; Stoeber, B. Lung Perfusion Imaging with Monosized Biodegradable Microspheres. *Biomacromolecules* **2010**, *11*, 561–567.

(133) Delgado, A.; Soriano, I.; Sánchez, E.; Oliva, M.; Évora, C. Radiolabelled Biodegradable Microspheres for Lung Imaging. *Eur. J. Pharm. Biopharm.* **2000**, *50*, 227–236.

(134) Zhang, R.; Hao, Z.; Ding, Z.; Lü, Z. Preparation and Characterization of Lung-Targeting Cefquinome-Loaded PLGA Microspheres. *J. Wuhan Univ. Technol. Sci. Ed* **2017**, *32*, 494–499.

(135) Lu, B.; Zhang, J. Q.; Yang, H. Lung-Targeting Microspheres of Carboplatin. *Int. J. Pharm.* **2003**, *265*, 1–11.

(136) Sangi, S.; SreeHarsha, N.; Bawadekji, A.; Ali, M. Al. Chemotherapeutic Drug Targeting to Lungs by Way of Microspheres after Intravenous Administration. *Drug Des. Devel. Ther.* **2018**, *12*, 3051–3060.

(137) Hirenkumar, M.; Steven, S. Poly Lactic-Co-Glycolic Acid (PLGA) as Biodegradable Controlled Drug Delivery Carrier. *Polymers (Basel).* **2012**, *3*, 1–19.

(138) Danhier, F.; Ansorena, E.; Silva, J. M.; Coco, R.; Le Breton, A.; Préat, V. PLGA-Based Nanoparticles: An Overview of Biomedical Applications. *J. Control. Release* **2012**, *161*, 505–522.

(139) Li, X.; Jiang, X. Microfluidics for Producing Poly (Lactic-Co-Glycolic Acid)-Based Pharmaceutical Nanoparticles. In *Advanced Drug Delivery Reviews*; Elsevier B.V., 2018; pp 101–114.

(140) Pandey, A.; Jain, D. S. Poly Lactic-Co-Glycolic Acid (PLGA) Copolymer and Its Pharmaceutical Application. In *Handbook of Polymers for Pharmaceutical Technologies: Processing and Applications Processing and Applications*; Thakur, V., Thakur, M., Eds.; Scrivener: Hoboken, New Jersey ; Salem, Massachusetts, 2015; Vol. 2, pp 151–172.

(141) Zhong, H.; Chan, G.; Hu, Y.; Hu, H.; Ouyang, D. A Comprehensive Map of FDA-Approved

Pharmaceutical Products. *Pharmaceutics* **2018**, *10*, 1–19.

(142) Ding, D.; Zhu, Q. Recent Advances of PLGA Micro/Nanoparticles for the Delivery of Biomacromolecular Therapeutics. *Mater. Sci. Eng. C* **2018**, *92*, 1041–1060.

(143) Fredenberg, S.; Wahlgren, M.; Reslow, M.; Axelsson, A. The Mechanisms of Drug Release in Poly(Lactic-Co-Glycolic Acid)-Based Drug Delivery Systems - A Review. *Int. J. Pharm.* **2011**, *415*, 34–52.

(144) Croom, K. F.; Goa, K. L. Levofloxacin: A Review of Its Use in the Treatment of Bacterial Infections in the United States. *Drugs* **2003**, *63*, 2769–2802.

(145) Blondeau, J. M. A Review of the Comparative In-Vitro Activities of 12 Antimicrobial Agents, with a Focus on Five New `respiratory Quinolones'. *J. Antimicrob. Chemother.* **1999**, *43*, 1–11.

(146) Torres, A.; Liapikou, A. Levofloxacin for the Treatment of Respiratory Tract Infections. *Expert Opin. Pharmacother.* **2012**, *13*, 1203–1212.

(147) Alam, M. R.; Hershberger, E.; Zervos, M. J. The Role of Fluoroquinolones in the Treatment of Skin and Soft Tissue Infection. *Curr. Infect. Dis. Rep.* **2002**, *4*, 426–432.

(148) McGregor, J. C.; Allen, G. P.; Bearden, D. T. Levofloxacin in the Treatment of Complicated Urinary Tract Infections and Acute Pyelonephritis. *Ther. Clin. Risk Manag.* **2008**, *4*, 843–853.

(149) Blokhina, S. V.; Sharapova, A. V.; Ol'khovich, M. V.; Volkova, T. V.; Perlovich, G. L. Solubility, Lipophilicity and Membrane Permeability of Some Fluoroquinolone Antimicrobials. *Eur. J. Pharm. Sci.* **2016**, *93*, 29–37.

(150) European Medicines Agency. Tavanic Solution for Infusion - EMEA/H/A-30/1262, 2012.

(151) European Medicines Agency. Tavanic Tablets - EMEA/H/A-30/1262, 2012.

(152) Rodvold, K. A.; Danziger, L. H.; Gotfried, M. H. Steady-State Plasma and Bronchopulmonary Concentrations of Intravenous Levofloxacin and Azithromycin in Healthy Adults. *Antimicrob. Agents Chemother.* **2003**, *47*, 2450–2457.

(153) Gotfried, M. H.; Danziger, L. H.; Rodvold, K. A. Steady-State Plasma and Intrapulmonary Concentrations of Levofloxacin and Ciprofloxacin in Healthy Adult Subjects. *Chest* **2001**, *119*, 1114–1122.

(154) Kiem, S.; Schentag, J. J. Interpretation of Antibiotic Concentration Ratios Measured in Epithelial Lining Fluid. *Antimicrob. Agents Chemother.* **2008**, *52*, 24–36.

(155) Rubinstein, E. History of Quinolones and Their Side Effects. *Chemotherapy* **2001**, *47*, 3–8.

(156) Carbon, C. Comparison of Side Effects of Levofloxacin versus Other Fluoroquinolones. *Chemotherapy* **2001**, *47*, 9–14.

(157) European Medicines Agency. Disabling and potentially permanent side effects lead to suspension or restrictions of quinolone and fluoroquinolone antibiotics https://www.ema.europa.eu/en/news/disabling-potentially-permanent-side-effects-lead-suspension-restrictions-quinolone-fluoroquinolone (accessed Jan 26, 2020).

(158) United States Food and Drug Administration. FDA reinforces safety information about serious low blood sugar levels and mental health side effects with fluoroquinolone antibiotics; requires label changes https://www.fda.gov/drugs/drug-safety-and-

availability/fda-reinforces-safety-information-about-serious-low-blood-sugar-levels-and-mental-health-side (accessed Jan 16, 2020).

(159) Gaspar, M. C.; Grégoire, N.; Sousa, J. J. S.; Pais, A. A. C. C.; Lamarche, I.; Gobin, P.; Olivier, J. C.; Marchand, S.; Couet, W. Pulmonary Pharmacokinetics of Levofloxacin in Rats after Aerosolization of Immediate-Release Chitosan or Sustained-Release PLGA Microspheres. *Eur. J. Pharm. Sci.* **2016**, *93*, 184–191.

(160) Hadiya, S.; Liu, X.; Abd El-Hammed, W.; Elsabahy, M.; Aly, S. A. Levofloxacin-Loaded Nanoparticles Decrease Emergence of Fluoroquinolone Resistance in Escherichia Coli. *Microb. Drug Resist.* **2018**, *24*, 1098–1107.

(161) Cheow, W. S.; Hadinoto, K. Factors Affecting Drug Encapsulation and Stability of Lipid-Polymer Hybrid Nanoparticles. *Colloids Surfaces B Biointerfaces* **2011**, *85*, 214–220.

(162) Cheow, W. S.; Chang, M. W.; Hadinoto, K. The Roles of Lipid in Anti-Biofilm Efficacy of Lipid-Polymer Hybrid Nanoparticles Encapsulating Antibiotics. *Colloids Surfaces A Physicochem. Eng. Asp.* **2011**, *389*, 158–165.

(163) Imran, M.; Shah, M. R.; Ullah, F.; Ullah, S.; Elhissi, A. M. A.; Nawaz, W.; Ahmad, F.; Sadiq, A.; Ali, I. Sugar-Based Novel Niosomal Nanocarrier System for Enhanced Oral Bioavailability of Levofloxacin. *Drug Deliv.* **2016**, *23*, 3653–3664.

(164) Bagga, P.; Siddiqui, H. H.; Akhtar, J.; Mahmood, T.; Zahera, M.; Khan, M. S. Gold Nanoparticles Conjugated Levofloxacin: For Improved Antibacterial Activity Over Levofloxacin Alone. *Curr. Drug Deliv.* **2017**, *14*, 1114–1119.

(165) Islan, G. A.; Cacicedo, M. L.; Bosio, V. E.; Castro, G. R. Development and Characterization of New Enzymatic Modified Hybrid Calcium Carbonate Microparticles to Obtain Nano-Architectured Surfaces for Enhanced Drug Loading. *J. Colloid Interface Sci.* **2015**, *439*, 76–87.

(166) Islan, G. A.; Ruiz, M. E.; Morales, J. F.; Sbaraglini, M. L.; Enrique, A. V.; Burton, G.; Talevi, A.; Bruno-Blanch, L. E.; Castro, G. R. Hybrid Inhalable Microparticles for Dual Controlled Release of Levofloxacin and DNase: Physicochemical Characterization and in Vivo Targeted Delivery to the Lungs. *J. Mater. Chem. B* **2017**, *5*, 3132–3144.

(167) Hung, L. H.; Teh, S. Y.; Jester, J.; Lee, A. P. PLGA Micro/Nanosphere Synthesis by Droplet Microfluidic Solvent Evaporation and Extraction Approaches. *Lab Chip* **2010**, *10*, 1820–1825.

(168) Montazeri, L.; Bonakdar, S.; Taghipour, M.; Renaud, P.; Baharvand, H. Modification of PDMS to Fabricate PLGA Microparticles by a Double Emulsion Method in a Single Microfluidic Device. *Lab Chip* **2016**, *16*, 2596–2600.

(169) Ma, J.; Hui, Y. S.; Zhang, M.; Yu, Y.; Wen, W.; Qin, J. Honeycomb Structures:Facile Synthesis of Biomimetic Honeycomb Material with Biological Functionality. *Small* **2013**, *9*, 497–503.

(170) Xu, Q.; Hashimoto, M.; Dang, T. T.; Hoare, T.; Kohane, D. S.; Whitesides, G. M.; Langer, R.; Anderson, D. G.; David, H. Preparation of Monodisperse Biodegradable Polymer Microparticles Using a Microfluidic Flow-Focusing Device for Controlled Drug Delivery. *Small* **2009**, *5*, 1575–1581.

(171) Swider, E.; Koshkina, O.; Tel, J.; Cruz, L. J.; de Vries, I. J. M.; Srinivas, M. Customizing Poly(Lactic-Co-Glycolic Acid) Particles for Biomedical Applications. *Acta Biomater.* **2018**, *73*, 38–51.

(172) Ramazani, F.; Chen, W.; Van Nostrum, C. F.; Storm, G.; Kiessling, F.; Lammers, T.; Hennink, W. E.; Kok, R. J. Strategies for Encapsulation of Small Hydrophilic and Amphiphilic Drugs in PLGA Microspheres: State-of-the-Art and Challenges. *Int. J. Pharm.* **2016**, *499*, 358–367.

(173) Christopher, G. F.; Anna, S. L. Microfluidic Methods for Generating Continuous Droplet Streams. *J. Phys. D. Appl. Phys.* **2007**, *40*, R319–R336.

(174) Liu, Z.; Fontana, F.; Python, A.; Hirvonen, J. T.; Santos, H. A. Microfluidics for Production of Particles: Mechanism, Methodology, and Applications. *Small* **2019**, *16*, 1904673.

(175) Rezvantalab, S.; Keshavarz Moraveji, M. Microfluidic Assisted Synthesis of PLGA Drug Delivery Systems. *RSC Adv.* **2019**, *9*, 2055–2072.

(176) Duncanson, W. J.; Lin, T.; Abate, A. R.; Seiffert, S.; Shah, R. K.; Weitz, D. A. Microfluidic Synthesis of Advanced Microparticles for Encapsulation and Controlled Release. *Lab Chip* **2012**, *12*, 2135–2145.

(177) Perez, A.; Hernández, R.; Velasco, D.; Voicu, D.; Mijangos, C. Poly (Lactic-Co-Glycolic Acid) Particles Prepared by Microfluidics and Conventional Methods. Modulated Particle Size and Rheology. *J. Colloid Interface Sci.* **2015**, *441*, 90–97.

(178) Anna, S. L.; Mayer, H. C. Microscale Tipstreaming in a Microfluidic Flow Focusing Device. *Phys. Fluids* **2006**, *18*, 121512.

(179) Tundo, P.; Selva, M. The Chemistry of Dimethyl Carbonate. *Acc. Chem. Res.* **2002**, *35*, 706–716.

(180) Dixit, K.; Athawale, R. B.; Singh, S. Quality Control of Residual Solvent Content in Polymeric Microparticles. *J. Microencapsul.* **2015**, *32*, 107–122.

(181) Kinoshita, K.; Parra, E.; Hussein, A.; Utoft, A.; Walke, P.; de Bruijn, R.; Needham, D. From Single Microparticles to Microfluidic Emulsification: Fundamental Properties (Solubility, Density, Phase Separation) from Micropipette Manipulation of Solvent, Drug and Polymer Microspheres. *Processes* **2016**, *4*, 49.

(182) Chaisri, W.; Ghassemi, A. H.; Hennink, W. E.; Okonogi, S. Enhanced Gentamicin Loading and Release of PLGA and PLHMGA Microspheres by Varying the Formulation Parameters. *Colloids Surfaces B Biointerfaces* **2011**, *84*, 508–514.

(183) Mylonaki, I.; Allémann, E.; Delie, F.; Jordan, O. Imaging the Porous Structure in the Core of Degrading PLGA Microparticles: The Effect of Molecular Weight. *J. Control. Release* **2018**, *286*, 231–239.

(184) Bruschi, M. L. Mathematical Models of Drug Release. In *Strategies to Modify the Drug Release from Pharmaceutical Systems*; 2015; pp 63–86.

(185) Lao, L. L.; Peppas, N. A.; Boey, F. Y. C.; Venkatraman, S. S. Modeling of Drug Release from Bulk-Degrading Polymers. *Int. J. Pharm.* **2011**, *418*, 28–41.

(186) Wiggins, J. S.; Hassan, M. K.; Mauritz, K. A.; Storey, R. F. Hydrolytic Degradation of Poly(d,l-Lactide) as a Function of End Group: Carboxylic Acid vs. Hydroxyl. *Polymer* **2006**, *47*, 1960–1969.

(187) Klose, D.; Siepmann, F.; Elkharraz, K.; Siepmann, J. PLGA-Based Drug Delivery Systems: Importance of the Type of Drug and Device Geometry. *Int. J. Pharm.* **2008**, *354*, 95–103.

(188) Gasmi, H.; Danede, F.; Siepmann, J.; Siepmann, F. Does PLGA Microparticle Swelling

Control Drug Release? New Insight Based on Single Particle Swelling Studies. *J. Control. Release* **2015**, *213*, 120–127.

(189) Vey, E.; Rodger, C.; Meehan, L.; Booth, J.; Claybourn, M.; Miller, A. F.; Saiani, A. The Impact of Chemical Composition on the Degradation Kinetics of Poly(Lactic-Co-Glycolic) Acid Copolymers Cast Films in Phosphate Buffer Solution. *Polym. Degrad. Stab.* **2012**, *97*, 358–365.

(190) Vey, E.; Roger, C.; Meehan, L.; Booth, J.; Claybourn, M.; Miller, A. F.; Saiani, A. Degradation Mechanism of Poly(Lactic-Co-Glycolic) Acid Block Copolymer Cast Films in Phosphate Buffer Solution. *Polym. Degrad. Stab.* **2008**, *93*, 1869–1876.

(191) Kłodzińska, S. N.; Wan, F.; Jumaa, H.; Sternberg, C.; Rades, T.; Nielsen, H. M. Utilizing Nanoparticles for Improving Anti-Biofilm Effects of Azithromycin: A Head-to-Head Comparison of Modified Hyaluronic Acid Nanogels and Coated Poly (Lactic-Co-Glycolic Acid) Nanoparticles. *J. Colloid Interface Sci.* **2019**, *555*, 595–606.

(192) Cheow, W. S.; Chang, M. W.; Hadinoto, K. Antibacterial Efficacy of Inhalable Levofloxacin-Loaded Polymeric Nanoparticles against E. Coli Biofilm Cells: The Effect of Antibiotic Release Profile. *Pharm. Res.* **2010**, *27*, 1597–1609.

(193) Masadeh, M. M.; Alzoubi, K. H.; Ahmed, W. S.; Magaji, A. S. In Vitro Comparison of Antibacterial and Antibiofilm Activities of Selected Fluoroquinolones against Pseudomonas Aeruginosa and Methicillin-Resistant Staphylococcus Aureus. *Pathogens* **2019**, *8*.

(194) Sierra, J. M.; Marco, F.; Ruiz, J.; Jiménez de Anta, M. T.; Vila, J. Correlation between the Activity of Different Fluoroquinolones and the Presence of Mechanisms of Quinolone Resistance in Epidemiologically Related and Unrelated Strains of Methicillin-Susceptible and -Resistant Staphylococcus Aureus. *Clin. Microbiol. Infect.* **2002**, *8*, 781–790.

(195) Kolate, A.; Kore, G.; Lesimple, P.; Baradia, D.; Patil, S.; Hanrahan, J. W.; Misra, A. Polymer Assisted Entrapment of Netilmicin in PLGA Nanoparticles for Sustained Antibacterial Activity. *J. Microencapsul.* **2015**, *32*, 61–74.

(196) Dillen, K.; Vandervoort, J.; Van Den Mooter, G.; Verheyden, L.; Ludwig, A. Factorial Design, Physicochemical Characterisation and Activity of Ciprofloxacin-PLGA Nanoparticles. *Int. J. Pharm.* **2004**, *275*, 171–187.

(197) Nemeth, J.; Oesch, G.; Kuster, S. P. Bacteriostatic versus Bactericidal Antibiotics for Patients with Serious Bacterial Infections: Systematic Review and Meta-Analysis. *J. Antimicrob. Chemother.* **2015**, *70*, 382–395.

(198) Klepser, M. E.; Ernst, E. J.; Petzold, C. R.; Rhomberg, P.; Doern, G. V. Comparative Bactericidal Activities of Ciprofloxacin, Clinafloxacin, Grepafloxacin, Levofloxacin, Moxifloxacin, and Trovafloxacin against Streptococcus Pneumoniae in a Dynamic in Vitro Model. *Antimicrob. Agents Chemother.* **2001**, *45*, 673–678.

(199) Golini, G.; Favari, F.; Marchetti, F.; Fontana, R. Bacteriostatic and Bactericidal Activity of Levofloxacin against Clinical Isolates from Cystic Fibrosis Patients. *Eur. J. Clin. Microbiol. Infect. Dis.* **2004**, *23*, 798–800.

(200) Tasso, L.; De Andrade, C.; Dalla Costa, T. Pharmacokinetic/Pharmacodynamic Modelling of the Bactericidal Activity of Free Lung Concentrations of Levofloxacin and Gatifloxacin against Streptococcus Pneumoniae. *Int. J. Antimicrob. Agents* **2011**, *38*, 307–313.

(201) Weber, M.; Steinle, H.; Golombek, S.; Hann, L.; Schlensak, C.; Wendel, H. P.; Avci-Adali, M. Blood-Contacting Biomaterials: In Vitro Evaluation of the Hemocompatibility. *Front.*

Bioeng. Biotechnol. **2018**, *6*, 99.

(202) Dobrovolskaia, M. A.; McNeil, S. E. Immunological Properties of Engineered Nanomaterials: An Introduction. *Handb. Immunol. Prop. Eng. Nanomater. Second Ed.* **2016**, *1*, 1–24.

(203) Dobrovolskaia, M. A.; Aggarwal, P.; Hall, J. B.; McNeil, S. E. Preclinical Studies to Understand Nanoparticle Interaction with the Immune System and Its Potential Effects on Nanoparticle Biodistribution. *Mol. Pharm.* **2008**, *5*, 487–495.

(204) Fornaguera, C.; Calderó, G.; Mitjans, M.; Vinardell, M. P.; Solans, C.; Vauthier, C. Interactions of PLGA Nanoparticles with Blood Components: Protein Adsorption, Coagulation, Activation of the Complement System and Hemolysis Studies. *Nanoscale* **2015**, *7*, 6045–6058.

(205) Thasneem, Y. M.; Sajeesh, S.; Sharma, C. P. Effect of Thiol Functionalization on the Hemo-Compatibility of PLGA Nanoparticles. *J. Biomed. Mater. Res. - Part A* **2011**, *99 A*, 607–617.

(206) Tracy, M. A.; Ward, K. L.; Firouzabadian, L.; Wang, Y.; Dong, N.; Qian, R.; Zhang, Y. Factors Affecting the Degradation Rate of Poly(Lactide-Co-Glycolide) Microspheres In Vivo and In Vitro. *Biomaterials* **1999**, *20*, 1057–1062.

(207) Wadas, T. J.; Wong, E. H.; Weisman, G. R.; Anderson, C. J. Coordinating Radiometals of Copper, Gallium, Indium, Yttrium, and Zirconium for PET and SPECT Imaging of Disease. *Chem. Rev.* **2010**, *110*, 2858–2902.

(208) Wattendorf, U.; Merkle, H. P. PEGylation as a Tool for the Biomedical Engineering of Surface Modified Microparticles. *J. Pharm. Sci.* **2008**, *97*, 4655–4669.

(209) Owens, D. E.; Peppas, N. A. Opsonization, Biodistribution, and Pharmacokinetics of Polymeric Nanoparticles. *Int. J. Pharm.* **2006**, *307*, 93–102.

(210) Madani, F.; Bessodes, M.; Lakrouf, A.; Vauthier, C.; Scherman, D.; Chaumeil, J. C. PEGylation of Microspheres for Therapeutic Embolization: Preparation, Characterization and Biological Performance Evaluation. *Biomaterials* **2007**, *28*, 1198–1208.

(211) Sousa, I.; Claro, V.; Pereira, J. L.; Amaral, A. L.; Cunha-Silva, L.; De Castro, B.; Feio, M. J.; Pereira, E.; Gameiro, P. Synthesis, Characterization and Antibacterial Studies of a Copper(II) Levofloxacin Ternary Complex. *J. Inorg. Biochem.* **2012**, *110*, 64–71.

(212) Thakur, A.; Rodríguez-Rodríguez, C.; Saatchi, K.; Rose, F.; Esposito, T.; Nosrati, Z.; Andersen, P.; Christensen, D.; Häfeli, U. O.; Foged, C. Dual-Isotope SPECT/CT Imaging of the Tuberculosis Subunit Vaccine H56/CAF01: Induction of Strong Systemic and Mucosal IgA and T-Cell Responses in Mice upon Subcutaneous Prime and Intrapulmonary Boost Immunization. *Front. Immunol.* **2018**, *9*, 2825.

(213) Yang, L.; Gradl, R.; Dierolf, M.; Möller, W.; Kutschke, D.; Feuchtinger, A.; Hehn, L.; Donnelley, M.; Günther, B.; Achterhold, K.; et al. Multimodal Precision Imaging of Pulmonary Nanoparticle Delivery in Mice: Dynamics of Application, Spatial Distribution, and Dosimetry. *Small* **2019**, *15*.

(214) Taplin, V. G.; MacDonald, N. S. Radiochemistry of Macroaggregated Albumin and Newer Lung Scanning Agents. *Semin. Nucl. Med.* **1971**, *1*, 132–152.

(215) Sun, H.; Li, H.; Sadler, P. J. Transferrin as a Metal Ion Mediator. *Chem. Rev.* **1999**, *99*, 2817–2842.

(216) Price, E. W.; Cawthray, J. F.; Bailey, G. A.; Ferreira, C. L.; Boros, E.; Adam, M. J.; Orvig,

C. H 4octapa: An Acyclic Chelator for 111In Radiopharmaceuticals. *J. Am. Chem. Soc.* **2012**, *134*, 8670–8683.

(217) Price, E. W.; Orvig, C. Matching Chelators to Radiometals for Radiopharmaceuticals. *Chem. Soc. Rev.* **2014**, *43*, 260–290.

(218) Harris, W. R.; Chen, Y.; Wein, K. Equilibrium Constants for the Binding of Indium(III) to Human Serum Transferrin. *Inorg. Chem.* **1994**, *33*, 4991–4998.

(219) Ando, A.; Ando, I.; Hiraki, T.; Hisada, K. Relation between the Location of Elements in the Periodic Table and Various Organ-Uptake Rates. *Int. J. Radiat. Appl. Instrumentation.* **1989**, *16*, 57–80.

7 Appendix

Research manuscript:

Agnoletti M, Rodrıguez-Rodriguez C, Kłodzinska SN, Esposito TVF, Saatchi K, Mørck Nielsen H, Häfeli UO. Monosized Polymeric Microspheres for Passive Lung Targeting: Biodistribution and Pharmacokinetics after Intravenous Administration. *ACS Nano.* 2020, 14, 6693-6706.

Appendix

Monosized Polymeric Microspheres for Passive Lung Targeting: Biodistribution and Pharmacokinetics after Intravenous Administration

Research manuscript

Agnoletti M, Rodrıguez-Rodriguez C, Kłodzinska SN, Esposito TVF, Saatchi K, Mørck Nielsen H, Häfeli UO

ACS Nano, 2020, 14, 6693-6706

ACSNANO

www.acsnano.org

ARTICLE

Monosized Polymeric Microspheres Designed for Passive Lung Targeting: Biodistribution and Pharmacokinetics after Intravenous Administration

Monica Agnoletti, Cristina Rodríguez-Rodríguez, Sylvia N. Kłodzińska, Tullio V. F. Esposito, Katayoun Saatchi, Hanne Mørck Nielsen,* and Urs O. Häfeli*

Cite This: *ACS Nano* 2020, 14, 6693−6706

Read Online

ACCESS | Metrics & More | Article Recommendations | Supporting Information

ABSTRACT: **Local as well as systemic therapy is often used to treat bacterial lung infections. Delivery of antibiotics to the vascular side of infected lung tissue using lung-targeting microspheres (MS) is a good alternative to conventional administration routes, allowing for localized high levels of antibiotics. This delivery route can also complement inhaled antibiotic therapy, especially in the case of compromised lung function. We prepared and characterized monodisperse poly(lactic-*co*-glycolic acid) (PLGA) MS loaded with levofloxacin using a flow-focusing glass microfluidic chip. *In vitro* characterization showed that the encapsulated LVX displayed a biphasic controlled release during 5 days and preserved its antibacterial activity. The MS degradation was investigated *in vitro* by cross-sectioning the MS using a focused ion beam scanning electron microscope and *in vivo* by histological examination of lung tissue from mice intravenously administered with the MS. The MS showed changes in the surface morphology and internal matrix, whereas the degradation *in vivo* was 3 times faster than that *in vitro*. No effect on the viability of endothelial and lung epithelial cells or hemolytic activity was observed. To evaluate the pharmacokinetics and biodistribution of the MS, complete quantitative imaging of the ^{111}indium-labeled PLGA MS was performed *in vivo* with single-photon emission computed tomography imaging over 10 days. The PLGA MS distributed homogeneously in the lung capillaries. Overall, intravenous administration of 12 μm PLGA MS is suitable for passive lung targeting and pulmonary therapy.**

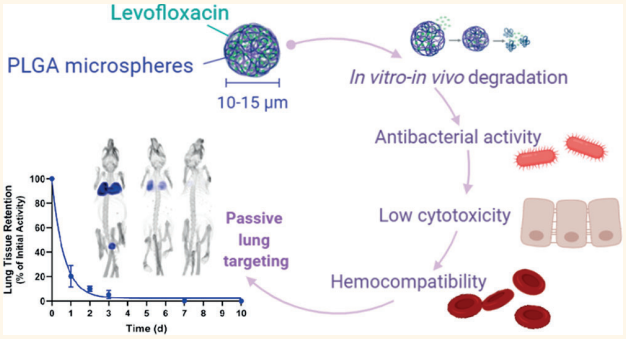

KEYWORDS: *microfluidics, levofloxacin, PLGA, microspheres, passive lung targeting, FIB-SEM, SPECT/CT*

Lower respiratory tract infections, such as pneumonia or bronchiolitis, are some of the leading causes of mortality and morbidity worldwide. In 2016, 2.4 million deaths were caused by such infections, making them the sixth leading cause of mortality for all ages and the leading cause of death among children under 5 years of age.[1] The recommended treatment for bacterial infections in the lungs includes oral or intravenous (IV) administration of amoxicillin, tetracyclines, macrolides, respiratory fluoroquinolones, such as levofloxacin and moxifloxacin, or, in the case of pseudomonal infections, administration of antipseudomonal fluoroquinolones, such as levofloxacin or ciprofloxacin, in combination with an antipseudomonal β-lactam antibiotic.[2,3] Although fluoroquinolones have been used extensively in the last decades, their use has recently been associated with long-lasting, disabling, and potentially permanent side effects, such as tendon inflammation and rupture, depression, as well as problems with memory and sleeping.[4,5] This brought the European Medicines Agency and the United States Food and Drug Administration to restrict their use in patients with underlying conditions, which predispose them to the occurrence of side effects.[4,5] Additionally, the uncontrolled use of antibiotics, including fluoroquinolones, in the last decades has dramatically increased the amount of

Received: December 12, 2019
Accepted: May 11, 2020
Published: May 11, 2020

https://dx.doi.org/10.1021/acsnano.9b09773
ACS Nano 2020, 14, 6693−6706

antibiotic-resistant pathogens.[6] In the clinic, this translates to the need for larger doses of antibiotics in order to obtain effective drug concentrations in the lungs. Such high doses are associated with an increase in undesirable side effects.

The obstacles encountered during antibiotic treatment have directed the attention of researchers toward development of formulations that allow targeted delivery of sufficiently high antibiotic doses directly to the infection site. This is particularly interesting when considering the treatment of pulmonary infections as delivering the antibiotic selectively to the lungs will not only reduce the dose needed to achieve a therapeutic effect and reduce systemic side effects caused by the antibiotic, but also diminish the risk of development of multi-drug-resistant bacteria. Although guidelines for treating lung infections currently recommend oral and IV administration routes, many lung-targeted inhalation drug delivery systems have been developed and investigated during the last decades. Several dry powder and nebulized suspensions, emulsions, and solutions are approved (*e.g.*, tobramycin (TOBI Podhaler)[7,8] and colistimethate sodium (Colobreathe)[9,10] for *Pseudomonas aeruginosa* infections) or investigated at preclinical and clinical stages.[11,12]

However, for patients with compromised lung function or respiratory tract obstruction (*e.g.*, due to inflammation and mucus plugs), the delivery of antibiotics by inhalation is difficult and often not sufficiently effective to eliminate all of the pathogens. For this reason, targeted delivery of drugs to the lungs from the vasculature around the thin alveolar epithelium is considered to be the most relevant, and using biocompatible drug carriers with sustained drug release will minimize the dosing frequency. To entrap the IV-injected particulate carrier system in the alveolar capillaries, the particles must be sized slightly larger than the capillary diameter (*i.e.*, 7.5 ± 2.3 μm in healthy adults,[13] 6.6 ± 1.6 and 7.5 ± 1.7 μm in rats and dogs[14]), leading to the complete entrapment in the lungs after being pumped through the heart and into the pulmonary blood circulation. This passive lung targeting strategy is currently approved in nuclear medicine for determining lung perfusion in humans with ^{99m}Tc-labeled macroaggregated albumin (MAA) (Pulmolite, Pharmalucence, MA, USA; DraxImage, Draxis Health, Montreal, Canada), where only 0.5−0.7% of healthy lung capillaries are embolized after IV injection of a standard dose of MAA (*i.e.*, 200,000−700,000 MAA particles).[15−17] Passive lung targeting was also recently investigated in preclinical work for the treatment of lung tumors (with cisplatin),[18] tuberculosis (with rifampicin),[19] and pulmonary infections (with erythromycin,[20] azithromycin,[21] ofloxacin,[22] and cefquinome[23,24]). However, previous works that evaluated particles for IV treatment of pulmonary infection displayed a particle size distribution in the range of 3−50 μm. Such large particle size distributions are associated with a high risk of local vascular resistance alterations as not only capillaries but also arterioles could be clogged. This may result in incomplete dose delivery to the lungs and distribution in nontargeted organs, such as liver and kidneys.[20−22,24]

With the hypothesis that a narrow particle size distribution is essential for optimal passive lung targeting, we prepared microspheres (MS) loaded with the antibiotic levofloxacin (LVX) using a flow-focusing microfluidic chip. We combined a wide range of methods to optimize, characterize, and gain a comprehensive understanding of the physicochemical properties of the delivery system. The monodisperse, LVX-loaded poly(lactic-*co*-glycolic acid) (PLGA) MS were investigated for *in vitro* drug release, and the associated MS degradation was examined by assessing changes in the surface morphology and in the particle internal structure using the focused ion beam scanning electron microscopy (FIB-SEM) technique. The antibacterial activity, cytotoxicity, and hemocompatibility were evaluated, and the PLGA MS were radiolabeled with ^{111}indium (^{111}In) to quantitatively determine lung uptake in mice by imaging the MS *in vivo* with single-photon emission computed tomography (SPECT/CT) over 10 days and to determine if systemically administered drug delivery systems can target the lungs and potentially treat pulmonary infections.

RESULTS AND DISCUSSION

PLGA Microspheres Displayed a Mean Diameter of 12 μm and a Uniform Size Distribution. Monodisperse PLGA MS with a mean diameter of 12 μm and a coefficient of variation <5.2% were successfully prepared (Table 1 and Figure S1A−D).

Table 1. Particle Size, Drug Content and Encapsulation Efficiency of Fresh and Freeze-Dried Nonloaded and Levofloxacin-Loaded PLGA Microspheres[a]

Formulation (#, form)	Particle size (μm)	CV (%)	Theoretical LVX loading (% w/w)	LVX loading (% w/w)	EE (% w/w)
F0, fresh	12.3 ± 0.4 ns	3.5	-	-	–
F0, freeze-dried	12.5 ± 0.6 ns	4.6	-	-	–
F0i, fresh	11.4 ± 0.5 ns	4.5	-	-	–
DTPA-F0i, fresh	12.0 ± 0.6 ns	4.7	-	-	–
F1, fresh	12.2 ± 0.4 ns	3.5	15	2.2 ± 0.1	13.7 ± 2.0
F1, freeze-dried	11.5 ± 0.4 ns	3.3	15	* 1.8 ± 0.5 ns	12.2 ± 3.10
F2, fresh	12.7 ± 0.5 ns	3.9	15	3.9 ± 0.6 ns	26.5 ± 3.9
F2, freeze-dried	12.1 ± 0.5 ns	4.7	15	* 3.5 ± 0.4	23.4 ± 2.9
F3, fresh	12.5 ± 0.5 ns	3.3	30	5.6 ± 0.4	18.4 ± 0.8
F3, freeze-dried	12.1 ± 0.6 ns	5.2	30	5.0 ± 0.3 ns	16.3 ± 1.1

[a]CV, coefficient of variation (calculated based on 500 microspheres); EE, encapsulation efficiency; LVX, levofloxacin, *p < 0.05, calculated based on three independent batches (N = 3); ns, not significantly different. For particle size, statistical multiple comparisons between all formulations were done. For LVX loading and EE, multiple comparisons between fresh and freeze-dried formulations as well as the different loaded formulations were done. The statistical analysis of the EE followed the analysis of the loading.

No significant differences in physicochemical properties were observed between the fresh and freeze-dried formulations (Table 1). The high uniformity of particle size was achieved using flow focusing in the microfluidic chip, producing uniform droplets (Movie S1), which each turned into a solid and also uniform microsphere after solvent extraction and evaporation. This exquisite control was made possible by controlling many experimental parameters, including flow rates, polymer concentration, and composition of the dispersed phase (DP) and the continuous phase (CP). More specifically, only few combinations of the DP and CP flow rates resulted in the production of monodisperse MS, whereas others resulted in polydisperse MS. In general, in the range of tested flow rates Q (Q_{DP} = 0.5−5 μL/min and Q_{CP} = 30−150 μL/min), we found that particle size decreased by increasing the flow rate of the CP and thus by increasing the flow rate ratio, as previously shown.[25] Moreover, polydispersity decreased by increasing the concentration of PLGA in the DP (0.5−5% w/w), due to the increased viscosity of the DP. From the systematic optimization, the optimal

https://dx.doi.org/10.1021/acsnano.9b09773
ACS Nano 2020, 14, 6693−6706

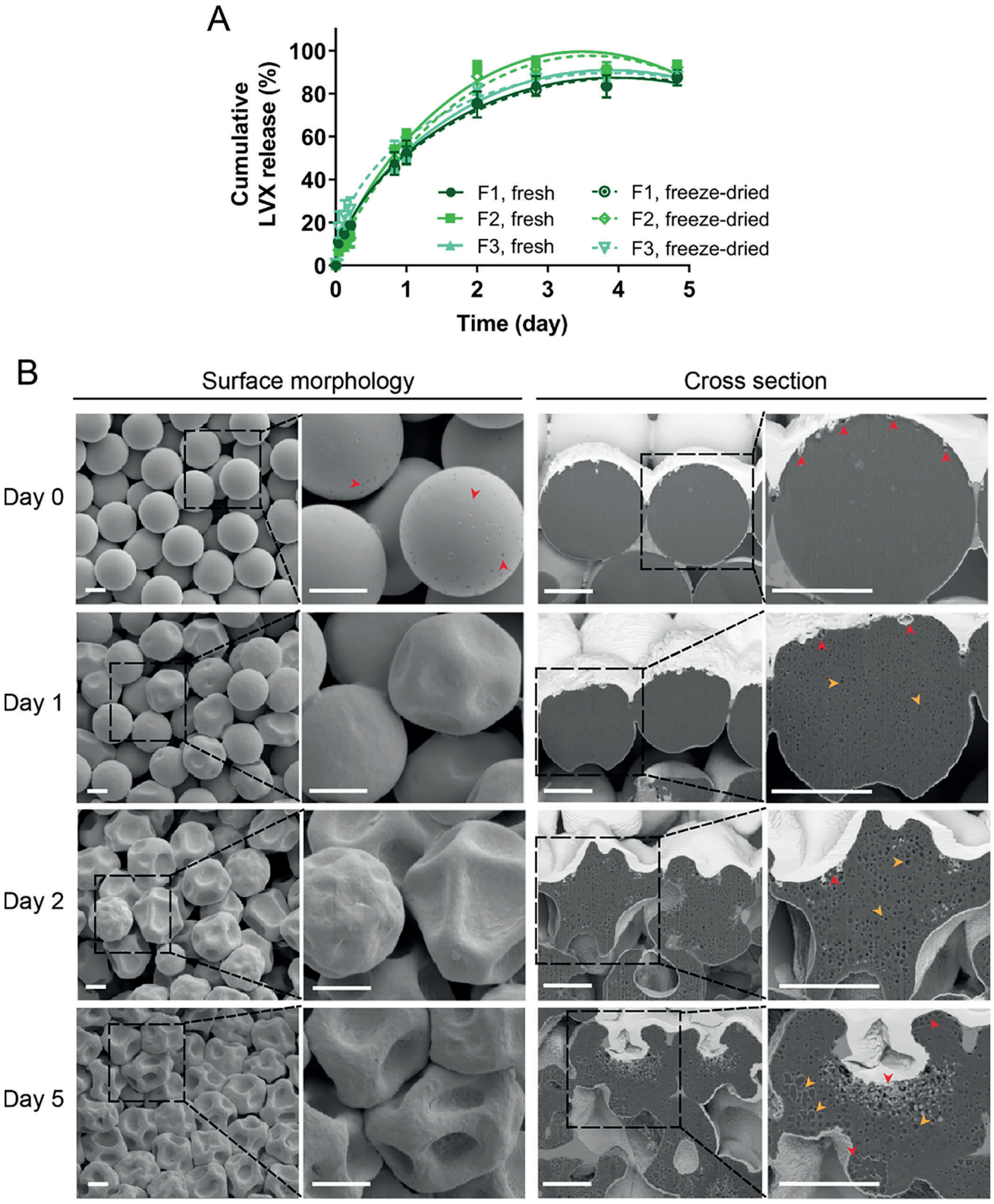

Figure 1. Degradation of PLGA microspheres and associated release of the drug levofloxacin. (A) *In vitro* cumulative release profiles of LVX from PLGA MS (F1, fresh and freeze-dried (dark green); F2, fresh and freeze-dried (light green); F3, fresh and freeze-dried (teal)) in phosphate buffered saline (PBS) and 37 °C, fitted by the Peppas−Sahlin model. Results are expressed as mean ± SD ($N = 3$, $n = 1$). (B) SEM images of F2 PLGA MS and their cross section during degradation. Red arrowheads point to some of the surface pores. Orange arrowheads point to some of the internal cavities. Scale bars: 5 μm.

https://dx.doi.org/10.1021/acsnano.9b09773
ACS Nano 2020, 14, 6693−6706

conditions were found to be Q_{DP} = 3 μL/min, Q_{CP} = 90 μL/min, and 5% (w/v) PLGA concentration in the DP.

Controlled particle size and uniform size distribution are critical for safe passive lung targeting. According to the United States Pharmacopeia, ">90% of albumin aggregated particles must have a size between 10 and 90 μm and no microparticles may be larger than 150 μm".[26] With a more monodisperse particle size distribution, higher selectivity in lung targeting is achieved as measured by the amount of particles reaching the capillaries, without embolizing larger arterioles or accumulating in other organs (*e.g.*, liver, kidneys). According to the literature,[18−24] all previous preclinical work was done with particles with size distributions between 3 and 50 μm that resulted in high lung uptake and relatively high levels of particle biodistribution to other organs.

All of the LVX-loaded PLGA MS had a spherical shape and smooth surface, with evidence of small surface cavities (Figure 1B, day 0). The nonloaded PLGA MS presented a smooth and uniform surface morphology, as shown in Figure S1E−H. A difference in surface morphology between nonloaded and loaded PLGA particles was also reported by Bragagni *et al.*,[27] where prilocaine-loaded PLGA MS showed large surface cavities (or a partially collapsed spherical shape). This effect was concluded to be attributed to the plasticizing effect of the loaded prilocaine.

The LVX-loaded PLGA MS formulations F1, F2, and F3 had a LVX content of approximately 2, 4, and 5.5%, respectively (Table 1). Saturating the CP with LVX doubled both the LVX content and the encapsulation efficiency (EE) (F1 *vs* F2), indicating that by reducing the diffusion of the drug from the organic (*i.e.*, DP) to the water phase (*i.e.*, CP) the drug content of highly water-soluble drugs in hydrophobic polymeric particles can be significantly increased, in agreement with previous work.[28] The LVX content (drug-to-polymer ratio), but not the EE, further significantly increased when the anhydrous form of LVX was replaced with the hemihydrate form (F2 *vs* F3), and the theoretical drug loading was increased from 15 to 30%. The higher drug loading together with an unchanged EE may indicate superior loading of the hemihydrate form but also saturation of the loading capacity. The LVX loading in F3 PLGA MS was satisfactory considering the high water solubility of LVX and the hydrophobic nature of PLGA combined with the oil/water (O/W) single emulsion method of preparation.

These findings support previous reports on the importance of the method of preparation of polymeric MS and formulation parameters (*e.g.*, polymer M_w, composition and concentration of the polymer, type and concentration of the emulsifier, water miscibility of the organic solvent or cosolvents used) for an efficient encapsulation of small hydrophilic and amphiphilic drugs.[29] In line with these reports, increasing the PLGA concentration from 10 to 20% resulted in an increase in gentamicin loading from 2.7 to 6.2% in PLGA MS prepared with the water/oil/water (W/O/W) double emulsion method.[30] Previous work on 2−3 μm PLGA particles loaded with LVX and prepared using W/O/W double emulsion showed a maximum LVX content of 10%.[28,31]

The residual amount of poly(vinyl alcohol) (PVA) present in the suspension of PLGA MS after three washing steps corresponded to 3.3% of the total amount of PVA added per batch (Table S1).

Encapsulated Levofloxacin Was Slowly Released within 5 Days during PLGA Degradation. All LVX-loaded PLGA MS formulations showed similar release profiles, with a fast release of 10−20% of the encapsulated dose within the first 5 h, followed by a gradual slow release up to maximum 85% within 5 days (Figure 1A). This illustrates a typical biphasic diffusion-driven release curve[32] of the LVX-loaded PLGA MS, where the initial fast release is likely due to surface-bound LVX detaching from the MS or to LVX molecules encapsulated close to the periphery of the particles that are easily accessible by hydration and can thus diffuse out through the polymeric matrix. The slow release phase is due to the diffusion of LVX molecules through the pores formed by polymer hydration and degradation. The kinetic profiles of LVX release from all of the PLGA MS were best fitted by the Peppas−Sahlin model, having the highest correlation coefficient values (R^2 = 0.9847−0.9964) and the lowest root mean squared error (RMSE = 2.04−4.83) (Table S2 and Figure S2). According to the Peppas−Sahlin model, the drug release from the polymeric matrix occurs as a result of the combination of two independent mechanisms: the diffusion of the drug (first term of Peppas−Sahlin equation, Table S2) and the transition of the polymer from a semirigid to a flexible state, generating a relaxation of the polymer chains (second term of Peppas−Sahlin equation, Table S2).[33,34] The contribution of the Fickian diffusion was much greater than the polymer relaxation (k_1 = 65.1−76.8 *vs* k_2 = −11.7 to −16.5), indicating that the drug release of LVX from all PLGA MS is mainly controlled by the Fickian diffusion. However, the relaxation mechanism is not negligible as the purely Fickian diffusion exponent *m* (Peppas−Sahlin equation, Table S2) is not equal to *n* in the Korsmeyers−Peppas equation (Table S2).[33,34]

Similar release profiles have previously been reported for 3−5 μm LVX-loaded PLGA MS with a higher and faster burst release of 40% within the first 30 min followed by a slow release phase of 72 h.[28] Larger PLGA MS of 17 μm prepared using the double emulsion W/O/W method also showed to have a biphasic release curve with a dominant burst phase corresponding to 70% of the encapsulated LVX within 30 min.[28] PLGA (Resomer RG 502H, lactide/glycolide ratio 50:50, M_w 7−17 kDa, acid terminated) MS loaded with rifampicin showed to have similar biphasic release profile with 50−80% of rifampicin released after 12 h and release rates directly proportional to the polymer concentrations (3−30%).[35] On the other hand, a completely different release profile was observed for gentamicin-loaded PLGA (lactide/glycolide ratio 60:40) MS where the drug was released over 60 days with a triphasic profile with rates indirectly proportional to the PLGA concentration used.[30] A shift from a bi- to a triphasic release profile was shown by Mylonaki *et al.* over 30 days for atorvastatin-loaded PLGA MS of 16−18 μm prepared with PLGA of increasing M_w.[32] Different release profiles of LVX and ofloxacin were observed in the case of more hydrophilic delivery systems: an almost complete and immediate release of LVX (90% within 30 min) from cross-linked chitosan MS was presented by Gaspar *et al.*, confirming that water-soluble polymers are more suitable for fast release systems of LVX.[36] A different release profile was observed for albumin MS encapsulating ofloxacin, which was completely released within 6 h, showing a fast release of 42% in the first hour.[22] Overall, this shows how release kinetics depend on different factors, including the polymer type (copolymer ratio, crystallinity, M_w), particle diameter, polymer−drug interaction, and diffusion coefficient of the drug.[30,32,37]

To gain a better understanding of particle degradation and its relation to the release mechanism, the MS surface morphology and internal polymeric structure were investigated. Polymer degradation was evident upon exposure to the release medium as both LVX-loaded and nonloaded MS assumed a partially

https://dx.doi.org/10.1021/acsnano.9b09773
ACS Nano 2020, 14, 6693−6706

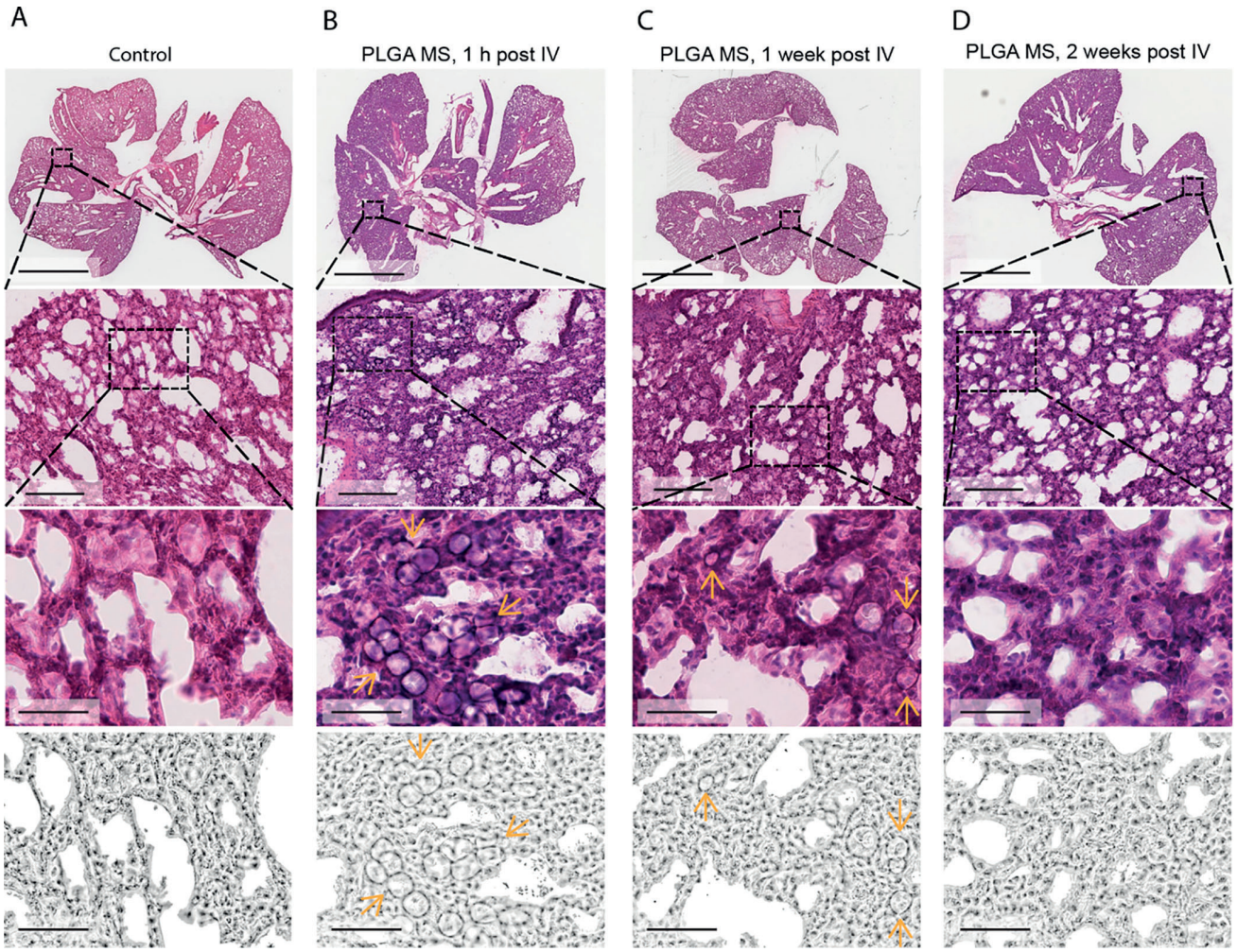

Figure 2. Representative histology images over time of lungs exposed to PLGA microspheres (F0) after intravenous injection. Representative images of H&E stained histological 30 μm coronal lungs sections at 0×, 10×, and 40× magnification after different treatments (first−third rows), and processed images after hematoxylin extraction (fourth row; see Figure S4 for full-sized images). For more details, see the Materials and Methods section. (A) Healthy and untreated lungs. (B−D) Healthy lungs after 1 h, 1 week, and 2 weeks of injection of 3 mg/mouse PLGA MS (corresponding to approximately 300,000 PLGA MS/mouse). Orange arrows point to some of the MS. Scale bars: (first row) 5 mm, (second row) 200 μm, (third and fourth row) 50 μm.

collapsed spherical shape, whereas the surface became rough and porous (Figures 1B and S3). Small pores were visible on the surface of the LVX-loaded PLGA MS and cavities in the internal matrix already after 1 day (cross section images in Figure 1B), whereas no pores were observed on the surface of the nonloaded PLGA MS (Figure S3). The pores and cavities increased in size over time (cross section images in Figure 1B, days 2−5 *vs* day 1). On day 5, substantial degradation of the MS was observed, with the appearance of large cavities close to the surface of the MS. The presence of wrinkles on the surface of MS could not be attributed to the vacuum used during the scanning electron microscopy (SEM) investigation, as optical microscopy images of the MS showed the same behavior (Figure S3). This formation of wrinkles and partially collapsed surface morphology has previously been described[38,39] as the initial event of heterogeneous degradation of PLGA films. The wrinkles occur on the soft surface layer as a consequence of water diffusion in the bulk matrix and the consequent decrease in the polymer glass transition temperature. The hydrolysis of PLGA results in the formation of glycolic acid and lactic acid, which locally decrease the microenvironment pH and catalyze further degradation of the polymer. Although this process takes place in the entire polymer matrix, neutralization of the degradation product on the particle surface by the release media results in reduced autocatalytic activity at the surface.[38,39] Further wrinkling of the particle surface was observed until complete dissolution of the polymer matrix on day 21, similarly to previous reports for 16−18 μm PLGA MS.[32] The nonloaded PLGA MS showed the same degradation mechanism, though without visible surface pores on day 0 (Figure S3).

To evaluate whether the degradation of the MS occurred in a similar manner *in vivo* after IV administration, the MS were administered to mice and their appearance *in situ* in the lungs was assessed. The PLGA MS seemed to degrade faster *in vivo* than *in vitro*, with all MS seemingly dissolved after 1 week (Figure 2C), whereas *in vitro*, the MS took 3 weeks to completely disintegrate (Figure S3). Similarly, Tracy *et al.* showed that the degradation of PLGA MS *in vivo* was 1.7−2.6 times faster than *in vitro*, independently of the polymer end group or molecular weight.[40] They hypothesized that this could be attributed to the presence

https://dx.doi.org/10.1021/acsnano.9b09773
ACS Nano 2020, 14, 6693−6706

Table 2. Minimum Inhibitory Concentration Values of Levofloxacin-Loaded PLGA Microspheres against *E. coli*, *P. aeruginosa*, and *S. aureus*[a]

	MIC range[b] (μg/mL)								
			F0	F1		F2		F3	
bacteria strain	aLVX	hLVX	fresh[c]	fresh[c]	freeze-dried	fresh[c]	freeze-dried	fresh[c]	freeze-dried
E. coli ATCC 25922	0.03	0.03	>30	0.5	1	1	1	0.25	0.5
P. aeruginosa PA01	1	1	>30	4	4	4	4	4	4
S. aureus 15981	0.5	0.5	>30	4	4	4	4	2	4

[a]MIC, minimum inhibitory concentration; aLVX, anhydrous levofloxacin; hLVX, hemihydrate levofloxacin; $N = 1$, $n = 3$. [b]MIC values for F1, F2, and F3 were corrected for the LVX amount released from the PLGA MS during the experimental time (20 h). [c]The fresh MS were stored at 4 °C for 48 h prior to MIC experiments, whereas the freeze-dried MS were dried immediately after preparation. Drug loading of those batches was not significantly different from fresh or freeze-dried MS.

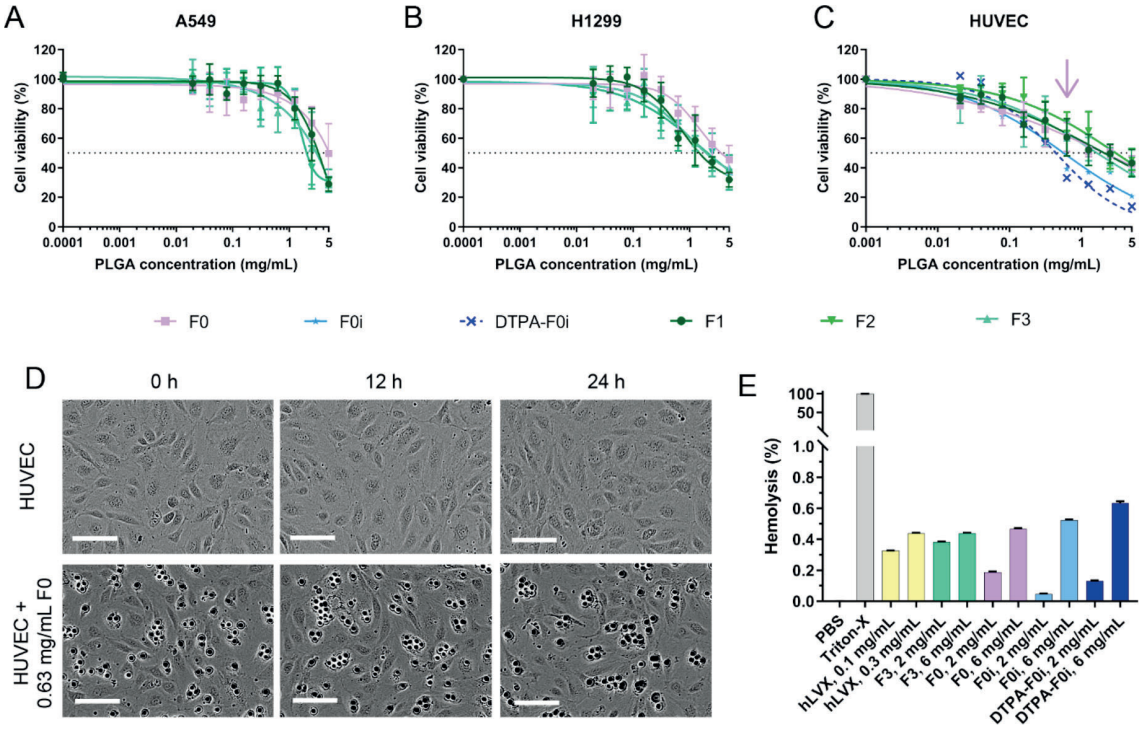

Figure 3. Cytotoxicity and hemocompatibility of PLGA microspheres. (A–C) Cell viability (%) of A549, H1299m and HUVEC cells incubated for 24 h with F0 (light purple), F0i (light blue), DTPA-F0i (blue), F1 (dark green), F2 (light green), F3 (teal) microspheres (MS). The dotted line represents 50% viability. Data are presented as mean ± SD, $N = 3$, except for F0i and DTPA-F0i, where $N = 1$. (D) Representative phase contrast images of HUVEC cells taken using the IncuCyte live-cell analysis system at 0, 12, and 24 h after treatment with media (control, top) or F0 at 0.63 mg/mL PLGA concentration (concentration indicated with the pink arrow in C) (bottom). Scale bars: 100 μm. (E) Hemolysis (%) of human red blood cells caused by free LVX, nonloaded PLGA MS, and LVX-loaded PLGA MS were assessed after 1 h incubation at different concentrations. Data are presented as mean ± SD ($N = 1$, $n = 3$).

of lipids and biological compounds *in vivo* acting as plasticizers and resulting in increasing the uptake of water into the polymer.[40] This results in faster degradation and may explain why particles are only visible in the lungs during the first week. No major surface wrinkling was observed for the MS in the lung tissue. This may be due to relatively low resolution of optical microscopy and the visual interference from the surrounding tissue.

Levofloxacin Antimicrobial Activity Decreased upon Encapsulation in PLGA Microspheres. Both anhydrous and hemihydrate LVX presented the same minimum inhibitory concentration (MIC) against the tested pathogens. However, upon encapsulation of LVX in PLGA particles, a decrease in antimicrobial activity was observed. All three formulations showed an increase in MIC to 4 μg/mL, from 0.5 and 1 μg/mL active compound against *Staphylococcus aureus* and *P. aeruginosa*, respectively. A larger increase in MIC as compared to the nonformulated drug was observed for the formulations when tested against *Escherichia coli*, with an increase from 0.03 to 0.5–1 μg/mL (Table 2). Similarly, a small increase in MIC toward *S. aureus* and *P. aeruginosa* for ciprofloxacin after formulation into PLGA nanoparticles has previously been reported by Dillen *et al.*[41] A 3-fold increase in MIC toward *P. aeruginosa* was also reported for netilmicin after encapsulation in PLGA nanoparticles, and this increase in MIC was attributed to the progressive release of netilmicin from the particles.[42] A small difference in MIC was observed for some of the fresh and freeze-dried formulations, in particular, formulation F1 against *E. coli* and formulation F3 against *E. coli* and *S. aureus*. However, the difference between the MICs for these formulations corresponds

https://dx.doi.org/10.1021/acsnano.9b09773
ACS Nano 2020, 14, 6693–6706

to a 2-fold dilution and is not considered significant, as the precision of the broth dilution method is generally regarded to be within a 2-fold concentration range.[43] Moreover, the dose of LVX delivered and released from the 3 mg dose of PLGA MS is expected to have a bactericidal effect in mice already at 1 h after delivery. In fact, its concentration in the murine alveolar lining fluid is calculated to be much greater (~400×) than the concentration needed for LVX to display a bacteriostatic effect against *P. aeruginosa* and *S. pneumoniae*. No growth inhibition was observed upon exposure to the nonloaded F0 PLGA MS in the tested concentration range (30−0.234 μg/mL, corresponding to the amount of PLGA in LVX-loaded MS) (Table 2). This is in accordance with literature, as PLGA nanoparticles show no inhibition of bacterial growth at concentrations below 1 mg/mL.[44]

PLGA Microspheres Showed Low Toxicity for Endothelial, Lung Epithelial, and Red Blood Cells at the *In Vivo* Dose. As the particles are intended for IV administration and passive targeting to the lungs, the cytotoxicity of PLGA MS was evaluated on endothelial (HUVEC), alveolar lung epithelial (A549), and human lung epithelial (H1299) cell lines. Nonloaded PLGA MS presented IC_{50} values of 1.5, 5, and 1.4 mg/mL for HUVEC, A549, and H1299, respectively (Figure 3A−C), in line with previous reports.[45,46] The LVX-loaded PLGA MS presented similar toxicity for the three tested cell lines with IC_{50} values of 1.4−2 mg/mL for HUVEC (corresponding to 0.03−0.08 mg/mL of loaded LVX), 2.5−3.5 mg/mL for A549 (corresponding to 0.06−0.09 mg/mL of loaded LVX), and 0.7−1.5 mg/mL for H1299 (*i.e.*, 0.01−0.04 mg/mL of loaded LVX) (Figure 3A−C). The cytotoxicity of LVX-loaded PLGA MS (*i.e.*, F1, F2, F3) was not related to the initial fast release of the loaded LVX, as no cytotoxicity was observed at the corresponding concentrations of free LVX (Figure S5A−C). These results indicate that loading the PLGA MS with LVX does not substantially affect the cytotoxicity, similar to the report by Gaspar *et al.* applying bronchial Calu-3 cells for testing.[28] F0i and DTPA-F0i PLGA MS slightly reduced cell viability of HUVEC cells at PLGA MS concentrations above 0.5 mg/mL compared to F0 PLGA MS (Figure 3C). This may be due to the presence of the amino group added to the PLGA to allow chelator conjugation, as nonloaded PLGA MS showed an IC_{50} of 1.4 mg/mL when tested on HUVEC cells. The cytotoxicity of the F0i PLGA MS was not affected by conjugation of DTPA to the amino groups on the PLGA (Figure 3C). The integrity of all cell lines exposed to formulations was confirmed by microscopic observation using the IncuCyte live-cell imaging system. Representative images of HUVEC cells exposed to 0.63 mg/mL of F0 PLGA MS are presented in Figure 3D.

The hemolytic effect of a drug delivery system is an important factor to consider before IV administration. Nonloaded (*i.e.*, F0, F0i, DTPA-F0i) and LVX-loaded PLGA MS (*i.e.*, F3, loaded MS with the highest LVX content) as well as free LVX did not lyse human erythrocytes in the tested concentration range. Additionally, none of the tested formulations induced more than 0.4% hemolysis, even at concentrations corresponding to 3× the dose administered *in vivo* for the components, namely, 6 and 0.3 mg/mL, respectively, for PLGA MS and free LVX, as shown in Figure 3E. The results indicate that the PLGA MS are hemocompatible and approved for safe administration *in vivo*. Previous reports indicate no hemolysis caused by PLGA was observed up to 3 mg/mL of PLGA nanoparticles;[47] however, to the authors' knowledge, no higher concentrations have been reported.

^{111}In-Labeled PLGA Microspheres Distributed Homogeneously in the Lung Capillaries Immediately after Intravenous Injection. The PLGA MS were radiolabeled first by functionalizing the surface with amino groups by adding PLGA-block-poly(ethylene glycol)-amine (PLGA-PEG-NH_2) to the DP (*i.e.*, formulation F0i PLGA MS, **1**, Figure 4A). The

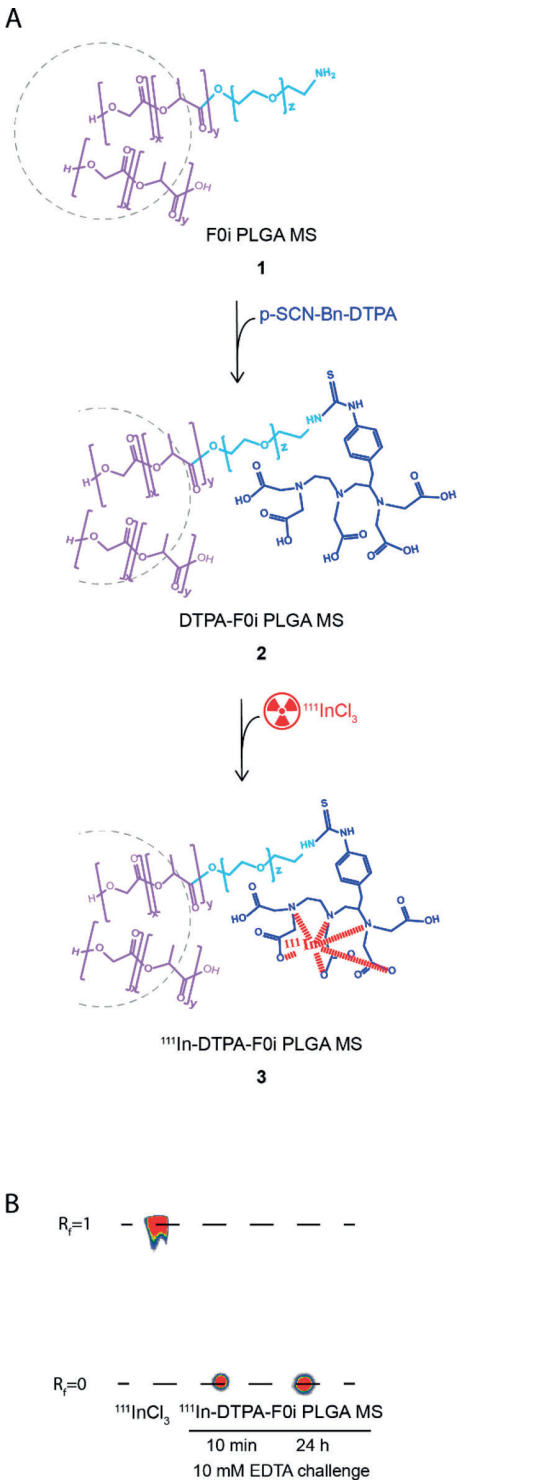

Figure 4. Synthesis of radiolabeled PLGA microspheres. (A) Synthesis of ^{111}In-DTPA-F0i PLGA MS. (B) Radiolabeling efficiency and stability over 24 h using ITLC.

https://dx.doi.org/10.1021/acsnano.9b09773
ACS Nano 2020, 14, 6693−6706

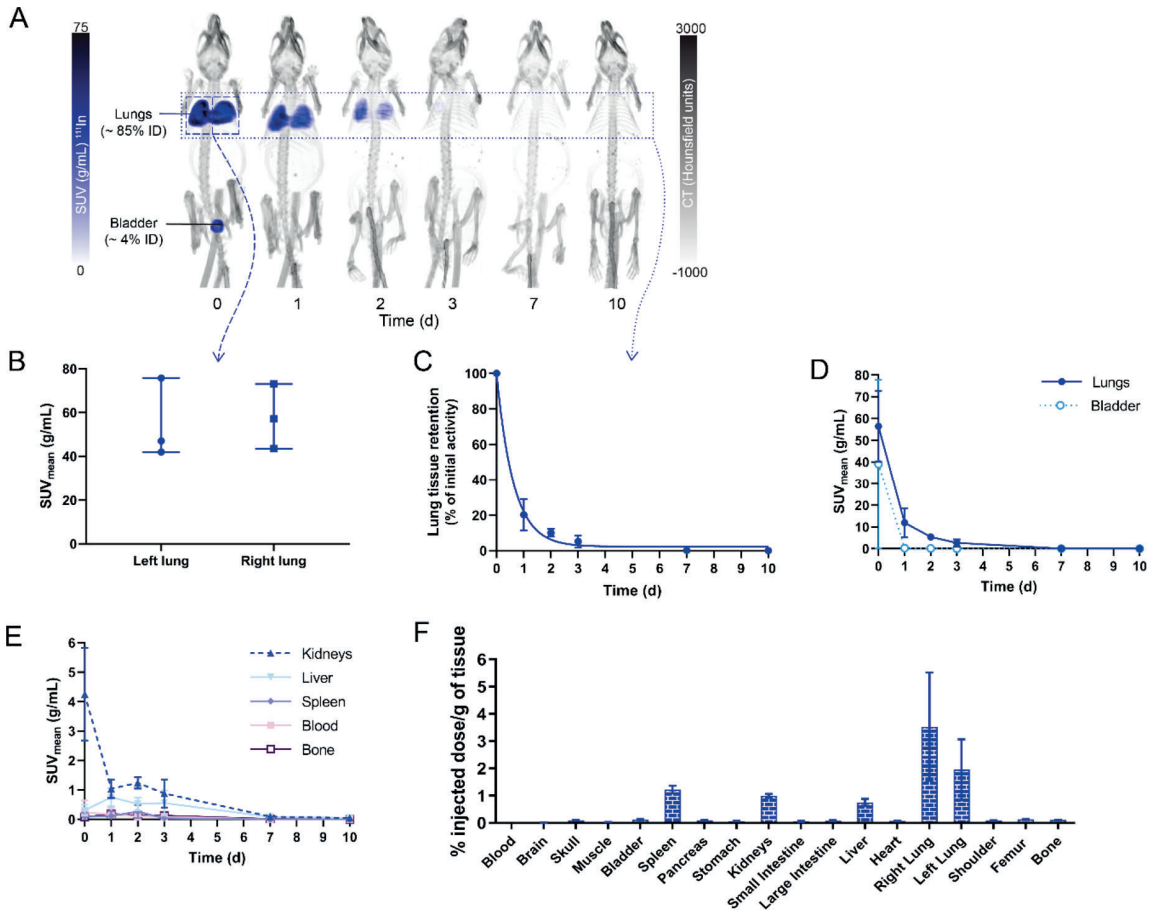

Figure 5. Pharmacokinetics and biodistribution of radiolabeled PLGA microspheres. (A) Representative maximum intensity projection SPECT/CT overlay images (dorsal view) of healthy C57BL/6 mice showing the *in vivo* distribution of ^{111}In-DTPA-F0i PLGA MS after IV tail injection over time. The radioactivity is shown in blue. (B) Left and right lung distribution of ^{111}In-DTPA-F0i PLGA MS immediately after IV injection, calculated from the SPECT images ($N = 3$), in standardized uptake value (SUV) (g/mL) (mean ± SD). (C) Lung tissue retention of PLGA MS. (D,E) Organ SUV in g/mL (mean ± SD) of the ^{111}In-DTPA-F0i PLGA MS over 10 days, calculated from the SPECT images ($N = 3$). (F) Biodistribution (mean ± SD, $N = 3$) of ^{111}In-DTPA-F0i PLGA MS on day 10 after injection. Tissue uptake is expressed as % of injected dose (ID)/g of tissue.

amino functionality was then used to attach the *p*-SCN-Bn-DTPA (resulting in DTPA-F0i PLGA MS, **2**, Figure 4A) and finally radiolabeling with the gamma emitter ^{111}In (**3**, Figure 4A). The labeling efficiency was approximately 5%, whereas the radiochemical purity measured using instant thin-layer chromatography (ITLC) was approximately 97% (Figure 4B). The ^{111}In-DTPA-PLGA MS remained at the origin (retention factor, $R_f = 0$) after incubation with 10 mM EDTA for 10 min at room temperature (RT), whereas the free $^{111}In^{3+}$ migrated with the solvent front ($R_f = 1$). The ^{111}In labeling presented high stability after 24 h incubation in 10 mM EDTA, a strong chelator, indicating very strong binding between DTPA and ^{111}In (Figure 4B).

To study the *in vivo* pharmacokinetics and biodistribution of the MS, healthy mice were IV injected with ^{111}In-DTPA-F0i PLGA MS and SPECT/CT images taken at different time points. Following IV administration, the ^{111}In-DTPA-F0i PLGA MS immediately accumulated in the lungs (Figure 5A, Movie S2). This is expected as particles present in IV fluids will pass through the heart and into the pulmonary circulation. This represents the first stage of filtration in which any material with a particle size larger than ~5 μm is trapped in the small pulmonary capillaries. The pulmonary distribution of the MS within both lobes is homogeneous (Figure 5B), which supports the hypothesis that passive lung targeting after IV administration of drug-releasing delivery systems with a monodisperse distribution could lead to more homogeneous localization in lung tissue compared to conventional pulmonary inhalation of aerosols of MS.

SPECT/CT images of maximum intensity projections are represented in Figure 5A. Assessment of the organ-specific time activity curves for ^{111}In-DTPA-F0i PLGA MS showed a rapid deposition in the lungs within the first 15 min (Figure 5A, day 0) and a slow elimination over 3 days (Figure 5A,C,D). To be able to visualize the uptake in other organs that presented less uptake, the intensity of each scan was adjusted individually to visualize small amounts of radioactivity in other organs (Figure S6A). This figure clearly showed that after 2−3 days postinjection, some radioactivity accumulated and stayed in the kidneys for days, following the same trend as free $^{111}In^{3+}$ (Figure S7A, 0−48 h). This activity might come from the degradation of MS and is characteristic for free $^{111}In^{3+}$ (Figures S7A−C). From our degradation studies (*in vitro*, Figures 1 and S3, and histology-based *in vivo*, Figure 2), we concluded that *in vivo* degradation of PLGA MS seemed to happen at a faster kinetic rate. Here, we can conclude that the F0i PLGA MS seem to disappear to a large

https://dx.doi.org/10.1021/acsnano.9b09773
ACS Nano 2020, 14, 6693−6706

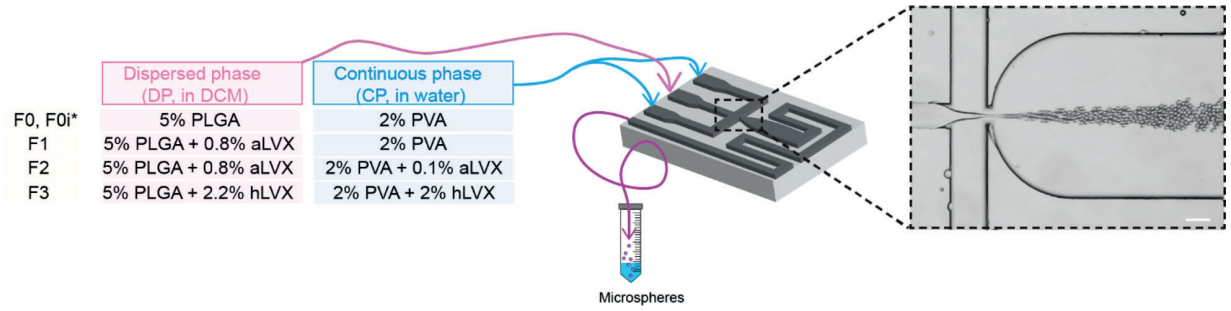

Figure 6. Preparation of microspheres on a flow-focusing microfluidic chip. aLVX, anhydrous LVX; hLVX, hemihydrate LVX; PVA, poly(vinyl alcohol); *F0i contains 50% (w/w) PLGA-PEG-NH_2 for radioactive imaging. Inset of the microfluidic chip is the snapshot during the production of droplets taken with optical microscope. Scale bar: 150 μm. Full video available in the Supporting Information (Movie S1).

extent from the lungs in approximately 3 days after injection (Figure 5A,C,D). After the last SPECT/CT scan on day 10, a biodistribution revealed that overall only 0.02% of the injected activity remained in the animals, with no radioactivity present in organs other than the lungs and the excretory organs liver, kidneys, and spleen (Figures 5F and S6I).

However, it should be noted that a small amount of radioactivity (up to 4%) was excreted immediately upon injection through the urinary tract into the bladder as seen by the high activity in the bladder during the first imaging time point (Figures 5A and 5D, day 0, and Movie S2). This is potentially due to immediate release of primarily the ^{111}In-DTPA complex associated with the PEG linker and partially hydrolyzed PLGA polymer rather than free noncomplexed $^{111}In^{3+}$. This is supported by the high labeling purity of ^{111}In-DTPA-PLGA MS; by the absence of detection of $^{111}In^{3+}$ in the MS batch observed even after 10 mM EDTA challenge (Figure 4B); and by the distribution and elimination of radioactivity after IV injection of free $^{111}In^{3+}$, which showed 25-fold higher levels of activity in the kidneys (~20% of the injected radioactivity) compared to that in the bladder (~2% of the injected radioactivity) (Figure S7A)—clearly something we did not see after the embolization with ^{111}In-DTPA-F0i PLGA MS. Additionally, the ^{111}In-DTPA linked to short peptides was previously reported not to be excreted through the urinary pathway but accumulated in the cortex and medulla of the kidneys,[48,49] similarly to ^{99m}Tc-DTPA commonly used in clinical routine for the evaluation of glomerular filtration rate.[50]

CONCLUSION

In summary, we have successfully prepared antibiotic-loaded biodegradable MS as a passive lung-targeting drug delivery system. The prepared PLGA MS displayed highly homogeneous size distributions with a mean diameter of 12 μm suitable for alveolar capillary targeting. Almost exclusive distribution to the lungs after IV injection was seen, and the MS remained there for at least a week. Biodistribution and pharmacokinetics illustrated that the particles immediately and homogeneously localized to the lung capillaries with up to 85% of the dose and confirmed continuous degradation and elimination from the target site *via* the urinary excretion pathway without any observed side effects. The particles were feasibly prepared by an optimized flow-focused microfluidics system, encapsulated a selected antibiotic of which up to approximately 80% was released as an active drug in a sustained manner over a period of 5 days *in vitro*. Other potent drug molecules can be encapsulated alone or in combination for the preparation of therapeutically effective dosage forms. Thus, the present work demonstrates an approach to explore lung-targeting MS further.

MATERIALS AND METHODS

Materials. Resomer RG 502H (PLGA 50:50, M_w 7−17 kDa, acid terminated), levofloxacin hemihydrate (Pharmaceutical Secondary Standard), levofloxacin anhydrous, and poly(vinyl alcohol) (M_w 30−70 kDa, 87−90% hydrolyzed) were all purchased from Sigma-Aldrich (St. Louis, MO, USA). PLGA-PEG-NH_2 (M_w PLGA 10 kDa, M_w PEG: 1 kDa) was bought from Nanosoft Polymers (Winston-Salem, NC, USA). (*S*)-2-(4-Isothiocyanatobenzyl)diethylenetriamine pentaacetic acid (*p*-SCN-Bn-DTPA) was purchased from Macrocyclics (Plano, TX, USA). ^{111}Indium ($^{111}InCl_3$) in 0.1 M HCl was supplied by BWXT (Vancouver, BC, Canada). Dichloromethane (DCM) and PBS at pH 7.4 were obtained from VWR (Radnor, PA, USA). 3-(4,5-Dimethylthiazol-2-yl)-2,5-diphenyltetrazolium bromide (MTT) and 4-(2-hydroxyethyl)piperazine-1-ethanesulfonic acid (HEPES) were purchased from Sigma-Aldrich. Ultrapure water for sample preparation was obtained from a PURELAB flex machine (ELGA LabWater, High Wycombe, UK).

P. aeruginosa PA01 (reference strain, wild-type), *S. aureus* 15981 (clinical isolate strain), and *E. coli* ATCC 25922 (reference strain) were kindly provided by the Institute of Immunology and Microbiology, University of Copenhagen. Mueller Hinton broth (MHB) was purchased from Sigma-Aldrich. Human lung adenocarcinoma cells (A549) and human non-small cell lung cancer (H1299) cells were purchased from American Type Cell Cultures (ATCC, Manassas, VA, USA). RPMI-1640 medium, Eagle's minimum essential medium (EMEM), fetal bovine serum (FBS), penicillin−streptomycin (10,000 U/mL), 0.25% (w/v) trypsin-ethylenediaminetetraacetic (EDTA) (1×), and UltraPure sucrose were purchased from Thermo Fisher (Waltham, MA, USA). Human umbilical vein endothelial cells (HUVEC), endothelial basal medium-2 (EBM-2), and endothelial growth medium-2 (EGM-2) single quots supplements were purchased from Lonza (Walkersville, MD, USA). A 4% (w/v) paraformaldehyde solution in PBS was purchased from Boster Biological Technology (Pleasanton, CA, USA).

Microfluidic Preparation of PLGA Microspheres. PLGA MS were prepared using a previously described flow-focusing microfluidic glass chip design.[51] The geometries were 150 and 240 μm wide channels for the DP and the CP channels, respectively, and with a 100 μm wide and 90 μm long orifice. All channels were 45 μm deep. The chip was connected through a 4 linear connector 4-way system (Mitos Edge Connector, Dolomite, Roystone, UK) and Teflon microtubing to the reservoirs of the DP and the CP. They, in turn, were connected to Flow EZ pressure pumps and flow sensors (Fluigent, France) that injected the solutions in the central and outer channels, ensuring superior control of the flow rates, compared to traditional syringe pumps (Figure 6).

The MS preparations were optimized by varying the composition of both the DP and CP, as shown in Figure 6, and keeping the flow rates constant at Q_{DP} = 3 μL/min and Q_{CP} = 90 μL/min. The organic DP consisted of a 5% (w/v) PLGA in DCM and for the loaded particles (*i.e.*,

https://dx.doi.org/10.1021/acsnano.9b09773
ACS Nano 2020, 14, 6693−6706

F1, F2, F3), 0.8−2.2% (w/v) of LVX, corresponding to 15% (for F1 and F2), and 30% (for F3) of theoretical drug loading. Anhydrous (F1, F2) as well as hemihydrate (F3) forms of the LVX were added to DP and also to the CP for F2 and F3 to increase the loading. The CP was 2% (w/v) PVA in ultrapure water, 0.22 μm filtered (Q-max PES syringe filters, Frisenette, Knebel, Denmark) prior to use, saturated with LVX for F2 (0.1% w/v) and F3 (2% w/v). To radiolabel MS (F0i) for the *in vivo* imaging studies, the DP was a 5% (w/v) solution of polymer in DCM. The polymer consisted of PLGA and PLGA-PEG-NH_2 at a weight ratio of 50:50. All solutions were prepared immediately prior to injection in the chip. After collection over 20−80 min depending on the desired batch size, the MS were washed three times with cycles of resuspension in purified water and centrifugation at 500*g* for 5 min at 4 °C and freeze-dried without any cryo- and lyo-protectants.

Radiolabeling of PLGA Microspheres. The F0i PLGA MS (9 mg) were prepared for radiolabeling. In order to avoid precipitation of the MS during radiolabeling, the whole amount was divided into six batches of 1.5 mg. Each batch was resuspended in 150 μL of $NaHCO_3$ (0.1 M, pH 8.0) and sonicated for 5 s. Then, 3.5 μL of 142 mg/mL *p*-SCN-Bn-DTPA in DMSO was added and shaken in an Eppendorf Thermomixer R (Brinkmann Instruments, Westbury, NY, USA) at 850 rpm and 20 °C overnight. Unreacted DTPA was removed by centrifugation (500*g*, 5 min, 4 °C), and the MS were washed with ultrapure water and resuspended in 200 μL of HEPES buffer (0.1 M, pH 7.0) for radiolabeling. $^{111}InCl_3$ (49.95 MBq, 3 μL in 0.1 M HCl) was added to the MS, and the mixture was incubated for 1 h 45 min on an Eppendorf shaker at 850 rpm at 20 °C. Noncomplexed $^{111}In^{3+}$ was removed by centrifugation (500*g*, 5 min, 4 °C), and the MS were washed with ultrapure water. The activity of the MS was measured with a dose calibrator (CRC-55tR; Capintec, Florham Park, NJ, USA). The six batches were pooled together to achieve samples with uniform MS labeling for *in vivo* administration.

The labeling efficiency was determined for the pooled radiolabeled MS and calculated from the ratio between the activity on the ^{111}In-DTPA-F0i PLGA MS and the activity initially added. The radiochemical purity and stability of ^{111}In-DTPA-F0i PLGA MS were assessed with ITLC using green Tec-Control strips as the stationary phase (Biodex Medical Systems, Shirley, NY, USA) and 10 mM EDTA in ultrapure water (pH 4.0) as the mobile phase after incubating the MS with 10 mM EDTA for 10 min and 24 h at RT. ITLCs were exposed to a photosensitive phosphor sheet (Packard, Mississauga, ON, Canada) for 5 min. The phosphor sheet was then developed using a cyclone phosphor imager (Packard) to determine the location of radioactivity on the ITLCs from which γ-rays were being emitted. The ^{111}In-DTPA-F0i PLGA MS remain at the origin ($R_f = 0$), whereas the free $^{111}In^{3+}$ migrated with the mobile phase to the solvent front ($R_f = 1$). Activity peaks were then integrated using Optiquant software to determine the radiochemical purity and stability.

Residual PVA Quantification. The residual amount of PVA present on the MS in suspension was quantified indirectly, by quantifying the residual amount of PVA in the suspension of 3 mg of PLGA MS using a colorimetric method based on the formation of a colored complex between the two adjacent hydroxyl groups of PVA and an iodine molecule.[52] Briefly, the supernatants obtained during the MS washing process were collected, and 0.4 mL of the solution was mixed with 1.5 mL of boric acid solution (0.65 M) and 0.3 mL of I_2/KI solution (0.05/0.15 M). The samples were incubated for 20 min, and the absorbance was measured at 630 nm with the SPECTROstar Nano UV−vis spectrophotometer (BMG LABTECH, Ortenberg, Germany).

Particle Size Distribution and Morphology. The particle size distribution of fresh and freeze-dried MS was determined using light microscopy. The MS were suspended in water and imaged with an Olympus IX71 inverted microscope (Olympus, Tokyo, Japan). Images were analyzed with ImageJ, and the diameters of at least 500 MS were measured in six fields from three different images ($N = 3$). Gaussian fit for obtaining the histogram of distribution was performed using GraphPad Prism 8 (GraphPad Software, La Jolla, CA, USA). The morphology of the fresh MS was analyzed by SEM after sputter-coating with a 6 nm layer of gold using a Leica EM ACE200 coater (Leica Mikrosysteme, Vienna, Austria). The images were acquired with a FEI Quanta 3D FEG microscope (FEI, Hillsboro, OR, USA) at an acceleration voltage of 2.0 kV.

Levofloxacin Content. LVX content in PLGA MS was assessed spectroscopically. The LVX-loaded PLGA MS were dissolved in acetonitrile for 4 h under magnetic stirring and analyzed with a SPECTROstar Nano UV−vis spectrophotometer (BMG LABTECH). Absorbance was detected at 298 nm where the interference with PLGA was negligible. The LVX loading was determined from the mass ratio of the encapsulated LVX to the total MS produced (eq 1), whereas the EE was defined as the mass ratio of the encapsulated LVX to the LVX initially added (eq 2).

$$\text{LVX loading (\%)} = \frac{\text{LVX encapsulated in the MS}}{\text{PLGA} + \text{LVX encapsulated in the MS}} \times 100 \quad (1)$$

$$\text{EE (\%)} = \frac{\text{LVX encapsulated in the MS}}{\text{LVX initially added}} \times 100 \quad (2)$$

Studies were conducted in triplicates on independent batches of MS ($N = 3$).

***In Vitro* Levofloxacin Release.** The *in vitro* release studies were carried out in PBS under sink conditions. The LVX-loaded PLGA-MS (3 mg) were dispersed in 2 mL of the release medium in an Eppendorf microcentrifuge tube (Sigma-Aldrich) and incubated at 37 °C under constant rotation. At predetermined time points, the test tube was centrifuged at 500*g* for 5 min at RT, and a 150 μL sample of the supernatant was collected and analyzed by UV−vis spectroscopy at 288 nm using a calibration curve (3−30 μg/mL LVX in PBS). The withdrawn sample was replaced with 150 μL of 37 °C release medium, the MS redispersed, and the test tube placed back in the incubator.

The cumulative release of LVX (%) was calculated according to eq 3:

$$\text{cumulative LVX release (\%)} = \sum_{t=0}^{t} \frac{\text{LVXreleased}_t}{\text{LVXenc}} = \frac{V_s \times \sum_{t=0}^{t} C_{t-1} + V_{tot} \times C_t}{M_{LVXenc}} \quad (3)$$

where LVXreleased_t is the amount of LVX released at time *t*, LVXenc is the amount of LVX loaded in the MS, V_{tot} and V_s are the total volume of the release reservoir and the volume of the sample withdrawn at each time point, respectively, and C_t is the concentration of LVX released at time point *t*.

The cumulative LVX release (%) *versus* time curves were fitted by five different mathematical models of drug release (*i.e.*, zero order, first order, Higuchi, Korsmeyer−Peppas, Peppas−Sahlin)[33] using MATLAB software (Mathworks, Natick, MA, USA, version R2019a). The R^2 and the RMSE were obtained and used to evaluate the goodness of the fitting and to choose the model that best described the experimental data.

The release study was performed on three separate days (corresponding to biological triplicates, $N = 3$), each in one technical replicate ($n = 1$) from an independent batch of each type of MS.

***In Vitro* PLGA Microspheres Degradation: Imaging and Cross Section.** The degradation of the MS matrix during the drug release study was investigated by analyzing both the surface modification and the internal matrix organization after cross sectioning of the MS. At predetermined time points (*i.e.*, 0, 1, 2, 5, 10, 14, 21 days), the MS were collected, resuspended in water, concentrated, and a drop was mounted on an aluminum stub and dried overnight at RT. Once completely dried, the MS were sputter coated with a 20 nm layer of iridium (Leica EM MED020, Leica Microsystems Canada, Concord, ON, Canada) on a rotate-tilt stage for improved uniform coating. Cross sections of the MS from each time point were prepared using a FIB and imaged with an SEM (Helios NanoLab 650, FEI, Hillsboro, OR, USA). The cross sections were prepared by tilting the sample to 52° and then applying a platinum protection layer on the surface of the particles of interest. This protection layer was used to prevent any surface damage by the ion beam and applied by gradually increasing the beam current from 7.7 pA to 2.5 nA in a stepwise manner until the ideal coating conditions were

https://dx.doi.org/10.1021/acsnano.9b09773
ACS Nano 2020, 14, 6693−6706

achieved. Then, a regular cross section of approximately 8−12 MS was selected for milling. The cross section face was gradually polished by decreasing the ion beam current from 2.5 to 0.79 nA, and selected particle surfaces were then further polished using an 80 pA ion beam current. SEM images were acquired at low keV for true surface imaging in the secondary electron mode (1 keV, 50 μA) and in backscattered electron mode (2 keV, 0.2 nA) for imaging cross sections. All images were corrected for tilt in the imaging setup (−38°) and acquired with 1536 × 1024 pixels at 30 μs/pixel dwell time and saved as 16-bit TIF files. Figure S8 summarizes the steps of the FIB-SEM procedure.

***In Vivo* PLGA Microsphere Degradation.** Twelve female mice C57BL/6 were tail vein injected with 100 μL of 30 mg/mL F0 PLGA MS (corresponding to approximately 300,000 PLGA MS from the same preparation per mouse). The exact number of MS was determined with flow cytometry (CytoFLEX Flow Cytometer, Beckman Coulter, Mississauga, ON, Canada). At each time point (*i.e.*, 0, 1, 2 weeks), three mice were sacrificed by CO_2 asphyxiation under isoflurane anesthesia. The lungs were harvested, rinsed in ice cold PBS, and fixed *via* submersion overnight in 4% (w/v) paraformaldehyde in PBS. The lungs were then moved to a 15% (w/v) sucrose solution in PBS for 10 h at 4 °C, after which they were placed in a 30% (w/v) sucrose solution in PBS at 4 °C until analysis, that is, for maximum of 3 weeks, with weekly replacements of fresh sucrose solution. The tissue samples were cut in 30 μm thick coronal sections, stained with hematoxylin and eosin (H&E) using a standard protocol, film coverslipped using TissueTek-Prisma and Coverslipper (Sakura Finetek, Torrance, CA, USA), and mounted onto microscope slides for imaging (Histowiz, Brooklyn, NY, USA). Whole-slide images were taken at 40× magnification and digitized with the Aperio AT2 slide scanner (Leica Biosystems Canada, Concord, ON, Canada). Each group contained three mice corresponding to three biological replicates ($N = 3$). To make the embolized MS imprint clearly visible from the 30 μm thick histology sections, image analysis was performed using Image Pro Plus (Media Cybernetics, Rockville, MD, USA, version 6.0), taking advantage of the fact that MS lodged in the capillaries or arterioles stretching the endothelial cells in a circular fashion around the MS. To make this clearly visible, the "blue" information from the histology pictures in RGB space, which highlights the nuclei, as they were stained blue from the hematoxylin dye in the H&E stain, was first extracted. To further highlight the cells, local equalization was applied, thus enhancing the differences between nuclei and the surrounding areas. MS could thus be shown very clearly as circular endothelial cell rings.

Antibacterial Activity of Levofloxacin-Loaded PLGA Microspheres. The MIC of LVX and PLGA MS containing LVX was determined using the broth microdilution method according to the Clinical and Laboratory Standards Institute guidelines.[53] Bacterial growth inhibition of the LVX-loaded PLGA MS was assessed against *E. coli* ATCC 25922, *P. aeruginosa* PA01, and *S. aureus* 15981. The LVX solutions (both anhydrous LVX and hemihydrate LVX) and the LVX-loaded PLGA MS suspensions (F1, F2, F3, both fresh and freeze-dried MS) were prepared in 2-fold dilutions in MHB in amounts corresponding to a concentration range of 8−0.007 μg/mL of LVX in solution and encapsulated LVX in a 96-well flat-bottomed plates (Costar Corning 3596 cell culture plates, Corning, NY, USA). The nonloaded PLGA MS were tested in PLGA concentrations corresponding to the amount of PLGA in the LVX-loaded MS (30−0.029 μg/mL). The samples were then inoculated with bacteria in log phase to achieve a final concentration of (2−5) × 10^5 colony forming units/mL and incubated for 20 h at 37 °C in an INCUCELL incubator (MMM Medcenter Einrichtungen, Munich, Germany) before visual inspection of growth. The MIC values were determined as the lowest concentration showing no visible bacteria growth. The experiment was performed once in triplicate ($N = 1$, $n = 3$).

***In Vitro* Compatibility Assessment.** *Cell Culturing.* The HUVEC cell culture was maintained in EBM-2 supplemented with (EGM-2) SingleQuots kit, whereas the H1299 and A549 cell cultures were maintained in RPMI1640 or FK-12 media, respectively, supplemented with 10% (v/v) FBS, penicillin (100 U/mL), and streptomycin (100 μg/mL). All cells were cultured in T-75 flasks (Corning, Corning, NY, USA) at standard culture conditions of 37 °C, 5% CO_2, and 95% humidity. Once the cells reached approximately 80% confluence, they were detached from the culture flasks using 0.25% (w/v) trypsin−EDTA solution (isotonic solution containing 2.5 and 0.3 mg/mL of trypsin and EDTA, respectively). During culturing growth, medium was replaced every 2 days.

Cytotoxicity. Cytotoxicity of nonloaded and LVX-loaded PLGA MS on HUVEC, H1299, and A549 cells was determined using the MTT assay. Briefly, the cells were seeded in flat-bottomed and transparent 96-well plates at densities of 10,000 cells/well (HUVEC) or 5000 cells/well (A549, H1299) and incubated at 37 °C for 24 h until approximately 80% confluency was achieved. The cells were washed with 37 °C PBS and exposed to 200 μL of culture medium containing MS in nine concentrations over a 2-fold serial dilution series (5−0.012 mg/mL). Cells incubated in culture medium (untreated cells) were used as the negative control. After the cells were incubated with the different formulations for 24 h, 5 μL of 5 mg/mL MTT reagent was added and the cells were subsequently incubated for 3.5 h (HUVEC) or 3 h (H1299 and A549) at 37 °C until the formation of formazan crystals. The medium was then removed, and 150 μL of DMSO was added to each well to dissolve the formazan crystals and lyse the cells. After complete dissolution, the absorbance was measured at 540 and 650 nm to subtract the background of the cells using a Synergy MX plate reader (BioTek, Winooski, VT, USA). Cell viability was calculated according to eq 4:

$$\text{cell viability (\%)} = \frac{A_{\text{treated cells @ 540 nm}} - A_{\text{treated cells @ 650 nm}}}{A_{\text{untreated cells @ 540 nm}} - A_{\text{untreated cells @ 650 nm}}} \times 100 \quad (4)$$

where $A_{\text{treated cells @ 540 nm}}$ and $A_{\text{untreated cells @ 540 nm}}$ are the absorbances at 540 nm of the wells incubated with either the MS or LVX and culture media, respectively, whereas $A_{\text{treated cells @ 650 nm}}$ and $A_{\text{untreated cells @ 650 nm}}$ are the respective background absorbances at 650 nm.

IC_{50} values representing 50% dehydrogenase inhibition in the cells as a result of the treatment were determined by fitting the data with a nonlinear regression function with variable slope with GraphPad Prism 8. The cell viability (%) versus concentration curves were fitted using eq 5:

$$\text{cell viability (\%)} = \frac{100}{\frac{1 + X^{\text{Hill slope}}}{IC_{50}{}^{\text{Hill slope}}}} \quad (5)$$

where X is the concentration of the formulation, Hill slope is a factor that describes the steepness of the linear part of the curve, and IC_{50} is the concentration of the formulations that inhibits 50% of cell dehydrogenase activity. The cytotoxicity assay was performed in biological ($N = 3$) and technical ($n = 3$) triplicates.

Cell Morphology Changes. The effects of the MS on HUVEC, H1299, and A549 cell morphology were investigated with a live cell imaging system. Cells were grown on a 96-well microplate tray and exposed to MS and LVX, as described in the previous section, and placed in an IncuCyte ZOOM live-cell analysis system (Essen Biosciences, Ann Arbor, MI, USA), equipped with a 10× objective in a 5% CO_2 incubator at 37 °C. Real-time images of each well were taken every 3 h for a period of 48 h.

Hemocompatibility. Hemocompatibility of the MS was investigated with the hemolysis assay, following a method described by Evans *et al.*[54] Briefly, blood from a healthy human donor was collected in K_2-EDTA-coated Vacutainer and centrifuged at 700*g* for 5 min at RT to obtain human red blood cells (hRBC). After the plasma was discarded, the hRBC were washed twice with 150 mM NaCl in ultrapure water and twice with PBS with cycles consisting of gently mixing, centrifuging at 700*g* for 5 min at RT, and gently removing the supernatant. The hRBCs were diluted to 3% (v/v) in PBS, and 100 μL of this dispersion was added to 100 μL of F0, F0i, DTPA-F0i, F3, and LVX in PBS at 4 and 12 mg/mL concentrations, corresponding to final 1× (2 mg/mL) and 3× (6 mg/mL) of the *in vivo* dose (used in the histology and imaging studies) when related to blood volume of the mouse (1.5 mL). Triton X-100 at a concentration of 2% (v/v) and PBS were used as positive and negative controls, respectively. The Eppendorf tubes were incubated for 1 h at 37 °C on an orbital shaker, and the hRBCs were pelleted by

https://dx.doi.org/10.1021/acsnano.9b09773
ACS Nano 2020, 14, 6693−6706

centrifugation at 700*g* for 5 min at RT. The supernatant was transferred to a round-bottom 96-well plate (Falcon, Corning, NY, USA), and the absorbance of hemoglobin was measured at 450 nm using a Synergy MX plate reader (BioTek). The hemolysis (%) was calculated according to eq 6:

$$\text{hemolysis (\%)} = \frac{A_{\text{sample}} - A_{\text{negative control}}}{A_{\text{positive control}} - A_{\text{negative control}}} \times 100 \quad (6)$$

where A_{sample} is the absorbance of supernatant from the hRBC incubated with the different concentrations of the formulations, whereas $A_{\text{negative control}}$ and $A_{\text{positive control}}$ are the absorbances of the supernatants from the hRBC incubated with PBS and Triton X-100, respectively, that correspond to 0 and 100% hemolysis. The hemolysis assay was performed once in technical triplicates ($N = 1$, $n = 3$).

***In Vivo* Pharmacokinetics and Biodistribution of PLGA Microspheres.** *SPECT/CT Imaging.* The *in vivo* studies were conducted in accordance with the Canadian Council on Animal Care (CCAC) and protocol A16-0150 approved by the Animal Care Committee (ACC) of the University of British Columbia. Five-month-old healthy female C57BL/6 mice were purchased from Charles River and allowed free access to food and water. The mice were allocated into two groups of three individuals (corresponding to three biological replicates, $N = 3$). Each animal was anesthetized using isoflurane on a precision vaporizer (5% in oxygen for induction, and between 1.5 and 2% in oxygen for maintenance) and received a subcutaneous dorsal injection of lactated Ringer's solution (0.5 mL) for hydration prior to each imaging scan. After the induction of anesthesia, an injection of 100 μL of 30 mg/mL ^{111}In-DTPA F0i PLGA MS in saline was administered *via* the tail vein. The administered dose corresponded to approximately 300,000 MS weighing 3 mg, resulting in 2 mg/mL target concentration of PLGA MS in the 1.5 mL average blood volume of a mouse. Similarly, the control group was administered an injection of 100 μL $^{111}InCl_3$ in saline *via* the tail vein. The average injected activities were 2.04 and 9.25 MBq for the ^{111}In-DTPA-F0i PLGA MS and the control group, respectively. Immediately after injection, whole-body images were acquired at different time points: 0, 1, 2, 3, 7, and 10 days for PLGA MS and 0, 4, 24, and 48 h for $^{111}InCl_3$. A multimodal SPECT/CT scanner (VECTor/CT, MILabs, The Netherlands) equipped with a XUHS-2 mm mouse pinhole collimator was used for the study. The first measurements (corresponding to day 0) were performed within 15 min after injection. Throughout the entire scanning procedure, the respiratory rate and body temperature of the mice were monitored and isoflurane dose and animal bed temperature adjusted accordingly. Following each SPECT acquisition, a whole-body CT scan (55 kV, 615 μA) was obtained to gain anatomical information, and both images were registered. The ^{111}In photopeak window was centered at 171 keV with a 20% energy window width (background weight 2.5), 0.4 mm^3 voxel, 128 subsets, and 5 iterations using the SROSEM image reconstruction algorithm. The images were decay corrected and after CT registration, and attenuation correction was applied. For visual representation, the reconstructed volumes of SPECT scans were postfiltered with a 3D Gaussian filter. Volumes of interest were manually defined using AMIDE[55] (UCLA, USA, version 1.0.4) to determine the time−activity pattern per target organ. The presented regions were heart, lungs, liver, kidneys, bladder, and bone. The average organ activity per volume was obtained from the SPECT images, and the standardized uptake value (SUV) was extracted from each organ using eq 7:

$$\text{SUV (g} \times \text{mL}^{-1}) = \frac{\text{organ activity concentration (MBq} \times \text{mL}^{-1})}{\text{injected dose (MBq)}} \times \text{body weight (g)} \quad (7)$$

To relate the scanner units (counts/voxel) to radioactivity concentration, a calibration factor was determined by scanning a source with a known concentration of $^{111}In^{3+}$.

Biodistribution. Following the last scan at day 2 for $^{111}InCl_3$ and at day 10 for ^{111}In-DTPA-F0i PLGA MS, mice were euthanized by CO_2 asphyxiation under isoflurane anesthesia. Cardiac puncture was promptly performed to recover blood, and the organs of interest were harvested (brain, skull, muscle, femur, bladder, spleen, pancreas, stomach, kidneys, small intestine, large intestine, liver, heart, right and left lungs, shoulder, and tail), rinsed with PBS, and blotted dry. Each organ was weighed, and the radioactivity was quantified using a calibrated gamma counter (Packard Cobra II Autogamma counter, PerkinElmer, Waltham, MA, USA) followed by calculating the amount relative to the injected dose per gram of tissue (%ID/g) and per organ (%ID/organ), respectively.

Statistical Analysis. All of the *in vitro* and *in vivo* experiments and measurements were conducted in triplicate, unless otherwise specified. Results are presented as mean ± SD. Statistical analyses of data from *in vitro* and *in vivo* experiments were performed with GraphPad Prism 8 (GraphPad Software). Probability values of $p < 0.05$ were considered statistically significant.

ASSOCIATED CONTENT

Supporting Information

The Supporting Information is available free of charge at https://pubs.acs.org/doi/10.1021/acsnano.9b09773.

Morphology and size distribution of PLGA microspheres (Figure S1); poly(vinyl alcohol) quantification during washing (Table S1); mathematical models of the *in vitro* release profiles (Table S2); representative drug release fitting models (Figure S2); degradation of F0 *vs* F0i PLGA microspheres (Figure S3); representative full-size processed histology images of lungs exposed to PLGA microspheres (F0) after intravenous injection over time (Figure S4); cell toxicity of PLGA microspheres, normalized for levofloxacin content (Figure S5); pharmacokinetics and biodistribution of radiolabeled PLGA microspheres (Figure S6); pharmacokinetics and biodistribution of $^{111}InCl_3$ after intravenous administration (Figure S7); steps to obtain cross sections of PLGA microspheres with FIB-SEM (Figure S8) (PDF)

Movie S1: Production of microspheres by flow focusing (AVI)

Movie S2: SPECT/CT animated image 15 min after intravenous administration of ^{111}In-DTPA-PLGA microspheres (MPG)

AUTHOR INFORMATION

Corresponding Authors

Hanne Mørck Nielsen − *Department of Pharmacy, Faculty of Health and Medical Sciences, University of Copenhagen, Copenhagen DK-2100, Denmark;* orcid.org/0000-0002-7285-9100; Email: hanne.morck@sund.ku.dk

Urs O. Häfeli − *Department of Pharmacy, Faculty of Health and Medical Sciences, University of Copenhagen, Copenhagen DK-2100, Denmark; Faculty of Pharmaceutical Sciences, University of British Columbia, Vancouver, BC V6T 1Z3, Canada;* orcid.org/0000-0003-0671-4509; Email: urs.hafeli@ubc.ca

Authors

Monica Agnoletti − *Department of Pharmacy, Faculty of Health and Medical Sciences, University of Copenhagen, Copenhagen DK-2100, Denmark; Faculty of Pharmaceutical Sciences, University of British Columbia, Vancouver, BC V6T 1Z3, Canada;* orcid.org/0000-0002-5103-9568

Cristina Rodríguez-Rodríguez − *Faculty of Pharmaceutical Sciences and Department of Physics and Astronomy, University of British Columbia, Vancouver, BC V6T 1Z3, Canada;* orcid.org/0000-0002-3313-4422

Sylvia N. Kłodzińska − *Department of Pharmacy, Faculty of Health and Medical Sciences, University of Copenhagen,*

https://dx.doi.org/10.1021/acsnano.9b09773
ACS Nano 2020, 14, 6693−6706

Copenhagen DK-2100, Denmark; orcid.org/0000-0001-7443-2234

Tullio V. F. Esposito − *Department of Pharmacy, Faculty of Health and Medical Sciences, University of Copenhagen, Copenhagen DK-2100, Denmark; Faculty of Pharmaceutical Sciences, University of British Columbia, Vancouver, BC V6T 1Z3, Canada;* orcid.org/0000-0003-4047-0405

Katayoun Saatchi − *Faculty of Pharmaceutical Sciences, University of British Columbia, Vancouver, BC V6T 1Z3, Canada;* orcid.org/0000-0002-5372-6791

Complete contact information is available at: https://pubs.acs.org/10.1021/acsnano.9b09773

Author Contributions

M.A., H.M.N., and U.O.H. designed the experiments. M.A. analyzed the data. M.A., C.R.R., S.N.K., T.V.F.E., and K.S. performed the experiments: M.A. prepared and characterized the microspheres; M.A. and S.N.K. performed the antimicrobial activity study; M.A. and T.V.F.E. performed the cytotoxicity study; K.S. modified the microspheres with DTPA; M.A. and T.V.F.E. radiolabeled and characterized the radiotracer; M.A., T.V.F.E., and C.R.R. performed the SPECT/CT, biodistribution and histology studies, and analyzed the data. M.A. and S.N.K. drafted the manuscript. All authors revised and approved the final manuscript. H.M.N. and U.O.H. oversaw the research. U.O.H. provided financial support.

Notes

The authors declare no competing financial interest.

ACKNOWLEDGMENTS

The authors would like to thank the Lundbeck Foundation, Denmark (Joint Professorship to UOH, Grant No. 2014-4176), for financial support of this project. Furthermore, the Core Facility for Integrated Microscopy (University of Copenhagen, Denmark) is acknowledged for access to their SEM facilities and support, and G. Owen and the Centre for High-Throughput Phenogenomics (University of British Columbia, Canada) are acknowledged for their help with the cross section images with the FIB-SEM. The authors would also like to thank M. Osooly for her skillful assistance in the SPECT/CT imaging and *ex vivo* biodistribution, J. Hodasova for her support with histology experiments, and the Canada Foundation for Innovation (Project No. 25413) for its support of the imaging facility (http://invivoimaging.ca/). K.S. acknowledges the generous support of BWXT Isotope Technology Group for the supply of the radioisotope.

REFERENCES

(1) Troeger, C.; Blacker, B.; Khalil, I. A.; Rao, P. C.; Cao, S.; Zimsen, S. R. M.; Albertson, S. B.; Stanaway, J. D.; Deshpande, A.; Farag, T.; Forouzanfar, M. H.; Abebe, Z.; Adetifa, I. M. O.; Adhikari, T. B.; Akibu, M.; Al Lami, F. H.; Al-Eyadhy, A.; Alvis-Guzman, N.; Amare, A. T.; Amoako, Y. A.; et al. Estimates of the Global, Regional, and National Morbidity, Mortality, and Aetiologies of Lower Respiratory Infections in 195 Countries, 1990−2016: A Systematic Analysis for the Global Burden of Disease Study 2016. *Lancet Infect. Dis.* **2018**, *18*, 1191−1210.

(2) Woodhead, M.; Blasi, F.; Ewig, S.; Huchon, G.; Leven, M.; Ortqvist, A.; Schaberg, T.; Torres, A.; van der Heijden, G.; Verheij, T. J. M. Guidelines for the Management of Adult Lower Respiratory Tract Infections. *Eur. Respir. J.* **2005**, *26*, 1138−1180.

(3) Torres, A.; Liapikou, A. Levofloxacin for the Treatment of Respiratory Tract Infections. *Expert Opin. Pharmacother.* **2012**, *13*, 1203−1212.

(4) European Medicines Agency. Disabling and Potentially Permanent Side Effects Lead to Suspension or Restrictions of Quinolone and Fluoroquinolone Antibiotics; https://www.ema.europa.eu/en/news/disabling-potentially-permanent-side-effects-lead-suspension-restrictions-quinolone-fluoroquinolone (accessed 2020-01-26).

(5) United States Food and Drug Administration. FDA Reinforces Safety Information About Serious Low Blood Sugar Levels and Mental Health Side Effects with Fluoroquinolone Antibiotics; Requires Label Changes; https://www.fda.gov/drugs/drug-safety-and-availability/fda-reinforces-safety-information-about-serious-low-blood-sugar-levels-and-mental-health-side (accessed 2020-01-16).

(6) Guitor, A. K.; Wright, G. D. Antimicrobial Resistance and Respiratory Infections. *Chest* **2018**, *154*, 1202−1212.

(7) European Medicines Agency. Tobi Podhaler - EMEA/H/C/002155 - IAIN/0042; https://www.ema.europa.eu/en/medicines/human/EPAR/tobi-podhaler (accessed 2020-05-16).

(8) Vazquez-Espinosa, E.; Marcos, C.; Alonso, T.; Giron, R. M.; Gomez-Punter, R. M.; Garcia-Castillo, E.; Zamora, E.; Cisneros, C.; Garcia, J.; Valenzuela, C.; Ancochea, J. Tobramycin Inhalation Powder (TOBI Podhaler ®) for the Treatment of Lung Infection in Patients with Cystic Fibrosis. *Expert Rev. Anti-Infect. Ther.* **2016**, *14*, 9−17.

(9) European Medicines Agency. Colobreathe - EMEA/H/C/001225 - IAIN/0043; https://www.ema.europa.eu/en/medicines/human/EPAR/colobreathe (accessed 2020-05-16).

(10) Schwarz, C. Colobreathe® for the Treatment of Cystic Fibrosis-Associated Pulmonary Infections. *Pulm. Ther.* **2015**, *1*, 19−30.

(11) Ngan, C. L.; Asmawi, A. A. Lipid-Based Pulmonary Delivery System: A Review and Future Considerations of Formulation Strategies and Limitations. *Drug Delivery Transl. Res.* **2018**, *8*, 1527−1544.

(12) Zhou, Q. T.; Leung, S. S. Y.; Tang, P.; Parumasivam, T.; Loh, Z. H.; Chan, H. K. Inhaled Formulations and Pulmonary Drug Delivery Systems for Respiratory Infections. *Adv. Drug Delivery Rev.* **2015**, *85*, 83−99.

(13) Hogg, J. C.; Coxson, H. O.; Brumwell, M. L.; Beyers, N.; Doerschuk, C. M.; MacNee, W.; Wiggs, B. R. Erythrocyte and Polymorphonuclear Cell Transit Time and Concentration in Human Pulmonary Capillaries. *J. Appl. Physiol.* **1994**, *77*, 1795−1800.

(14) Short, A. C.; Montoya, M. L.; Gebb, S. A.; Presson, R. G.; Wagner, W. W.; Capen, R. L. Pulmonary Capillary Diameters and Recruitment Characteristics in Subpleural and Interior Networks. *J. Appl. Physiol.* **1996**, *80*, 1568−1573.

(15) American College of Radiology. ACR-SPR-STR Practice Parameter for the Performance of Pulmonary Scintigraphy. Revised 2014 (Resolution 30); https://www.acr.org/-/media/ACR/Files/Practice-Parameters/Pulmonary_Scintigraphy.pdf (accessed 2020-02-18).

(16) Parker, J. A.; Coleman, R. E.; Grady, E.; Royal, H. D.; Siegel, B. A.; Stabin, M. G.; Sostman, H. D.; Hilson, A. J. W. SNM Practice Guideline for Lung Scintigraphy 4.0. *J. Nucl. Med. Technol.* **2012**, *40*, 57−65.

(17) Bajc, M.; Neilly, J. B.; Miniati, M.; Schuemichen, C.; Meignan, M.; Jonson, B. EANM Guidelines for Ventilation/Perfusion Scintigraphy: Part 1. Pulmonary Imaging with Ventilation/Perfusion Single Photon Emission Tomography. *Eur. J. Nucl. Med. Mol. Imaging* **2009**, *36*, 1356−1370.

(18) Huo, D.; Deng, S.; Li, L.; Ji, J. Studies on the Poly(Lactic-Co-Glycolic) Acid Microspheres of Cisplatin for Lung-Targeting. *Int. J. Pharm.* **2005**, *289*, 63−67.

(19) Zhang, W.; Jiang, X.; Hu, J.; Fu, C. Rifampicin Polylactic Acid Microspheres for Lung Targeting. *J. Microencapsulation* **2000**, *17*, 785−788.

(20) Fan, Y.; Shan-Guang, W.; Yu-Fang, P.; Feng-Lan, S.; Tao, L. Preparation and Characteristics of Erythromycin Microspheres for Lung Targeting. *Drug Dev. Ind. Pharm.* **2009**, *35*, 639−645.

(21) Ramaiah, B.; Harsha Nagaraja, S.; Kapanigowda, U. G.; Boggarapu, P. R.; Subramanian, R. High Azithromycin Concentration in Lungs by Way of Bovine Serum Albumin Microspheres as Targeted Drug Delivery: Lung Targeting Efficiency in Albino Mice. *Daru, J. Pharm. Sci.* **2016**, *24*, 14.

(22) Harsha, S.; R, C.; Rani, S. Ofloxacin Targeting to Lungs by Way of Microspheres. *Int. J. Pharm.* **2009**, *380*, 127−132.
(23) Zhang, R.; Hao, Z.; Ding, Z.; Lü, Z. Preparation and Characterization of Lung-Targeting Cefquinome-Loaded PLGA Microspheres. *J. Wuhan Univ. Technol., Mater. Sci. Ed.* **2017**, *32*, 494−499.
(24) Qu, S.; Dai, C.; Yang, F.; Huang, T.; Xu, T.; Zhao, L.; Li, Y.; Hao, Z. A Comparison of Two Methods for the Preparation Cefquinome-Loaded Gelatin Microspheres for Lung Targeting. *Pharm. Res.* **2018**, *35*, 43.
(25) Wu, T.; Luo, Z.; Ding, W.; Cheng, Z.; He, L. Monodisperse Droplets by Impinging Flow-Focusing. *Microfluid. Nanofluid.* **2017**, *21*, 129.
(26) United States Pharmacopeia. Technetium Tc-99m Albumin Aggregated Injection. In *United States Pharmacopeia (USP) 32 - National Formulary (NF) 27*; United States Pharmacopeial Convention: Rockville, MD, 2009; pp 3656−3657.
(27) Bragagni, M.; Gil-Alegre, M. E.; Mura, P.; Cirri, M.; Ghelardini, C.; Di Cesare Mannelli, L. Improving the Therapeutic Efficacy of Prilocaine by PLGA Microparticles: Preparation, Characterization and *In Vivo* Evaluation. *Int. J. Pharm.* **2018**, *547*, 24−30.
(28) Gaspar, M. C.; Pais, A. A. C. C.; Sousa, J. J. S.; Brillaut, J.; Olivier, J. C. Development of Levofloxacin-Loaded PLGA Microspheres of Suitable Properties for Sustained Pulmonary Release. *Int. J. Pharm.* **2019**, *556*, 117−124.
(29) Ramazani, F.; Chen, W.; Van Nostrum, C. F.; Storm, G.; Kiessling, F.; Lammers, T.; Hennink, W. E.; Kok, R. J. Strategies for Encapsulation of Small Hydrophilic and Amphiphilic Drugs in PLGA Microspheres: State-of-the-Art and Challenges. *Int. J. Pharm.* **2016**, *499*, 358−367.
(30) Chaisri, W.; Ghassemi, A. H.; Hennink, W. E.; Okonogi, S. Enhanced Gentamicin Loading and Release of PLGA and PLHMGA Microspheres by Varying the Formulation Parameters. *Colloids Surf., B* **2011**, *84*, 508−514.
(31) Gaspar, M. C.; Grégoire, N.; Sousa, J. J. S.; Pais, A. A. C. C.; Lamarche, I.; Gobin, P.; Olivier, J. C.; Marchand, S.; Couet, W. Pulmonary Pharmacokinetics of Levofloxacin in Rats after Aerosolization of Immediate-Release Chitosan or Sustained-Release PLGA Microspheres. *Eur. J. Pharm. Sci.* **2016**, *93*, 184−191.
(32) Mylonaki, I.; Allémann, E.; Delie, F.; Jordan, O. Imaging the Porous Structure in the Core of Degrading PLGA Microparticles: The Effect of Molecular Weight. *J. Controlled Release* **2018**, *286*, 231−239.
(33) Bruschi, M. L. Mathematical Models of Drug Release. *Strategies to Modify the Drug Release from Pharmaceutical Systems*; Woodhead Publishing: Cambridge, UK, 2015; pp 63−86.
(34) Lao, L. L.; Peppas, N. A.; Boey, F. Y. C.; Venkatraman, S. S. Modeling of Drug Release from Bulk-Degrading Polymers. *Int. J. Pharm.* **2011**, *418*, 28−41.
(35) Doan, T. V. P.; Couet, W.; Olivier, J. C. Formulation and *In Vitro* Characterization of Inhalable Rifampicin-Loaded PLGA Microspheres for Sustained Lung Delivery. *Int. J. Pharm.* **2011**, *414*, 112−117.
(36) Gaspar, M. C.; Sousa, J. J. S.; Pais, A. A. C. C.; Cardoso, O.; Murtinho, D.; Serra, M. E. S.; Tewes, F.; Olivier, J. C. Optimization of Levofloxacin-Loaded Crosslinked Chitosan Microspheres for Inhaled Aerosol Therapy. *Eur. J. Pharm. Biopharm.* **2015**, *96*, 65−75.
(37) Zhou, W.; Qian, H; Yan, L.; Luo, D.; Xu, N.; Wu, J. Controlled Release of Clodronate from PLA/PCL Complex Microsphere. *Mater. Lett.* **2015**, *152*, 293−297.
(38) Vey, E.; Rodger, C.; Meehan, L.; Booth, J.; Claybourn, M.; Miller, A. F.; Saiani, A. The Impact of Chemical Composition on the Degradation Kinetics of Poly(Lactic-Co-Glycolic) Acid Copolymers Cast Films in Phosphate Buffer Solution. *Polym. Degrad. Stab.* **2012**, *97*, 358−365.
(39) Vey, E.; Roger, C.; Meehan, L.; Booth, J.; Claybourn, M.; Miller, A. F.; Saiani, A. Degradation Mechanism of Poly(Lactic-Co-Glycolic) Acid Block Copolymer Cast Films in Phosphate Buffer Solution. *Polym. Degrad. Stab.* **2008**, *93*, 1869−1876.
(40) Tracy, M. A.; Ward, K. L.; Firouzabadian, L.; Wang, Y.; Dong, N.; Qian, R.; Zhang, Y. Factors Affecting the Degradation Rate of Poly(Lactide-Co-Glycolide) Microspheres *In Vivo* and *In Vitro*. *Biomaterials* **1999**, *20*, 1057−1062.
(41) Dillen, K.; Vandervoort, J.; Van Den Mooter, G.; Verheyden, L.; Ludwig, A. Factorial Design, Physicochemical Characterisation and Activity of Ciprofloxacin-PLGA Nanoparticles. *Int. J. Pharm.* **2004**, *275*, 171−187.
(42) Kolate, A.; Kore, G.; Lesimple, P.; Baradia, D.; Patil, S.; Hanrahan, J. W.; Misra, A. Polymer Assisted Entrapment of Netilmicin in PLGA Nanoparticles for Sustained Antibacterial Activity. *J. Microencapsulation* **2015**, *32*, 61−74.
(43) Jorgensen, J. H.; Ferraro, M. J. Antimicrobial Susceptibility Testing: A Review of General Principles and Contemporary Practices. *Clin. Infect. Dis.* **2009**, *49*, 1749−1755.
(44) Kłodzińska, S. N.; Wan, F.; Jumaa, H.; Sternberg, C.; Rades, T.; Nielsen, H. M. Utilizing Nanoparticles for Improving Anti-Biofilm Effects of Azithromycin: A Head-to-Head Comparison of Modified Hyaluronic Acid Nanogels and Coated Poly (Lactic-Co-Glycolic Acid) Nanoparticles. *J. Colloid Interface Sci.* **2019**, *555*, 595−606.
(45) Grabowski, N.; Hillaireau, H.; Vergnaud, J.; Santiago, L. A.; Kerdine-Romer, S.; Pallardy, M.; Tsapis, N.; Fattal, E. Toxicity of Surface-Modified PLGA Nanoparticles toward Lung Alveolar Epithelial Cells. *Int. J. Pharm.* **2013**, *454*, 686−694.
(46) Sousa, F.; Cruz, A.; Fonte, P.; Pinto, I. M.; Neves-Petersen, M. T.; Sarmento, B. A New Paradigm for Antiangiogenic Therapy through Controlled Release of Bevacizumab from PLGA Nanoparticles. *Sci. Rep.* **2017**, *7*, 3736.
(47) Fornaguera, C.; Calderó, G.; Mitjans, M.; Vinardell, M. P.; Solans, C.; Vauthier, C. Interactions of PLGA Nanoparticles with Blood Components: Protein Adsorption, Coagulation, Activation of the Complement System and Hemolysis Studies. *Nanoscale* **2015**, *7*, 6045−6058.
(48) Wang, X.; Jaraquemada-Peláez, M. D. G.; Rodríguez-Rodríguez, C.; Cao, Y.; Buchwalder, C.; Choudhary, N.; Jermilova, U.; Ramogida, C. F.; Saatchi, K.; Häfeli, U. O.; Patrick, B. O.; Orvig, C. H_4 octox: Versatile Bimodal Octadentate Acyclic Chelating Ligand for Medicinal Inorganic Chemistry. *J. Am. Chem. Soc.* **2018**, *140*, 15487−15500.
(49) Akizawa, H.; Arano, Y.; Mifune, M.; Iwado, A.; Saito, Y.; Mukai, T.; Uehara, T.; Ono, M.; Fujioka, Y.; Ogawa, K.; Kiso, Y.; Saji, H. Effect of Molecular Charges on Renal Uptake of ^{111}In-DTPA-Conjugated Peptides. *Nucl. Med. Biol.* **2001**, *28*, 761−768.
(50) Taylor, A. T. Radionuclides in Nephrourology, Part 1: Radiopharmaceuticals, Quality Control, and Quantitative Indices. *J. Nucl. Med.* **2014**, *55*, 608−615.
(51) Bokharaei, M.; Schneider, T.; Dutz, S.; Stone, R. C.; Mefford, O. T.; Häfeli, U. O. Production of Monodispersed Magnetic Polymeric Microspheres in a Microfluidic Chip and 3D Simulation. *Microfluid. Nanofluid.* **2016**, *20*, 6.
(52) Procházková, L.; Rodríguez-Muñoz, Y.; Procházka, J.; Wanner, J. Simple Spectrophotometric Method for Determination of Polyvinylalcohol in Different Types of Wastewater. *Int. J. Environ. Anal. Chem.* **2014**, *94*, 399−410.
(53) Clinical and Laboratory Standards Institute (CLSI). *Methods for Dilution Antimicrobial Susceptibility Tests for Bacteria That Grow Aerobically*. 11th ed.; CLSI standard M07; Clinical and Laboratory Standards Institute: Wayne, PA, 2018.
(54) Evans, B. C.; Nelson, C. E.; Yu, S. S.; Beavers, K. R.; Kim, A. J.; Li, H.; Nelson, H. M.; Giorgio, T. D.; Duvall, C. L. *Ex Vivo* Red Blood Cell Hemolysis Assay for the Evaluation of pH-Responsive Endosomolytic Agents for Cytosolic Delivery of Biomacromolecular Drugs. *J. Visualized Exp.* **2013**, No. e50166.
(55) Loening, A. M.; Gambhir, S. S. AMIDE: A Free Software Tool for Multimodality Medical Image Analysis. *Mol. Imaging* **2003**, *2*, 131−137.

https://dx.doi.org/10.1021/acsnano.9b09773
ACS Nano 2020, 14, 6693−6706

Supporting Information

Monosized Polymeric Microspheres Designed for Passive Lung Targeting: Biodistribution and Pharmacokinetics after Intravenous Administration

Monica Agnoletti, [a,b] Cristina Rodríguez-Rodríguez, [b,c] Sylvia N. Kłodzińska, [a] Tullio V.F. Esposito, [a,b] Katayoun Saatchi, [b] Hanne Mørck Nielsen,[a,*] and Urs O. Häfeli [a,b,*]

[a] Department of Pharmacy, Faculty of Health and Medical Sciences, University of Copenhagen, Copenhagen, DK-2100, Denmark

[b] Faculty of Pharmaceutical Sciences, University of British Columbia, Vancouver, BC, V6T 1Z3, Canada

[c] Department of Physics and Astronomy, University of British Columbia, Vancouver, BC, V6T 1Z1, Canada

*Corresponding authors: urs.hafeli@ubc.ca (UOH), hanne.morck@sund.ku.dk (HMN)

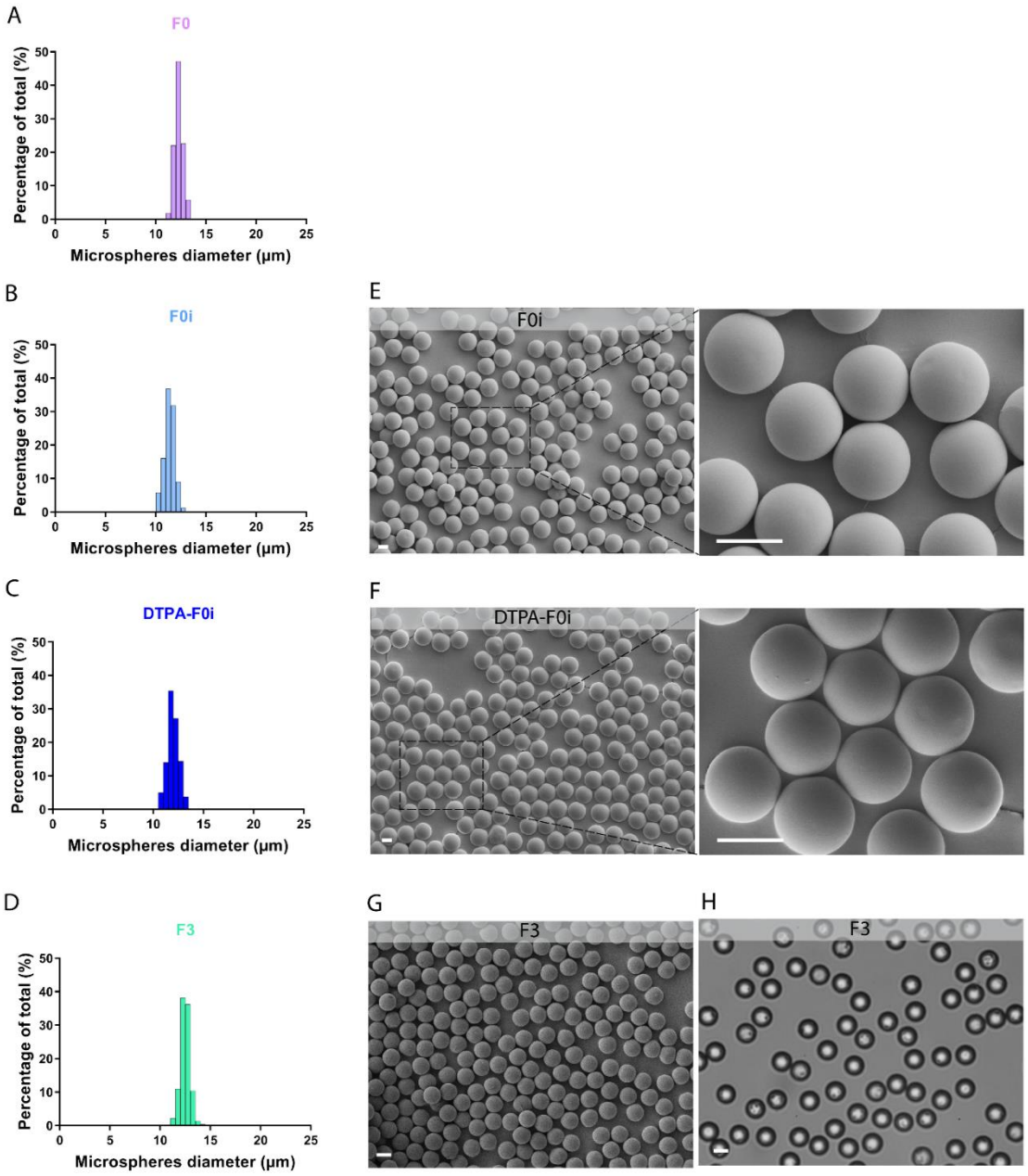

Figure S1. Morphology and size distribution of PLGA microspheres. (A-D) Size distribution of F0, F0i, DTPA-F0i and F3 PLGA MS. **(E-G)** Representative SEM images of F3, F0i and DTPA-F0i LVX-PLGA MS. Scale bars: 10 µm **(H)** Representative optical image of F3 LVX-loaded PLGA MS. Scale bar: 10 µm.

Table S1. Polyvinyl alcohol quantification during washing. PVA concentration present in the supernatant of the microsphere (MS) suspension, amount of PVA in the supernatant of the MS suspension and cumulative amount removed by the washing during up to three cycles of washing. Results are in triplicates (N = 3).

	PVA concentration (%, w/v) in the supernatant of the MS suspension	**Amount PVA (mg) in the supernatant of the MS suspension**	**Cumulative amount of PVA (%) removed during the different washing cycles †**
Before washing	2.015 ± 0.080	96.77 ± 3.81	-
After the 1st washing	0.016 ± 0.003	8.29 ± 1.60	88.7
After the 2nd washing	0.0001 ± 0.0005	0.05 ± 0.06	96.7
After the 3rd washing	0.0001 ± 0.0001	0.05 ± 0.06	96.7

† indicated as % of the amount of PVA measured in the dispersing medium after preparation and before washing

Table S2. Mathematical models of the *in vitro* release profiles. Estimated parameters, coefficient of determination, root mean squared error obtained from fitting experimental data to the main release kinetic mathematical models in MATLAB® software.

Mathematical model	Fitting parameters	Formulation					
		F1, fresh	**F1, FD**	**F2, fresh**	**F2, FD**	**F3, fresh**	**F3, FD**
Zero order $F = k_0 \times t$	**R^2**	0.6328	0.6476	0.5522	0.6144	0.6485	0.4411
	RMSE	20.69	20.12	26.10	23.88	21.15	24.90
	Parameters	k_0: 23.6	k_0: 23.6	k_0: 25.2	k_0: 24.8	k_0: 24.4	k_0: 24.7
First order $F = 100 \times (1 - e^{-k_{1^o} \times t})$	**R^2**	0.9689	0.9685	0.9735	0.9762	0.9789	0.9328
	RMSE	6.02	6.01	6.34	5.93	5.1	8.63
	Parameters	k_{1^o}: 0.69	k_{1^o}: 0.67	k_{1^o}: 0.94	k_{1^o}: 0.82	k_{1^o}: 0.74	k_{1^o}: 0.87
Higuchi $F = k_H \times t^{½}$	**R^2**	0.9560	0.9620	0.8863	0.9066	0.9538	0.9131
	RMSE	7.16	6.61	13.16	11.75	7.66	9.82
	Parameters	k_H: 45.3	k_H: 45.2	k_H: 48.9	k_H: 47.3	k_H: 46.8	k_H: 48.1
Korsmeyer-Peppas $F = k_{KP} \times t^n$	**R^2**	0.9648	0.9699	0.8882	0.9025	0.9584	0.9660
	RMSE	6.40	5.88	13.03	12.05	7.28	6.14
	Parameters	k_{KP}: 49.2 n: 0.420	k_{KP}: 48.8 n: 0.424	k_{KP}: 53.4 n: 0.415	k_{KP}: 50.7 n: 0.440	k_{KP}: 50.3 n: 0.431	k_{KP}: 55.8 n: 0.351
Peppas-Sahlin $F = k_1 \times t^m + k_2 \times t^{2m}$	**R^2**	0.9964	0.9948	0.9847	0.9927	0.9936	0.9888
	RMSE	2.04	2.44	4.83	3.29	2.86	3.52
	Parameters	k_1: 65.1 m: 0.69 k_2:-12.2	k_1: 63.7 m: 0.68 k_2:-11.7	k_1: 73.9 m: 0.81 k_2:-14.1	k_1: 67.5 m: 0.86 k_2:-11.9	k_1: 65.9 m: 0.73 k_2:-12.0	k_1: 76.8 m: 0.58 k_2:-16.5

FD: freeze-dried, k_0: zero-order release constant; k_{1^o}: first-order release constant; k_H: Higuchi release constant; k_{KP}: release constant incorporating structural and geometric characteristics of the drug-dosage form; n: diffusional exponent indicating the drug-release mechanism; k_1: constant related to the Fickian kinetics; k_2: constant related to relaxation kinetics; m: diffusional exponent, R^2: correlation coefficient values, RMSE: root mean squared error.

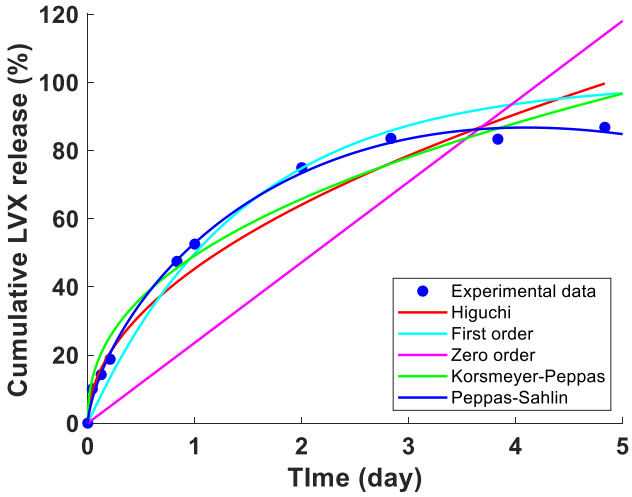

Figure S2. Representative drug release fitting models. Different kinetic models (Higuchi (red), First order (turquoise), Zero order (pink), Korsmeyer-Peppas (light green), Peppas-Sahlin (blue)) were fitted to the experimental release data of fresh F1 PLGA microspheres (blue dots).

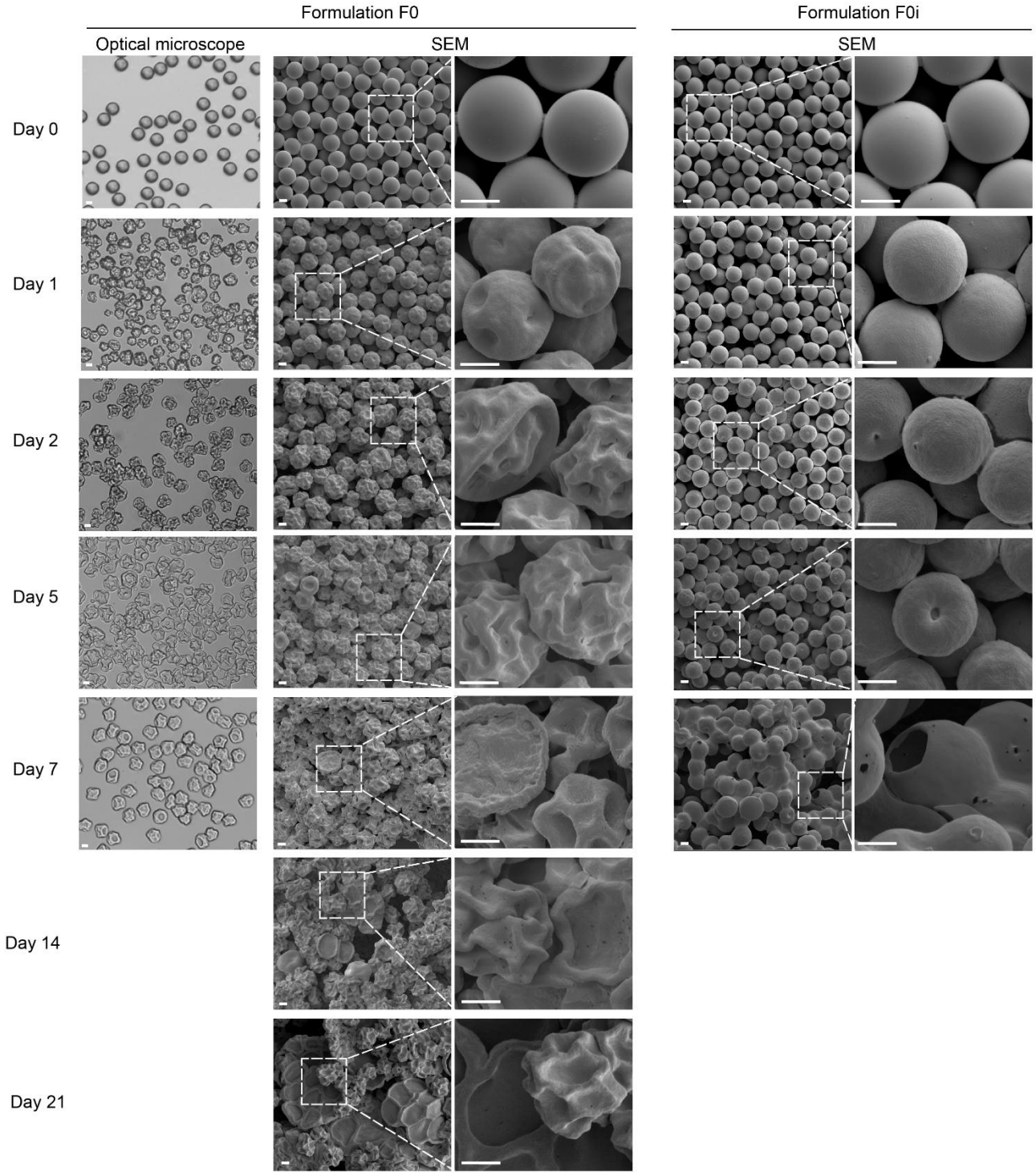

Figure S3. Degradation of F0 *vs* F0i PLGA microspheres. Optical microscope and SEM images of microspheres incubated in PBS at pH 7.4 and 37 °C. Scale bars: 5 µm.

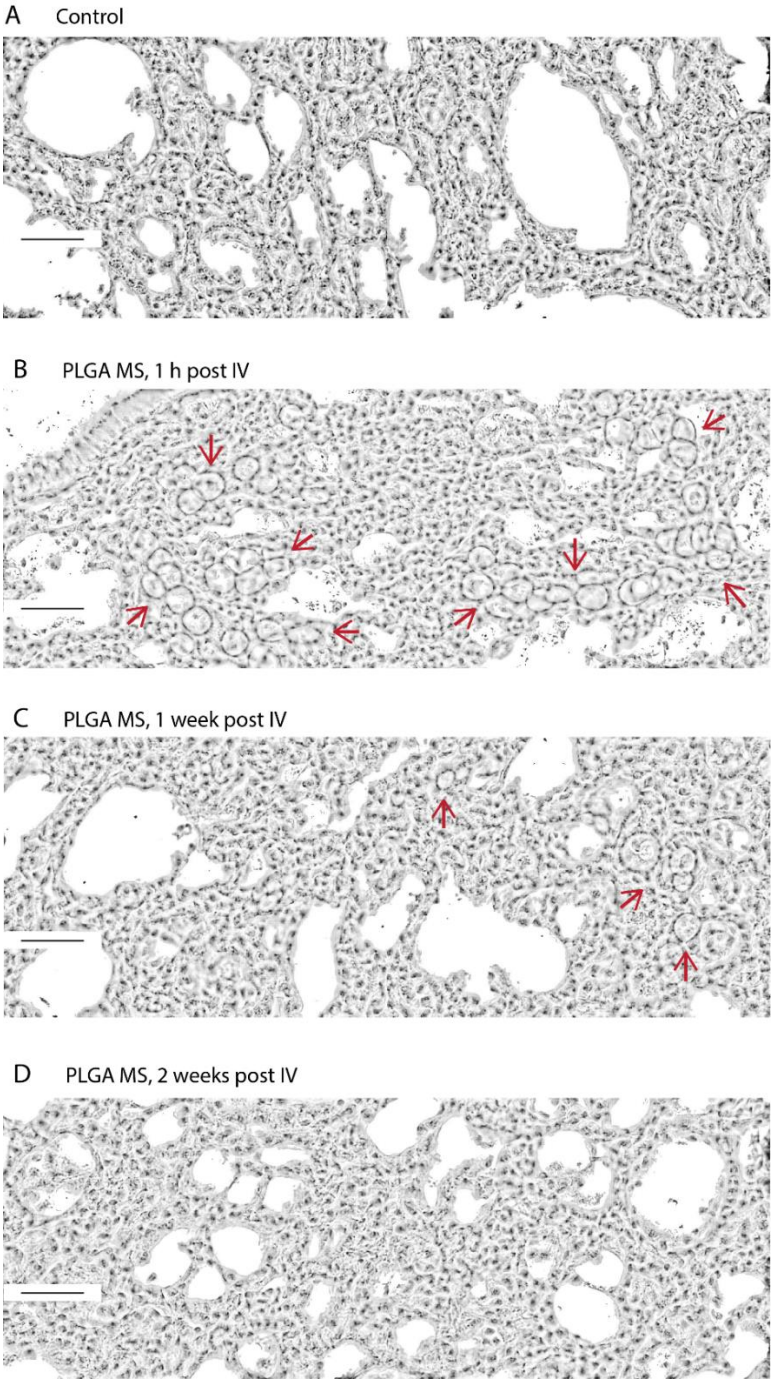

Figure S4. Representative full-size histology images of lungs exposed to PLGA microspheres (F0) after intravenous injection over time. Representative full-size processed images of the H&E stained histological 30-µm coronal lungs sections at 40× magnification after different treatments. **(A)** Healthy and untreated lungs. **(B,C,D)** Healthy lungs after 1 h, 1 week and 2 weeks of injection of 3 mg/mouse PLGA microspheres (corresponding to approximately 300,000 PLGA MS/mouse). Red arrows point to some of the microspheres. Scale bars: 50 µm.

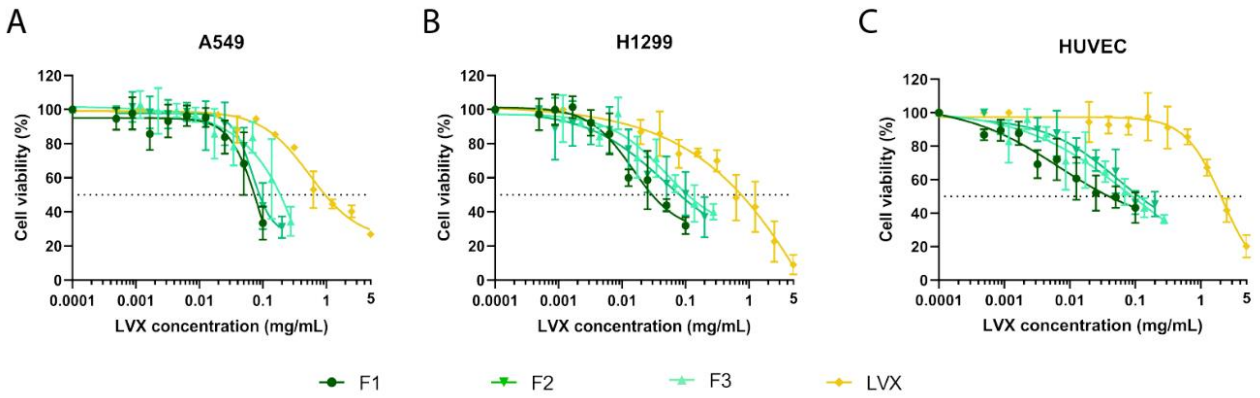

Figure S5. Cell toxicity of PLGA microspheres, normalized for levofloxacin content. Cell viability (%) of (**A**) A549, (**B**) H1299 and (**C**) HUVEC cells incubated for 24 h with F1 (dark green), F2 (light green), F3 (teal) PLGA microspheres and hemihydrate levofloxacin (yellow). The dotted line represents 50% viability. Data are presented as mean ± SD, N = 3, n = 3.

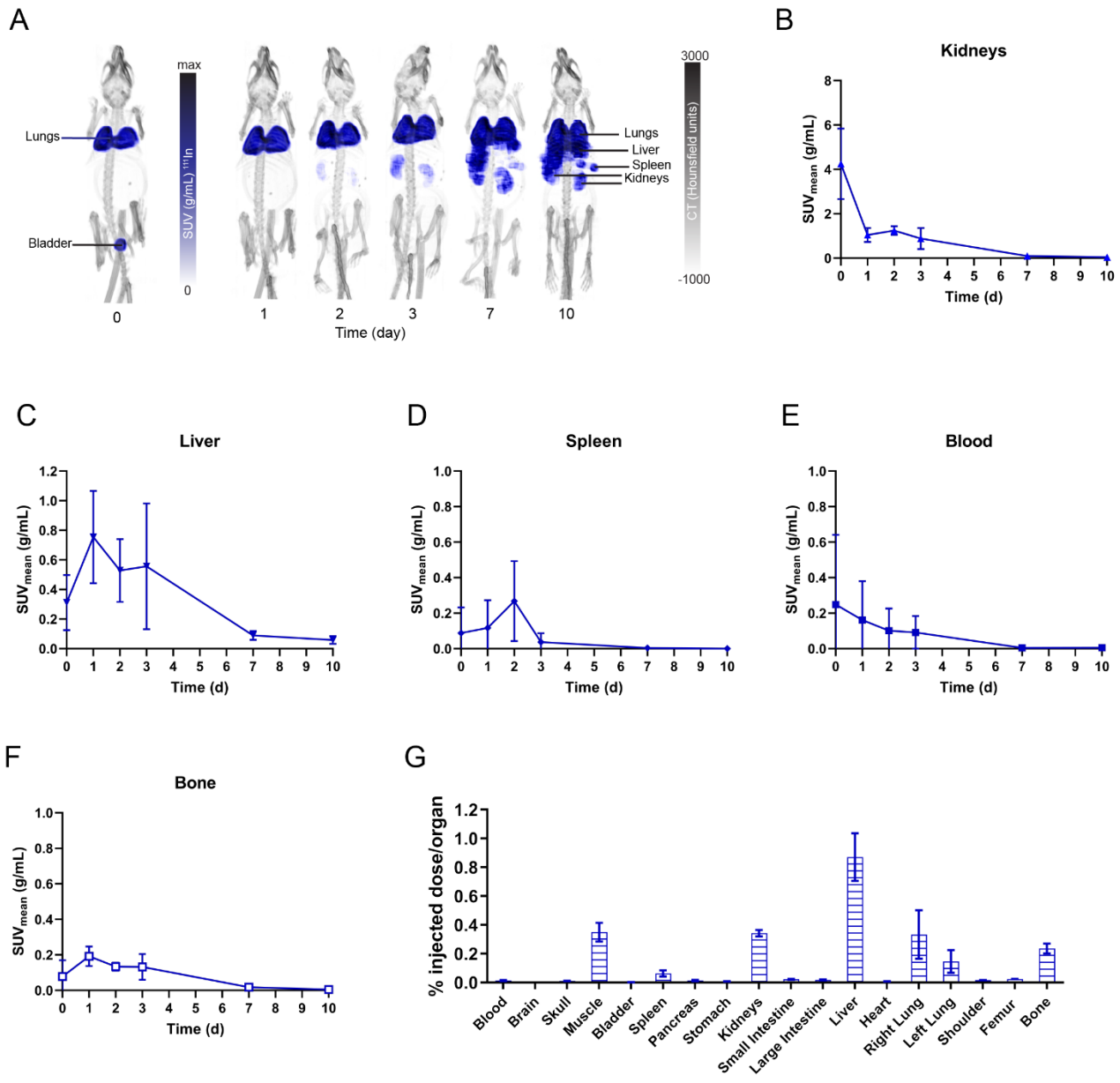

Figure S6. Pharmacokinetics and biodistribution of radiolabeled PLGA microspheres. **(A)** SPECT/CT images of ^{111}In-DTPA-PLGA MS at time points of 1 to 10 days are shown with intensity individually adjusted to visualize the small activity in other organs. Radioactivities shown are thus not to scale. **(B-F)** Organ SUV in g/mL (mean ± SD) of the ^{111}In-DTPA-F0i PLGA MS over 10 days, calculated from the SPECT images (N = 3) **(G)** Biodistribution (mean ± SD, N = 3) of ^{111}In-DTPA-PLGA MS on day 10 after injection. Tissue uptake is expressed as % of injected dose/organ.

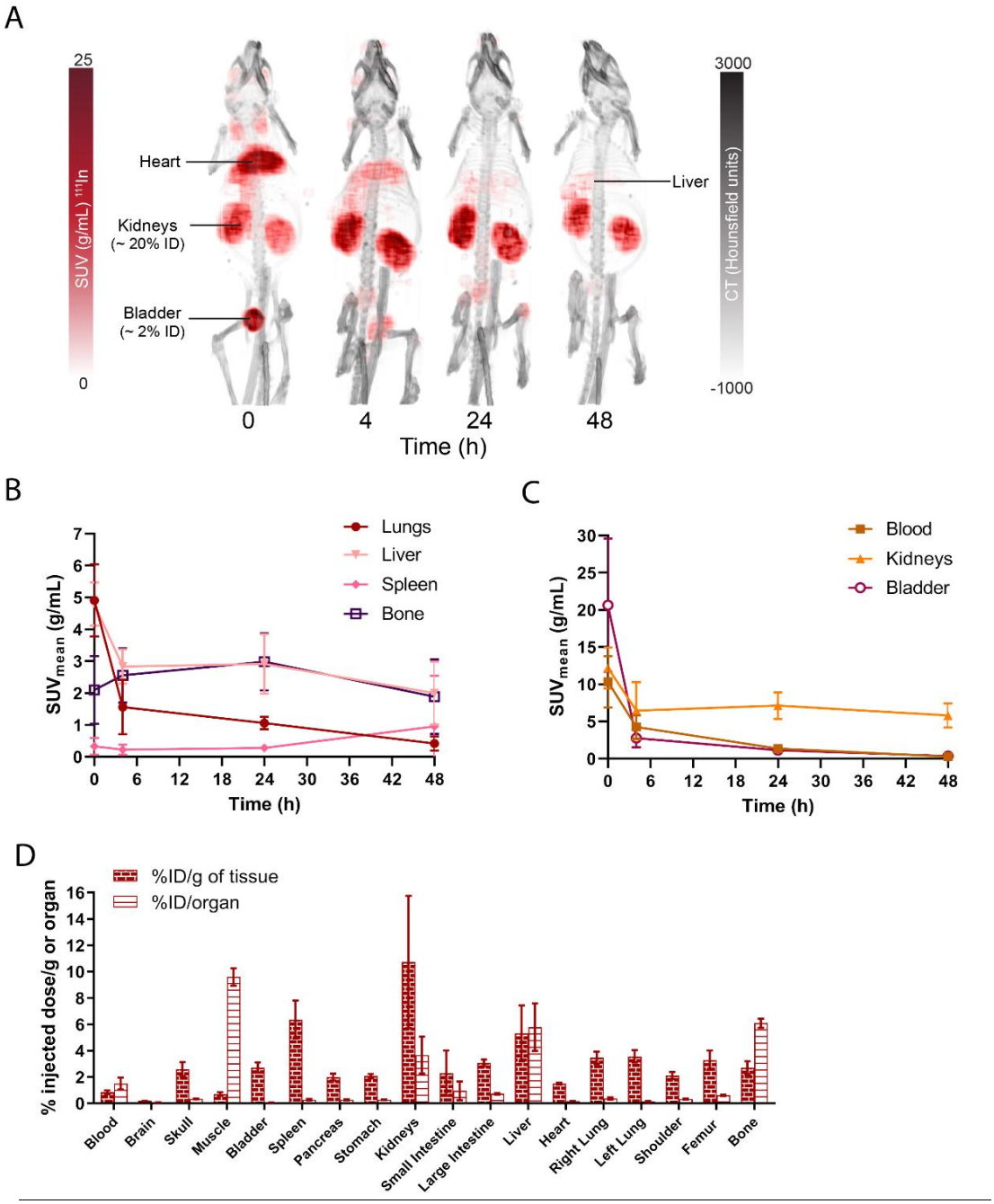

Figure S7. Pharmacokinetics and biodistribution of $^{111}InCl_3$ after intravenous administration. (A) Representative maximum intensity projections (MIPs) SPECT/CT overlay images (dorsal view) of healthy C57BL/6 mice showing the *in vivo* distribution of $^{111}InCl_3$ after intravenous tail injection over time. The radioactivity is shown in red. **(B-C)** Organ SUV in g/mL (mean ± SD) of the free $^{111}InCl$ over 48 h, calculated from the SPECT images (N = 3). **(D)** Biodistribution (mean ± SD, N = 3) of $^{111}InCl_3$ at 48 h after injection as % of injected dose (ID)/g of tissue and % of ID/organ.

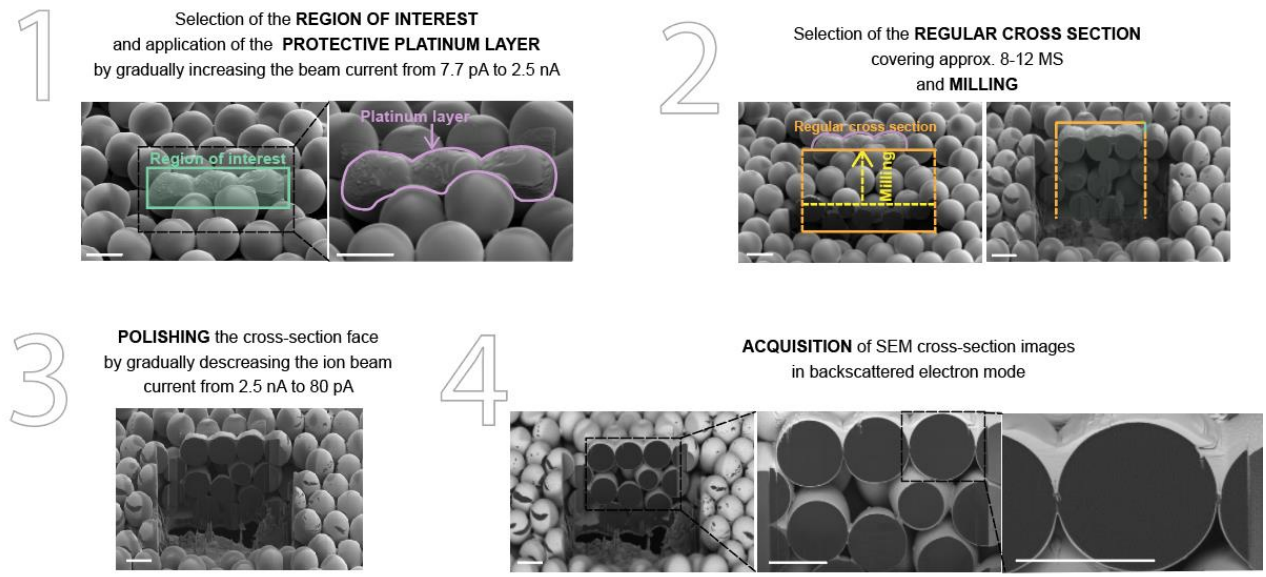

Figure S8. Steps to obtain cross-sections of PLGA microspheres with FIB-SEM. Scale bars: 10 µm.

Movie S1. Production of microspheres by flow focusing.

Movie S2. SPECT/CT animated image 15 min after intravenous administration of ^{111}In-DTPA-PLGA microspheres.